AN ABSTRACT OF THE THESIS OF

Nicholas C. Mehmel for the degree of Master of Science in Geology presented on September 15, 2020

Title: Assessment of Extraterrestrial Tracers Ir, Pt and ^{3}He in Polar Ice Cores

Abstract Approved:

_____

Edward J. Brook

This thesis focuses on the investigation of extraterrestrial tracers Ir, Pt and ^{3}He in polar ice cores. These tracers may be used to identify characteristics of interplanetary dust particles, and to quantify the flux of extraterrestrial material during impact events, certain volcanic eruptions, and stable background periods. In the first chapter I present novel Ir and Pt concentration records in ice cores from Summit Greenland, spanning the Tambora eruption of 1815 and the Tunguska impact event of 1908. A significant Pt signal is observed within a year of the Tambora eruption, but no observed signal is associated with the Tunguska event. Also presented here is a direct comparison between two established chemical digestion procedures, to assess what portions of the Ir and Pt signal are captured by each. An average Ir concentration of ~0.4 fg/g and average Pt concentration of ~15.7 fg/g are recorded, suggesting a total flux of interplanetary dust particles between 43.5 – 217 metric tons/day on Earth. In the second chapter, I present ^{3}He concentrations in very large ice samples (3+ kg) from Taylor Glacier, Antarctica, and report an average concentration among 7 samples of 5.32 x 10^{-17} ccSTP/g, with an average ^{3}He/^{4}He ratio of 98.77 R_A (SD: 34.4 R_A), where R_A is the atmospheric ^{3}He/^{4}He ratio comparable to stratospheric IDPs. Size fraction experiments and magnetic separation

experiments were also performed on ^{3}He- bearing particles in ice samples, and several bulk ice samples recorded $^{3}He/^{4}He$ ratios over 200 R_A.

Assessment of Extraterrestrial Tracers Ir, Pt and ^{3}He in Polar Ice Cores

by
Nicholas C. Mehmel

A THESIS

submitted to

Oregon State University

in partial fulfilment of
the requirements for the
degree of

Master of Science

Presented September 15, 2020
Commencement June 2021

Master of Science thesis of Nicholas C. Mehmel presented on September 15, 2020

APPROVED:

_____

Major Professor, representing Geology

_____

Dean of the College of Earth, Ocean, and Atmospheric Sciences

_____

Dean of the Graduate School

I understand that my thesis will become part of the permanent collection of Oregon State University libraries. My signature below authorizes release of my thesis to any reader upon request.

_____

Nicholas C. Mehmel, Author

ACKNOWLEDGEMENTS

I would like to thank my advisor, Ed Brook, for his continued support and encouragement throughout the pursuit of this thesis. His expertise and previous experience working with interplanetary dust particles in ice have helped guide me through this difficult exploratory work. He has served as an excellent mentor and role model, reaching above and beyond my expectations, and teaching me what science research is really about.

I also greatly appreciate the help provided by the members of my thesis committee. Dave Graham expertly guided me through the laboratory work on ^{3}He presented here, and treated me like a member of his own lab. We faced many challenges and setbacks while performing our measurements, but his complete mechanical mastery of the furnace, vacuum line and mass spec overcame each one. Brian Haley welcomed me to the Keck Lab with great enthusiasm, and his expert background in wet chemistry and trace metal analyses made PGE measurements possible. Maybe one day we will figure out how to get those Hf columns to work.

I owe a huge debt to Chris Russo, whose analytical expertise and countless hours helping me perform ICP-MS measurements taught me more than I could imagine about trace metal analyses. Chris performed all PGE measurements during the COVID-19 pandemic, which I can never fully repay him for. I want to thank Ed, Dave, Brian, and Chris, as well as Jesse Muratli, specifically for their logistical and emotional support following the Burt Hall fire of November, 2018. My proximity to the event, and the extreme setbacks it presented, left a heavy mental toll on me. Their timely support and encouragement kept me on track.

I must thank Philip Place from Rochester, as well as Geoff Hargreaves from the NSF Ice Core Facility, for retrieving and sending me the relevant ice samples. A great thanks to Monica Arianza and Joe McConnell at DRI for their excellent work dating and providing chemistry on Summit ice. Thank you to Andy Menking and Mike Kalk, for providing me with unique ice samples, and helping me with various tasks in the freezer. And a great thanks to all my friends in the CEOAS community, who helped make this project a success.

A resounding thank you must be paid to the Comer Family Foundation, for their generous financial support dedicated to the PGE portion of this research.

CONTRIBUTION OF AUTHORS

Three co-authors are specified in Chapter 1 of this thesis. Ed Brook provided the impetus for this PGE project by expanding on his previous pilot studies. He provided significant guidance with chapter organization and completed a large portion of chapter editing. Brian Haley helped conceptualize and implement laboratory methods for the project in the OSU Keck Lab, and collaborated on experimental design. Joe McConnell from DRI provided the continuous flow chemistry data presented and is responsible for the age model we used for ice samples.

Two co-authors are specified in Chapter 2 of this thesis. Ed Brook provided the impetus for this ^{3}He project as well, building on two previous published works investigating He isotopes in ice cores. He provided the bulk of editing for this chapter. Dave Graham, who runs the noble gas geochemistry lab at OSU, helped design the project and individual experiments from the start. We collaborated closely to perform all ^{3}He measurements presented here.

TABLE OF CONTENTS

CHAPTER 1: IRIDIUM AND PLATINUM ACCRETION IN POLAR ICE: RECORDS FROM SUMMIT, GREENLAND SPANNING THE TAMBORA ERUPTION OF 1815 AND TUNGUSKA IMPACT OF 1908

TABLE OF CONTENTS (Continued)

Page

TABLE OF CONTENTS (Continued)

Page

Chapter 1

IRIDIUM AND PLATINUM ACCRETION IN POLAR ICE: RECORDS FROM SUMMIT, GREENLAND SPANNING THE TAMBORA ERUPTION OF 1815 AND TUNGUSKA IMPACT OF 1908

1.1 ABSTRACT

Ir and Pt are often considered proxies for extraterrestrial input in marine sediment and polar ice core archives, and can be used to help identify significant impact events in Earth history. Certain volcanic eruptions can also leave behind Ir and Pt signatures, which complicates our interpretation of these trace signals. We present novel Ir and Pt concentration records from Summit, Greenland ice cores spanning the Tambora volcanic eruption of 1815 and the Tunguska impact event of 1908. An elevated Pt signal, reaching 271% of background concentrations, is observed within 1 year of the Tambora eruption. No significant signal in either element is observed during the Tunguska event. We also present a direct comparison of weak chemical digestion procedures developed by Gabrielli et al. (2004) and strong chemical digestion procedures developed by Petaev et al. (2013), and find that little difference exists between their observed signals. Average Ir and Pt concentrations in ice samples are 0.4 fg/g and 15.7 fg/g, respectively. Our results indicate that the majority of Ir and Pt in Greenland ice from the 1800-1900s C.E. is likely deposited by nano-meter sized meteoric smoke particles, and suggest a total flux of interplanetary dust particles between 43.5 – 217 metric tons/day, in close agreement with other published estimates.

1.2 INTRODUCTION

Iridium (Ir) and platinum (Pt) are often viewed as tracers of extraterrestrial (ET) input in terrestrial archives. These two platinum group elements (PGEs) leave behind clear signatures during ET impact events, because chondritic meteorites are up to 10,000x enriched in Ir and 3,000x enriched in Pt compared to Earth's crust (Anders and Grevesse, 1989). *Alvarez et al.* (1980)

famously attributed extraterrestrial cause to the K-Pg extinction event based on a large Ir anomaly. Smaller meteoroids and interplanetary dust particles (IDPs) that enter the Earth's atmosphere on a regular basis vaporize and re-condense in the upper atmosphere, producing nano-particles called meteoric smoke particles (MSP) often smaller than 50 μm (Plane, 2003). Measuring these PGEs in ice requires quantifying the relative proportions of terrestrial and extraterrestrial inputs, which vary greatly through time, particularly through Quaternary glacial cycles (Gabrielli et al., 2004). Compared to terrestrial dust, volcanic material is also enriched in PGEs originating from the mantle (McDonough & Sun, 1995) , and anomalies in Pt and Ir recorded in Greenland ice have been linked to volcanic events in Iceland (Gabrielli et al., 2008). Our primary motivation to improve understanding of PGEs in polar ice cores is to contribute to modern estimates of global IDP mass flux to Earth's surface, and to uncover the potential use of PGEs as stratigraphic tools in ice and sedimentary archives.

1.2.1 Background: IDP Flux and Entry Heating Process

The primary sources of IDPs in the solar system are collisions between asteroids and sublimation of comets as they near the sun (Plane, 2003). The total IDP flux into Earth's atmosphere is poorly constrained, with estimates varying from 5 to 200+ tons per day (Gabrielli et al., 2004; Mathews et al., 2001) depending on the method of measurement used to constrain the flux. Some workers have attempted to determine flux by directly measuring variables in outer space. For example Love & Brownlee (1993) obtained particle size estimates from the Long Duration Exposure Facility (LDEF), a soft metal plate fixed to a satellite that recorded collisions with IDPs of sufficient velocity. Other workers have attempted to quantify IDP abundance in the

middle atmosphere, using radar and other remote sensing techniques. For example, (Mathews et al., 2001) employed high performance radar at the Arecibo Observatory in Puerto Rico to identify the number and approximate mass of IDPs that travelled within the telescope's vertical beam. A third category of constraints targets chemical tracers of IDPs that are deposited and preserved in terrestrial archives, including marine sediments or ice sheets.

Most IDPs in space are undifferentiated and bulk-elemental in composition, but their relatively high carbon content and porous structures make them more fragile than most carbonaceous chondrites (Brownlee, 2016). Love & Brownlee (1993) estimate from the LDEF that the majority of IDP mass flux at the top of earth's atmosphere, referred to as "parental material" is between 200-220 μm diameter (which based on a ~2.8 g cm^{-3} meteorite density, equates to a ~10μg particle). Velocities at the top of Earth's atmosphere are now believed to average 25-30 km s^{-1}, but can range from 11.5-72 km s^{-1} depending on the particle orbit (Janches et al., 2006). These very high velocities cause most IDPs to undergo rapid frictional heating as they collide with air molecules in the atmosphere, causing their component minerals to vaporize. According to the CAMBOD chemical ablation model, all IDPs greater than 1 μg will reach their melting point (1800 K; 1500°C) and undergo some degree of ablation (Vondrak et al., 2008) A portion of relatively large particles will undergo partial ablation, losing all of their volatile elements during melt, but re-condensing into particles termed *cosmic spherules*: shiny, spherical particles ranging from 50-700 μm in diameter (0.2-500 μg in mass). It is important to note that particles of this size typically settle to Earth's surface within a day. The accretion rate of these cosmic spherules has been estimated by retrieving particles from the South Pole water well at Scott-Amundsen base in Antarctica. Comparison to model data indicates that about 90% of total incoming IDP mass is

ablated during atmospheric entry, and spherules only represent the remaining 10% of unablated material (Taylor et al., 1998).

The ablated material from IDPs is thought to combine with sulphate aerosols to form nanometer sized (<10 nm) meteoric smoke particles (MSPs) at or below 85km altitude (Plane, 2003; Saunders & Plane, 2011). Unlike spherules, these light particles do not sediment rapidly. Atmospheric circulation models predict that the MSPs remain airborne for months, and are preferentially pushed towards the winter pole by mesospheric meridional circulation prior to settling in the stratosphere within the polar vortex (Saunders et al., 2012). In fact, airborne measurements record a ~3x higher fraction of MSP-like particles within the northern hemisphere polar vortex than just outside of it (Curtius et al., 2005). The transport of MSPs into the mesosphere and troposphere is still poorly understood: some conceptual models predict a straightforward descent resulting in amplified deposition in the polar vortex (Gabrielli et al., 2004) while others argue that MSPs become well mixed again across latitudes by mid latitude tropopause folding (Saunders et al., 2012). Regardless, terrestrial collection currently offers the only method to *directly* measure cosmic dust concentration, composition, and spatial distribution.

1.2.2 *Terrestrial Archives, IDP Composition, and Previous Work Towards ET Tracers*

IDPs and their daughter MSPs can be collected on land or in marine sediments. Deep sea sediments are ideal for collecting larger cosmic spherules due to their long exposure times and low accumulation rates, allowing particles to collect in large concentrations. For example, spherules of diameter 200 μm or greater make up at least 20 ppb by weight of Pacific red clays (Murrell et al., 1980) However, over long periods, IDPs can weather in deep sea conditions.

Because most particles larger than 100 μm form magnetite upon atmospheric entry, many develop ferromagnetic properties and can be separated and collected from surrounding sediment using simple magnets (Brownlee, 1985). MSPs are too small to differentiate and collect from bulk marine sediment. Despite being a mere trace component of materials on earth, cosmic dust can contribute appreciable amounts of rare elements and isotopes to terrestrial sediments, including Ir, Pt, and ^{3}He (discussed in the following chapter).

Ir and Pt are very highly enriched in cosmic dust compared to terrestrial dust (Gabrielli et al., 2006) because they are both siderophile elements. During early Earth's planetary differentiation, bulk Ir and Pt migrated to the molten iron core, rather than crustal rocks (Plane, 2012). Undifferentiated chondritic material, the most common meteoric material, contains about 481 ppb Ir and 990 ppb Pt (Anders & Grevesse, 1989) Average terrestrial crust, on the other hand, contains 0.05 ppb Ir and 0.4 ppb Pt (Wedepohl, 1995). Alvarez et al. (1980) famously attributed extraterrestrial cause to the K-Pg extinction event based on a large Ir anomaly found in deep sea limestones exposed in Italy, Denmark and New Zealand. More recently, Ir and Pt have been explored as tracers in polar ice cores and snowpits, which provide a less contaminated matrix for IDP collection.

While Taylor et al. (1998) collected spherules from the South Pole water well, early attempts to measure Ir and Pt in ice used smaller size fractions. Karner et al. (2003) filtered particles sized 0.45μm – 20μm from 6 ~2 L ice samples (spanning ages 6-20ka) from the GISP2 ice core for measurement using instrumental neuron activation analysis (INAA). Their analysis recorded an average Ir concentration in ice of 2.52×10^{-2} fg/g ($\times 10^{-5}$ ppt), and a total accretion rate across earth of 0.22×10^{9} g/yr within this narrow size fraction. Contemporaneous research

indicated that even during large ET impact events, like the hypothesized K/Pg impact, a smaller nanophase size fraction (MSP-sized) formed by vapor recondensation may be the primary carrier phase of PGE tracers (Wdowiak et al., 2001). The methods used by Karner et al. likely missed these important MSPs. As a result, Gabrielli et al. (2004) established a new analytical method to determine sub fg/g concentrations of PGEs in ice using inductively coupled plasma sector field mass spectrometry (ICP-SFMS), specifically to target MSPs.

These new methods were applied by Gabrielli and co-workers to GRIP ice core samples from Summit, Greenland, spanning the Holocene and last glacial age (LGA) through 100 ka. A strong contrast was found between Holocene and LGA ice PGE concentrations and fluxes, with LGA ice experiencing strong crustal enrichment, theoretically due to enhanced dry and windy glacial conditions (Gabrielli et al., 2004). Holocene samples measured 0.3 fg/g Ir and 0.6 fg/g Pt respectively, which yields a global extraterrestrial input estimate of 78 $x10^9$ g/yr, significantly higher than the input of larger IDPs reported by Karner et al., (2003). A further exploration of MSPs was conducted by(Gabrielli et al., 2006) on Vostok and EPICA Dome C ice cores from Antarctica, finding higher PGE concentrations than in Greenland Holocene ice due to low snow accumulation rates (Medians = 1.9 fg/g Ir, 2.3 fg/g Pt in EDC, and 1.1fg/g Ir, 1.8fg/g Pt in Vostok). The most striking finding from this study was a significantly higher PGE flux during warm periods than cold periods, which opposed any known classical climatic profile for heavy metals and dust fluxes which always exhibit higher values during the last ice age and lower values during the Holocene. Regardless, the Dome C and Vostok records suggest an approximate global extraterrestrial input estimate of anywhere between 21 - 89 x 10^9 g/yr depending on the tracer and core used. The methods established by Gabrielli et al. for quantifying ultra-trace levels of

PGEs from polar ice and snow remain popular among more recent studies (Gabrielli et al., 2008; Soyol-Erdene et al., 2011; Tseren-Ochir et al., 2011).

IDPs and their ablated components can be identified and investigated based on their magnetic properties as well. (Lanci & Kent, 2006) used isothermal remanent magnetization (IRM) to selectively measure Fe- rich MSPs from Greenland ice based on their super-paramagnetic properties. Ice samples are cooled to 77K and allowed to warm; because MSPs are far smaller than terrestrial dust, they become mobile in the ice lattice at much lower temperatures (100K vs. >200K) allowing their paramagnetic properties to be measured separately (Suavet et al., 2008). Their estimate for ET magnetic particle sizes range from 7-17nm diameter, with a total particle concentration of 0.78 ± 22 ppb, both consistent with the PGE fluxes reported by Gabrielli et al (2004). Later measurements in Antarctic ice from Vostok indicate a remarkably similar MSP concentration despite vastly different accumulation rates between Greenland and Antarctica, suggesting that wet deposition dominates over dry deposition for MSPs (Lanci et al., 2007). Magnetic estimates of Greenland MSP concentrations are entirely consistent with chemical ICP-MS methods, whereas magnetic estimates of Antarctic MSP concentrations are significantly lower than chemical estimates (by about half; Lanci et al., 2012). The discrepancies between estimates suggest that chemical Ir and Pt measurements might include not only MSPs, but a portion of larger micrometeorite and terrestrial dust populations as well.

1.2.3 Strong HF Acid Digestion vs. Weak HNO_3 Suspension Methods

In an effort to measure all Ir and Pt present in ice from both MSPs and larger cemented particles, (Petaev et al., 2013) developed a far more aggressive chemical digestion method for

ice samples than those employed by Gabrielli et al.(2004). Earlier methods preconcentrated liquid samples by sub-boiling evaporation and kept MSP particles in solution by maintaining an analytical solution of 1% HNO_3 (%v/v). The new methods introduced concentrated HF and HNO_3 acids to the digestion process with intent to break down silicate minerals present in samples. They also suspended the final analytical solution in ~30% Aqua Regia, arguing (without substantiation) that PGEs are known to be unstable in 1% HNO_3 , making it unable to transfer all Ir and Pt into solution for measurement. Petaev et al. (2013) applied these chemical methods to the GISP2 Ice core from Summit, Greenland spanning the Bølling-Allerød/ Younger Dryas boundary (12.2-13.0 ka, 2.5-5 year resolution). They found a very large Pt anomaly, not accompanied by an Ir anomaly, producing Pt/Ir ratios exceeding anything ever found in terrestrial or extraterrestrial materials. While the chemical ratios of this anomaly are unusual and difficult to explain, the only materials known to have remotely similar Pt/Ir ratios and very low Al are magmatic iron meteorites (Wasson, 1999; Wasson & Choe, 2009). The results offer support to the hotly contested Younger Dryas Boundary impact hypothesis, even if they point towards an anomalously Pt-rich impactor. In 2018, a large impact crater from a kilometer wide Fe asteroid was identified in Northwest Greenland, but poor age constraints currently make it difficult to link this event to the Younger Dryas with any certainty (Kjær et al., 2018).

1.2.4 *Younger Dryas Boundary Impact Hypothesis*

The cause of the Younger Dryas (12.9-11.7ka), a ~1.2 kyr long cooling period in the midst of deglacial warming that is well documented in Greenland ice cores (Rasmussen et al., 2006), has not yet been determined. The remarkable 4-10°C temperature decline experienced in

Greenland (Buizert et al., 2014)is associated with abrupt shifts in atmospheric and oceanic circulation. A broad range of potential mechanisms have been proposed, but whether these were triggered by a unique catastrophic event, as suggested by a number of recent papers, is an open question for some (Broecker et al., 2010). Potential catastrophic events hypothesized to have set off the abrupt climate shift include outburst flooding from proglacial Lake Agassiz into the Atlantic (Broecker, 2006), an eruption of the Laacher See volcano at ~12.9ka (Baales et al., 2002), and an extraterrestrial impact event. The impact hypothesis has support from several lines of evidence, including minor terrestrial Ir spikes in magnetic fractions of bulk sediment (Firestone et al., 2007), the presence of Fe-rich microspherules at the YD boundary across the northern hemisphere continents (Bunch et al., 2012), shock synthesized nanodiamonds found in YD Boundary sediments (Kennett et al., 2009a; Kennett et al., 2009b) and possibly the impact crater referenced above. These lines of evidence have undergone great scrutiny in the academic community (Pinter et al., 2011), and have yet to coalesce into a viable theory, but support for the impact hypothesis has come in the form of Pt anomalies identified in Southern Chile by (Pino et al., 2019), and, as discussed above, in Greenland ice by Petaev et al. (2013); though these studies do not link impact events to significant climate shifts. With evidence this sparse, a further investigation of the relatively untested methods used by Petaev et al. is necessary to ensure that their findings are accurate and trustworthy.

1.2.5 *Volcanic PGE Input*

While Ir and Pt are heavily enriched in cosmic materials, they are also enriched to a lesser and more variable extent in volcanic materials and mafic rocks (McDonough & Sun, 1995) Ir

enrichment in volcanic emissions has been documented for quite some time, as identified in effusive (non-explosive) Kilauean eruptions, likely in the volatile form of Ir hexafluoride (IrF_6), hypothesized to have a very short atmospheric lifetime (Zoller et al., 1983). The first volcanic Ir enrichment recorded in polar ice came from very large particles in tephra layers in the Beardmore Glacier area in Antarctica (the tephra was likely deposited by nearby Pleiades Volcanos, (Koeberl, 1989). Gabrielli et al. (2006) believe they too found Ir and Pt anomalies in aerosol size fractions (analogous to MSPs) in Antarctic ice. Based on their super-chondritic, and highly variable fluxes of Ir and Pt measured from EPICA Dome C (EDC, which did not follow classical climate deposition patterns), and the high concentrations of volcanic heavy metals in the same samples, they suggest that samples were strongly influenced by volcanic aerosol deposition from nearby Mt. Erebus. The conclusion is not surprising, Mt. Erebus is an active hotspot volcano located in a rift zone (Gupta et al., 2009) thought to contribute significant trace elements to the Antarctic atmosphere, and whose gas plume can be detected across much of the Antarctic continent (Zreda-Gostynska et al., 1997). Furthermore, the deposition of other trace metals like Pb, Cd, and In in preindustrial ice from Taylor Dome, Antarctica closely matches modeled output rates to the atmosphere by effusive degassing of volcanos worldwide (Matsumoto & Hinkley, 2001).

Volcanic input to the Greenland ice sheet is not quite as well constrained. Recent work by Gabrielli et al. (2008) focused on Pt and Ir in Greenland snowpits, spanning 1991-1995. They find a well resolved Pt peak (~50fg g^{-1}) and a short Ir spike (~30 fg g^{-1}), along with concentration peaks in Al, Ag, Cd and Hg in the winter of 1991, corresponding very well with ash emitted by an eruption of the nearby Hekla Volcano in the same year. Smaller Ir and Pt excursions are also measured in following years, with peaks ranging from 8-10 fg g^{-1} in the summer of 1993 for both

elements. These later excursions are attributed to global atmospheric perturbations from the large eruption of Mt. Pinatubo (Philippines) in June, 1991. Though stratospheric input of Pinatubo's aerosols is a strong hypothesis, the global atmospheric aerosol budget was perturbed for at least 3 years following the Pinatubo eruption (McCormick et al., 1995), and amplified input from MSPs or vehicles equipped with catalytic converters (Barbante et al., 2001) cannot be ruled out.

Young ice and snow samples close to the surface offer an optimal matrix for studying Ir and Pt fluxes due to their precise and accurate dating via layer counting and their ease of collection. These samples are also are most susceptible to contamination/ mixing with heavy and trace metals from modern anthropogenic sources. For example, seasonal variations of Pt in Summit snowpits (1991-1995) closely parallel changes in Russian Pt production, suggesting that smelters in the Russian Arctic may perturb natural Pt signals (Barbante et al., 2003). Measurements of heavy metals (Cr, Cu, Zn, Co, Ni, Mo, Rh, Pd, Ag, Cd, Sb, Pt, Au, and U) from snow/ice cores in Mont Blanc and Monte Rosa in the European Alps indicate that input from these metals did not jump dramatically until the 1920s. Pt concentrations in particular remain below 0.2 fg g^{-1} throughout the 18^{th} and 19^{th} century, before climbing to 0.4- 0.6 pg g^{-1} in the 1930's (Barbante et al., 2004). These concentrations are 2-3 orders of magnitude higher than Pt concentrations measured in Greenland ice, suggesting only a small portion of anthropogenic Pt makes its way to Greenland (Gabrielli et al., 2008). Most recently Soyol-Erdene et al. (2011) measured Ir and Pt in Antarctic snowpits spanning the past 50 years. Average reported concentrations were 17 fg g^{-1} for Pt and 0.12 fg g^{-1} for Ir, with concentration peaks observed during the following volcanic deposition periods: Pinatubo (1993-1994), Cerro Hudson (1991-

1992), El Chichon (1982), Deception Island (1967-1970), and Mt. Agung (1964-1965), concluding that Pt and Ir are useful indicators of past eruptions. They do not observe anthropogenically enriched Pt in Antarctic snow until 1980.

While the potential sources of PGEs into polar ice are becoming clearer over time, the relative input from each of these sources is still poorly constrained. It is possible that the MSP input estimated from previous studies is overestimated, and that a larger portion of PGEs in ice samples are derived from volcanic sources than previously anticipated. In an attempt to divide these two separate inputs, we analyze ice from Greenland spanning two separate events: the Mt. Tambora eruption of 1815 C.E., and the Tunguska extraterrestrial impact of 1908 C.E.. By comparing records from these two events, we hope to unveil recognizable differences between extraterrestrial and volcanic inputs of PGEs.

1.2.6 *Tambora & Tunguska Events*

The eruption of Mt. Tambora (Sumbawa, Indonesia) on April 11, 1815 is considered the most powerful ash eruption since the last glacial maximum (LGM) almost 20kyr ago(Stothers, 1984). The explosion had an estimated volcanic explosivity index (VEI) of 7, ejecting approximately 10 billion tons of pycroclastic trachyandesite and exposing a caldera 6 km across and 600 m deep (Stothers, 1984). Plinian plumes and caldera collapse launched plumes over 43km in the air, injecting 60 mt of sulfur into the stratosphere (6x the amount injected by Pinatubo in 1991), resulting in a stratospheric veil of sulfate aerosols observed around the world (Oppenheimer, 2003). The widespread veil of sulfate aerosols triggered climate anomalies, but also left clear S signatures in multiple Greenland and Antarctic ice cores (Dai et al., 1991) that

were easily identified in our ice samples. Until now, no attempt has been made to identify PGE signatures from this event in any climate archive.

The Tunguska event on June 30th, 1908 over eastern Siberia is far more mysterious. It is classified as an impact event (though no impact crater has been found) attributed to an air burst of a carbonaceous chondritic meteoroid about 60-200m in size that disintegrated prior to hitting earth's surface (Lyne & Tauber, 1995). Though eyewitness accounts corroborating this hypothesis were limited, some shockwave approximating a 10-20 mt (TNT) blast clearly must have occurred at about 10km altitude in order to flatten 80 million trees over 2000+ km^2 (Chyba et al., 1993). Other geophysical model predictions predict the body broke up into smaller rocks between 30-45 km (Borovička et al., 2013). Recent geochemical evidence from microsamples in peat bogs near the Tunguska event, including nanodiamonds, appropriate δ^{13}C values and microinclusions of troilite suggest that these are all remnants of a meteoric body (Kvasnytsya et al., 2013). Surprisingly, these individual microsamples were not enriched in Ir (Kvasnytsya et al., 2013). In contrast, bulk sediment from Tunguska layers in local Siberian peat bogs are enriched in Ir, with concentrations 10-20x higher than those in preceding layers (Hou et al., 1998). So far, very few attempts have been made to identify tracers from this impact event (the largest in recorded history) outside of the Eurasian continent (K. L. Rasmussen et al., 1995).

1.2.7 *Research Significance and Primary Research Goals*

A better understanding of Ir and Pt signals in ice cores has the potential to improve estimates of IDP flux to earth, help better quantify siderophile budgets in various earth reservoirs, and enable the reconstruction of volcanic, meteoric, and even climate events in Earth

history that are undetectable by other means. Further research into MSPs alone has far reaching applications. They provide feeder materials for nucleation of noctilucent clouds (a visual indicator of greenhouse processes and modern climate change), they interact with aerosols and O_3 in the stratosphere (impacting ozone formation), and their Fe-rich composition may help fertilize the upper ocean with bio-available Fe (a potentially critical process to climate feedbacks; Plane, 2012; Watson et al., 2000). Cosmic dust also may have delivered complex organic matter and amino acids to the primitive earth, complementing early abiotic synthesis (Anders, 1989). Further measurements of ice samples spanning the Younger Dryas period are necessary to better assess the Younger Dryas impact hypothesis.

In this work we present ice core records of Ir and Pt from Summit, Greenland spanning the Tambora eruption of 1815 and the Tunguska impact of 1908, as well as background periods spanning the 1920's. A critical laboratory comparison of methods similar to those of Gabrielli et al (2004) and Petaev et al. (2013) was conducted to determine differences in signals obtained by each. Our primary research goals were to:

1. Develop a viable method of sub-femtogram level PGE measurement in ice cores at Oregon State University, College of Earth Ocean and Atmospheric Sciences.

2.*Constrain seasonal background variability of PGEs during the 1800s-1900s C.E in Summit, Greenland ice.*

3.Investigate PGE signals corresponding to the Tambora eruption of 1815 in Summit ice

4.Investigate PGE signals corresponding to the Tunguska impact of 1908 in Summit ice

5.Test the assertion from Petaev et al.(2013) that methods established by Gabrielli et all. (2004) miss a significant portion of total PGE signals in ice samples.

6.Provide another estimate of global IDP flux to the existing (small) collection of published estimates

1.3 METHODS

1.3.1 Sample Collection and Dating

Ice core samples spanning 35.45m to 44.61m and 61.23m to 70.33m depths were collected at Summit, Greenland during May, 2015 and sent to the National Ice Core Laboratory (NICL) for storage. Coring was conducted using the US Ice Drilling Program, 9.5 inch diameter Blue Ice Drill without drill fluid. All barrel and cutter head parts are composed of either hardened or uncoated steel, fiberglass, or plastic materials. Metal components that come in direct contact with the core were ultrasonic cleaned in acetone, 200 proof ethanol, and DI water then baked at 50°C overnight prior to drilling, while fiberglass and plastic parts were scrubbed with ethanol and rinsed with DI water (US Ice Drilling Program, 2019). In March of 2018, a cross-section of each meter-long core was cut and sent to the Desert Research Institute (DRI) for Continuous Flow Analysis (CFA) of major elements and compounds (Including Na, S, P, Ca, Ti, NH4, particulate content and stable isotopes) used to date the cores via volcanic synchronization and annual layer counting (McConnell et al., 2005). The resulting timescale from these measurements has sub-monthly temporal resolution. Continuous chemistry data can be found in Appendix A. The remainder of each core (each approximately 1 meter in length with a cross section of 10 cm x 6c m) was sent to Oregon State University for rare earth element (REE) and platinum group element (PGE) analysis.

Measured seasonal samples for this study span the depths of 3 (years 1914-1926) to target seasonal background signals, 40.15m to 41.59m (1906-1911) for Tunguska impact signals, and 66.23m to 67.35m (1813-1818) for Tambora eruption signals. Another subset of annual samples, spanning 61.23m to 64.51 (1825-1837) were split in half vertically in order to assess differences between two separate digestion methods. Depths for each seasonal or annual cut were determined from the chemically-derived timescale described above.

1.3.2 Cutting Procedure

Once ice samples were dated, seasonal sample depths were determined from the chemistry timescale and marked on the surface of each core depth using a felt tip permanent marker. Appropriate lengths were cut in a -25°C freezer using a LAGUNA 14 bx bandsaw. Carbon steel blades were used without cutting oil or lubrication, and ice was handled using nitrile gloves to prevent unnecessary surface contamination. Cut samples were placed in individually labeled plastic bags and transported in a cooler to a -10°C upright freezer. 10 total samples underwent the following procedures at any given time; at least 2 were always procedural blanks.

1.3.3 Sample Cleaning and Pre-Concentration Procedure

Seasonal ice samples (typically ranging in weight from 150g to 500g) were scraped with an acid-cleaned ceramic knife under a laminar flow hood using nitrile gloves, which removed approximately 0.25- 0.5cm from each flat edge of ice sample. The ceramic knife was rinsed with Milli-Q water between individual ice samples. Once scraped, samples were placed in 1L acid-cleaned Teflon beakers, capped and weighed, then placed on a laminar flow hood, uncapped,

and allowed to evaporate on hotplates set to 125°C. At this temperature now-aqueous samples could evaporate rapidly but not boil. Once sample volumes evaporated to below 15mL they were swirled in circles to stir up any sticking or settling particles, and poured into 30mL, conical bottom digestion vessels. Small volumes of ultrapure water (5-8mL) from an LDPE squirt bottle were used to "rinse down" the sides of the 1 L Teflon beaker to collect any remaining particles, and transferred to 30 mL digestion vessels as well. Remaining sample volume was evaporated to dryness in these digestion vessels on hotplate heating blocks set to 125°C. Once dried down samples were capped and transferred to a fume hood to begin chemical digestion. All 2 mL and 30 mL Teflon digestion vessels were cleaned before and between uses according to the revised cleaning methods referenced below, and stored in a laminar flow hood to dry prior to interaction with samples. Large, 1 L Teflon beakers were cleaned by scrubbing with lab soap and a gloved hand, rinsed 3x with Milli-Q, filled and stored with 10% HNO3 acid for 48+ hours, and rinsed 3x again with Milli-Q before placement in the laminar flow hood to dry.

1.3.4 Digestion Procedures- Strong HF Digestion

The vast majority of samples were digested using an aggressive chemical procedure modeled after those introduced by Petaev et al. (2013). Fischer Chemical brand, Optima grade concentrated hydrofluoric acid (HF), nitric acid (HNO_3), and hydrochloric acid (HCl) were used for all steps. A 1:1 mixture of 0.5 mL concentrated Optima grade HF and 0.5 mL concentrated Optima grade HNO_3 acid were added to each vessel, swirled, and all vessels were placed in heating racks on a hotplate set to 125°C for 8 hours a day on 3 consecutive days. Sealed samples were regularly swirled during this period to mix the solutions in the vessels. After 3 days, each vessel was

uncapped, and dried down at 125°C. Because this was not a Class 1000 clean room, a laminar flow hood was placed onto a cart and wheeled up to the fume hood to blow filtered air through the intake directly in front of the hotplate. Trials in early analytical rounds indicated that this hood arrangement reduced blank concentrations of Pt and Ir by over 50% (Round 3 in **Figure 1.1**). Once completely dried down, samples were brought back up with 1.4 mL of dilute aqua regia solution (0.3 mL Optima grade HCl, 0.1 mL Optima grade HNO_3 and 1mL Milli-Q), capped, and allowed to sit on the hotplate for >1 hour at 125°C. Once cooled, solutions were transferred to pre-weighed 2 mL Teflon vials, capped, and weighed again to obtain final solution weights. All final solution weights were monitored to ensure full sample transfer and record precise solution volumes. Full 2 mL Teflon vials were sealed with parafilm and brought to the temporary Keck Laboratory facilities at OSU (Research Way, Corvallis, OR) for measurement and analysis.

1.3.5 Digestion Procedure- Weak HNO_3 Digestion

Twelve larger, annual ice samples were split in half vertically to create "replicate" samples to undergo 2 separate digestion methods for comparison. One replicate was digested using the "strong digestion" methods described above, and one digested using "weak digestion" methods that follow based on those introduced by Gabrielli et al. (2004, 2006, 2008) and used in Balcerzak (2009), Petaev et al. (2013) and Sengupta et al. (2015). For the latter method, once melted ice samples were evaporated down to dryness in digestion vessels as described above this collection of samples was introduced only to 1.4 mL of 1% Optima grade HNO_3, set in a heating block on a hotplate at 125°C for 8 hours a day on 3 consecutive days, and transferred

directly to 2 mL Teflon vials for analysis. 4 samples underwent this procedure with 50% Optima grade HNO_3 acid instead of 1% HNO_3.

1.3.6 Procedural Blanks

For both digestion methods, procedural blanks were prepared as follows: Clean 1 L beakers sat open in the laminar flow hood while samples evaporated on hotplates next to them. Once most samples were ready to transfer to 30 mL digestion vessels, a 10 mL pipette was used to squirt 8 mL of Milli-Q along the sides of each blank beaker to "wash down" any adhered particles from the edges of the container. Blank beakers were heated along with the rest of the samples at 125°C, swirled, and transferred to 30mL digestion vessels to evaporate down to dryness. Once dry, blanks underwent the same digestion procedures as their accompanying samples. Samples could only be digested in groups of 10 due to available materials, and no individual round had less than 2 blanks. Blank beakers and digestion vessels were picked at random each round.

1.3.7 PGE and REE Measurement Methods

All measurements were performed on a ThermoScientific iCAP RQ ICP-MS equipped with an ESI Apex Omega desolvating nebulizer. Prior to each run the instrument was tuned for maximum sensitivity in ^{115}In and ^{138}U with minimal UO/U oxide formation (typically 0.30-0.31%). Sensitivity for In and U typically was between 250,000 cps and 350,000 cps per 0.05 ppb, respectively. These represent targeted sample aspiration rates of 200ul/min, with a true range between 180-240ul/min.

After initial trials during analytical rounds 1-4, all samples were analyzed in the following matrix: 0.125 mL of final digestion product solution (suspended in 1.4 mL dilute Aqua Regia or 1% HNO_3 depending on digestion procedure), 0.030 mL of In internal standard (equivalent to 50 ppt in final matrix), and a 2.845 mL mix of 5% HNO3 and 0.7% Hf (%v/v). An aggressive rinse procedure was used between samples to reduce cross contamination: 45 seconds in 2% HNO_3, 120 seconds in 5% HNO_3 + 0.7% HF, 45 seconds in 2% HNO_3, 120 seconds in Milli-Q water and 45 seconds in 2% HNO_3 before moving onto the next sample. Because drift in the monitored In internal standard never exceeded 1.8% during analyses, we elected not to apply an In correction to our PGE and REE measurements

Hf, Lu, Pt and Ir calibration blocks were composed 6 standards each ranging from 50-2000 ppt Hf, 0.5-20 ppt Lu, 0.2-20 ppt Pt and 0.01-1 ppt Ir, with one initial blank sample representing 0 ppt for all species. An "oxide check" solution of 2.5 ppt Lu and 250 ppt Hf was measured every 9 samples to assess variability in oxide formation rates over time. Limits of detection (LOD) were calculated using 3x the standard deviation of instrumental blank measurements, returning values of 0.0003 ppt for ^{191}Ir and 0.0018 ppt for ^{195}Pt. Analytical solutions never measured concentrations below 0.0005 ppt Ir or 0.03 ppt Pt in ice samples.

1.3.8 Method Modification Due to Laboratory Fire

Initial project methods intended to use Accuri Mars 6 microwave technology and E-Z prep vessels to digest ice samples and measure PGE concentrations. Due to a laboratory fire and destruction of said microwave, the alternative methods described above were created to mimic microwave digestions as closely as possible.

Prior to the laboratory fire, all laboratory procedures were intended to be conducted in dedicated Class 1000 clean room space with positive air pressure to minimize contamination. This space was made inoperable due to the laboratory fire, so an alternative, negative-pressure lab space located in Wilkinson 115 was used for sample preparation and digestion. This may have amplified measurement uncertainty and blank contamination over similar procedures conducted in a clean space. Although an alternative clean space later became available, once extensive sample prep procedures commenced in this negative-pressure space we elected to remain in the initial lab space for experiment consistency.

1.3.9 Test of Separating REEs from PGEs Using Column Chemistry

The elements hafnium (Hf) and lutetium (Lu) are known to produce oxide interferences on Pt and Ir during Inductively Coupled Plasma-Mass Spectroscopy (ICP-MS) analyses (Pearson & Woodland, 2000). Early phases of our experiment focused on developing a column chemistry method to isolate Pt and Ir in solution, while withholding Hf and Lu in column resin. Exploratory methods were derived largely from those laid out by Jarvis et al. (1997) and Petaev et al. (2013).

Trial experiments on Pt-Ir-Hf-Lu spiked solutions used AG 50W-X8 *cation exchange resin* (100-200 mesh) and column solution of 0.5M HCl. The small sample size and solution concentration necessitated the use of a very small column, approximately 0.5 cm in diameter and ~1-2 cm in height, accommodating ~0.5-1cc of slurried resin in trials (**Figure 1.2a**). Several elution experiments were conducted to test the feasibility of columns for our study, though no appropriate methods were discovered. We concluded due to the low concentrations and volumes of our solutions, necessary short length of our columns, and similar chemical behavior

between REEs and PGEs, that our interfering elements and elements of interest would always come off the column simultaneously (**Figure 1.2 b,c**). As a result, column chemistry of this type would not help us improve PGE measurements for our study.

1.3.10 Oxide Interferences

Without columns to separate Hf and Lu species, dealing with oxide interferences (particularly from $^{177}Hf^{16}O$, $^{178}Hf^{16}O$, $^{179}Hf^{16}O$, $^{180}Hf^{16}O$and $175Lu^{16}O$) became a priority concern for PGE measurements. Gabrielli et al. (2004) and Petaev et al. (2013) reported oxide corrections of <5% and 3% respectively in measured ice samples, indicating that oxide interferences were only a small portion of their measured signal when using front-end desolvation systems. Measured REE concentrations were not reported by Gabrielli et al., but Hf concentrations for the Petaev study were 2+ orders of magnitude lower than obtained here (Petaev samples averaged 0.13 ppt Lu and 0.97 ppt Hf in ice, whereas our samples averaged 0.17 ppt Lu and 43.80 ppt Hf in ice), making larger oxide corrections inevitable in our samples. We are unsure what caused the large discrepancy in measured Hf concentrations, but we discuss potential sources of contamination in the *Discussion* section. In our study, all sample measurements were performed using an *Apex Q Desolvating Nebulizer* to reduce oxide interferences.

High REE concentrations led to oxide interference percent of signals (%OS) reached as high as 80% for Ir and 95% for Pt in early trials. Improvements to wet chemistry and analytical methods brought these interferences to a mean of 63.1% for Ir (SD: 14.6%, Range: 37.8% - 81.7%), and 80.47% for Pt (SD: 9.4%, Range: 68.2% - 88.6%) percent of measured signal in seasonal background samples (years 1916.5-1919.5), 70.88% for Ir (SD: 9.4%, Range: 56.2% - 86.2%) and

89.2% for Pt (SD: 3.9%, Range: 84.1% - 94.9%) percent of measured signal in Tambora period samples (years 1813.5-1817.5), and 64.8% for Ir (SD: 11.2%, Range: 41.8% - 89.0%) and 83.1% for Pt (SD: 8.4%, Range: 67.4% - 91.5%) percent of measured signal in Tunguska period samples (years 1906.5-1910.5). This moderate reduction in oxide interference %OS (starting in analytical round 5 on 4/29/20) is attributed to more aggressive rinsing of autosampler between samples, and a slight addition of HF to sample solutions prior to measurement (both discussed previously). Despite our best efforts, we could not reduce oxide interference corrections any further.

Despite the large correction, oxide interferences remained very constant during individual analyses and among separate daily runs. An artificial "oxide check" solution, composed of 2.5 ppt Lu and 250 ppt Hf was repeated every 9 measurements to assess instrumental drift over time and between days. A summary of oxide formation rates during analysis can be found in **Figure 1.3**, with ^{179}Hf forming HfO with an m/z of 195 (interfering on ^{195}Pt) at a mean rate of 0.28% and ^{175}Lu forming LuO with an m/z of 191 (interfering with^{191} Ir) at a mean rate of 0.13% (over 10 separate days of instrument time). On any individual day, the SD of these rates never exceeded 0.014% for HfO formation or 0.022% for LuO formation. Oxide-corrected PGE values show no correlation with REE concentrations in samples (**Figure 1.4**), indicating that our post-measurement corrections eliminated false oxide signals. We attempted to test reproducibility of small signals (**Figure 1.5**) by saving 4 samples and measuring them during each analytical run. However, the relative standard deviation (**Table 1.1**) between runs was larger than those of procedural blanks, and even between adjacent samples, indicating that something changed in sample reservoirs once they were first opened for initial analysis. We do not believe that this test is accurately reproducing sample variability, and we suggest future reproducibility tests be

performed on replicate ice samples (discreet ice samples split in half along their vertical axes). In this study, samples of similar time period were measured together on the same day in an attempt to increase signal reproducibility and improve relative accuracy of records.

1.3.11 Reducing Blanks & Teflon Digestion Vessel Cleaning Procedures

Procedural blanks improved significantly over time as adjustments were made to digestion procedures, primarily in the form of Teflon cleaning improvements. Initial Teflon cleaning procedures included scrubbing inside digestion vessels with a gloved finger, rinsing 3x with Mili-Q water, and allowing vessels to soak submerged in 10% HNO_3 for 48 hours in a polyethylene Nalgene beaker. Acid was drained and vessels were rinsed again 3x with Milli-Q water, and placed in a laminar flow hood to dry. Improved cleaning procedures introduced lab soap to the gloved hand scrubbing procedure (NEUTRAD detergent), followed by rinsing 3x in Milli-Q, filling and capping vessels with 50% HNO_3 to heat at 125°C, draining acid while still hot, rinsing 3x with Milli-Q, filling and capping vessels with Milli-Q to heat at 125°C, draining Milli-Q while still hot, and placing under laminar flow hood to dry. All working polyethylene containers of concentrated digestion acids (Optima grade HNO_3, HCl, and HF) were replaced as well, in case of contamination.

Blank measurements also improved with more aggressive autosampler rinsing, presumably due to a reduction in cross-sample contamination. Less Hf and Lu could "stick" to the sampler and be carried from an REE rich sample or standard into a subsequent procedural blank sample-preventing artificial inflation of counts on all species of interest. A summary of blank measurements throughout the study period can be found in **Figures 1.1 & 1.6**. Blanks from initial

measurement trials (analytical rounds) regularly recorded Ir and Pt concentrations over 0.16 ppt and 0.15 ppt respectively. Analytical improvements introduced in analytical Round 5 (measured 4/29/20) and procedural improvements introduced in analytical Round 6 (measured 5/12/20) reduced these blank concentrations by a factor of 100. Procedural blanks for analytical rounds 6-10, extrapolated to a hypothetical 250g ice sample, averaged concentrations of 3,547 fg/g Hf (SD: 3,967 fg/g, 0.3% - 13.1% of average sample signal), 6.16 fg/g Lu (SD: 6.74 fg/g, 0.41% - 11.5% of average sample signal), 0.06 fg/g Ir (SD: 0.04 fg/g , 3.7% - 43.9% of average oxide-corrected sample signal), and 1.37 fg/g Pt (SD: 0.76 fg/g, 2.3% - 14.9% of average oxide-corrected sample signal).

1.3.12 Data Reduction: Corrections and Uncertainty

Several corrections were applied to raw ICP-MS count-per-second (cps) data to determine the concentration of elements in original ice samples and associated concentration uncertainties. During each analytical round (or day of measurement), average cps values from oxide-check solutions (2.5 ppt Lu, 250 ppt Hf) and REE standard calibration curves were used to determine average LuO and HfO oxide formation rates that interfere with PGE species. Daily oxide formation rates were multiplied by raw cps of Hf and Lu in ice samples and procedural blanks, and subtracted from raw PGE cps to determine oxide-corrected cps values. Hf and Lu cps values were not oxide-corrected because their interfering species were not measured. Dy-163 (1.29 ppb crustal abundance) and ^{159}Tb (1.2 ppb crustal abundance) are the only isotopes capable of significantly interfering with ^{179}Hf (0.4 ppb crustal abundance) and ^{175}Lu (0.8 ppb crustal abundance) respectively (Haynes et al., 2016; Meija et al., 2016) The relative low abundance of

these isotopes compared to our REEs of interest indicates that their oxide interferences are likely negligible. For reference, ^{195}Pt and ^{191}Ir crustal abundances are 1.6 ppt and 0.37 ppt respectively.

Oxide corrected cps values for samples then underwent a procedural blank correction. Each round of digestions produced 2-3 blanks, whose oxide corrected REE and PGE cps were averaged (and standard deviation saved for error propagation). Average cps values from procedural blank species were then subtracted from sample species to produce blank-corrected cps values. Blank-corrected cps values were then converted to concentrations using calibration factors (cps/ppt) from measured standard blocks, resulting in values that represent the concentration in ppt of species within the mass-spec centrifuge tubes. Weights of final digest solutions from 2 mL PFA vials and initial ice sample weights were used to determine dilution factors to calculate the concentration of relevant species in the original ice samples.

Standard error for calculated REE and PGE concentrations is calculated using standard uncertainty propagation methods, and incorporates the following factors: (1) standard *error* of measured cps for each sample as a representation of analytical uncertainty, (2) standard *error* of oxide formation rates throughout daily measurements, (3) standard *error* in counts for procedural blanks analyzed each day, (4) and standard *error* of the linear regression on the calibration block for each species as a representation of calibration uncertainty. Masses of final digest solutions and ice mass were used to apply these confidence intervals to original ice samples to calculate uncertainties for measurements in Greenland ice. Calculated standard errors were multiplied by 2 to generate approximate 95% confidence intervals, and plotted to represent uncertainty in our figures.

1.3.13 *Choice of ^{191}Ir and ^{195}Pt to Quantify Pt and Ir Concentrations*

Our decision to calculate concentrations using the isotopes ^{191}Ir and ^{195}Pt (and their respective interfering species ^{175}Lu and ^{179}Hf) was based on three primary factors: the natural abundance of each elemental isotope, the measured contribution of each isotope in procedural blanks, and the rate of oxide interference on PGE species (which is a function of relative natural abundances of interfering elements, as well as their oxide formation rate in the plasma chamber of the ICP-MS).

^{191}Ir has a lower natural abundance than ^{193}Ir (37.3% vs. 62.7%; Meija et al., 2016), but calculated blank Ir concentrations are 21.8% lower on average using this isotope likely due to oxide interference issues inflating certain ^{193}Ir measurements. Blank measurements based on ^{191}Ir are far less variable. Ir blank values have an average SD of 2.88 x 10^{-4} ppt (mean concentration: 4.27 x 10^{-4} ppt) as measured using ^{191}Ir, compared to 15.88 x 10^{-4} ppt (mean concentration: 5.47 x 10^{-4} ppt) as measured using ^{193}Ir. One potential cause for this is the lower rate of oxide interference for ^{191}Ir vs. ^{193}Ir: Only 0.14% of ^{175}Lu is oxidized to LuO, compared to 0.24% of ^{177}Hf. Lu is also over 2 orders of magnitude less abundant than Hf in our procedural blanks, and in our samples. These factors made ^{191}Ir the obvious choice for calculating Ir concentrations with the lowest possible uncertainty.

Unlike ^{191}Ir, ^{195}Pt is the most abundant stable isotope of Pt by a slight margin (33.78%, vs. 32.86% for ^{194}Pt and 25.21% for ^{196}Pt; Meija et al., 2016). The primary drawback of using this isotope is the oxide interference rate: 0.27% of ^{179}Hf is oxidized to HfO, compared to 0.24% and 0.22% for ^{178}Hf and ^{180}Hf respectively (natural isotopic abundances are 27.82% for ^{178}Hf, 13.62% for ^{179}Hf, and 35.08% for ^{180}Hf; Haynes et al., 2016). However, ^{195}Pt records the lowest and most

stable procedural blank concentrations over its counterparts: 0.010 ± 0.006 ppt as measured, vs. 0.012 ± 0.012 ppt for ^{194}Pt and 0.021 ± 0.014 ppt for ^{196}Pt, which likely experience noise from larger oxide interferences. It is unclear why the isotopic ratios of Pt blank values do not reflect natural abundances from any natural reservoir (chondritic material, crustal material, etc.) The relative low SD of blank concentrations using ^{195}Pt minimized uncertainties in Pt concentration calculations, though all 3 species behaved quite similarly. All Ir and Pt concentration records presented in our results section are derived from ^{191}Ir and ^{195}Pt.

1.3.14 Relevant Methodological Differences to Previous Studies

Relevant differences between "strong digest" methods from Petaev et al. (2013) and those conducted in this study include: 1) Petaev et al. rinsed outer layers of ice samples (ranging 30-70g) with ultrapure DI water to remove surface contamination, 2) pre-concentrated liquid samples in polypropylene beakers prior to transfer to Teflon digestion vessels, 3) their digestion was conducted at 150°C in an oven over one continuous week, 4) their chemistry was conducted in a class 1000 clean room, 5) they re-dissolved digestion products in 0.4mL of concentrated aqua regia (for an unknown period of time), prior to dilution with 1mL of Milli-Q, 6) their samples were measured on a GV instruments Platform ICP-MS, equipped with an APEX nebulizing inlet and 10% aqua regia as a wash solution between samples and a 10ppb LuHf oxide-check solution to determine oxide formation rates, 7) They measured samples directly from dilute aqua regia solution (we diluted aqua regia solutions with 3% HNO_3 to avoid instrument damage).

Gabrielli et al. (2004) established "weak digest" methods that also differ from ours in the following ways: 1) samples of approximately 60g were stripped of their 3 outermost annual

concentric layers using acid cleaned stainless steel knives, 2) melted samples were never dried down completely, merely to 1 mL before being brought up to a final concentration of 1% HNO_3, and 3) analytical measurements were performed on a Thermo Element2 ICP-MS with an Aridus desolvation/nebulization system, 4) procedural blanks for that study were conducted by pre-concentrating 30, 60 and 100 mL volumes of ultrapure water, and 5) all open-container procedures were conducted inside class 100 clean benches.

1.4 RESULTS

1.4.1 Seasonal Background Variability

Ir and Pt concentrations determined (using our strong digestion procedure) from a designated "background period" (1914- 1926) are illustrated in **Figure 1.7 and Figure 1.8** (normalized to terrestrial tracers), along with several other relevant tracers. Non-sea salt sodium (nssNa) records offer a potential proxy for seasonal sea ice extent, and is known to present well-marked winter maxima in central Greenland (Legrand & Mayewski, 1997). Non-sea salt calcium (nssCa) records provide a robust proxy for continental dust input, and tend to exhibit well-marked spring maxima in Greenland (Hammer, 1977). Maxima and minima in these tracers are used to estimate seasonal deposition of ice samples, to assess any seasonal variability in PGEs or REEs.

Concentrations of Ir do not appear to exhibit a clear seasonal signal, though approximately annual peaks are observed in the later part of the record (1922-1926), where measured uncertainty is highest. Pt, Hf and Lu do not appear to exhibit seasonal signals at any point in their respective records. It is worth noting that significant peaks in Hf and Lu concentrations (most notably in mid- 1916 and mid-1922) coincide with similar peaks in Ir and

amplified uncertainty in Pt, suggesting that the PGE records might be suffering from lingering artifacts in oxide interferences for these particular samples.

In analytical Rounds 2-4, before methods were finalized, average concentrations in ice for Ir averaged 0.706 fg/g ppt (SD: 0.905 fg/g) , which shifted up to 1.10 fg/g (SD: 1.10 fg/g) in Round 5 and settled at 0.479 fg/g (SD: 0.431 fg/g) in Round 6. Pt concentrations began at 18.6 fg/g (SD: 14.6 fg/g) in Rounds 2 - 4, shifted to 8.90 fg/g (SD: 13.8 fg/g) in Round 5, and settled at 19.6 fg/g (SD: 12.1 fg/g) in Round 6. Based on the methodological improvements discussed in the methods section, ONLY analytical Round 6 (covering a span of 3+ years) should be trusted as the most accurate estimate of "background" concentrations in the measured ice samples. In this collection of background samples, the mean Ir uncertainty (0.22 fg/g, 45.9% of the mean concentration, range: 0.0953 – 0.502 fg/g) was small compared to the sample range. Mean Pt uncertainty (3.98 fg/g, 20.3% of the mean concentration, uncertainty range: 1.93– 12.37 fg/g) was also small compared to the sample range. The only sample in this period with notably large uncertainties is 1918 Q1, though they are not larger than the variability of the record itself. A further illustration of sample averages for different periods, record variability and uncertainty values is provided in **Table 1.2**.

1.4.2 *Tambora Time Period, 1813- 1818*

Volcanic signals in the ice core were traced using a particulate content index (measured in ppm of dust equivalent between the size ranges of 0.8 to 10 µm, calculated assuming a spherical particle shape and density of 2.65 g/cm^3) and non-sea salt sulfur (nssS). Sulfur compounds commonly emitted in volcanic eruptions, notably SO_2 and SO_4, have previously been

used to identify the Tambora reference layer in Greenland ice (Melott et al., 2010). Our sample measurements record a brief, synchronous spike in both tracers precisely at the time of the eruption in April, 1815. The record also reveals a much larger, delayed nssS signal that spans a significantly longer period, lasting from early 1816 to mid 1817. Other high resolution Greenland ice core records exhibit a similar initial spike in SO_4 that does not greatly exceed seasonal variability, and a delayed primary signal from 1816 through 1817 (Cole-Dai et al., 1997; Dai et al., 1991; Oppenheimer, 2003). The initial small peak that coincides with particulate content may represent deposition of larger, heavier particles in the days following the eruption, while the lagged primary signal likely represents deposition of smaller sulfate aerosol particles that that were injected to the stratosphere at the time of the eruption, and slowly mixed back into the troposphere over the following years.

Of the PGE and REE species, Pt alone displays a convincing peak that may correlate to the eruption (**Figure 1.9,** and normalized to terrestrial tracers in **Figure 1.10**). The sample spanning the third quarter of 1815 records a maximum Pt concentration of 38 fg/g, 271% of the preceding samples from 1814. The same sample also records a modest peak in Ir of 0.538 fg/g, which is only 225% of samples preceding it. The PGE peaks occur approximately halfway between the initial spike in particulate content and nssS, and the larger, delayed nssS peak. REEs do not display a similar signal at this time, but their signals do resemble the second nssS peak beginning in 1816. Hf in particular rises dramatically at this time, elevating to 280% of preceding concentrations.

Because samples were deliberately cut to represent equal periods of time, Ir and Pt flux records (**Figure 1.14**) are quite analogous to concentration records. Ir flux during this period

ranges from 3.06-13.7 fg $cm^{-2}a^{-1}$, whereas Pt flux ranges from 159.35- 766.0 fg $cm^{-2}a^{-1}$. Very low Ir/Pt mass ratios persist through the record, averaging 0.019 (SD = 0.008).

1.4.3 Tunguska Time Period, 1906 - 1911

Very few tracers recorded any significant excursions synchronous with the Tunguska Impact of 1908 (**Figure 1.11** and **Figure 1.12**). Ammonium (NH_4) appears to be very slightly perturbed from the normal annual signal right around the time the Tunguska impactor landed in Siberia (June, 1908). Though this perturbation (near 0.8 µM) serves as a peak in the 1906-1911 record, it is not particularly high compared to our entire NH_4 record (which spans 1896-1926 and reaches a peak of 1.601 µM). This is not the first time an ammonium perturbation was observed during this period: (Melott et al., 2010) records a very abrupt and very large NH_4 peak from late 1908-1909 in a GISP2 core (also located at Summit, Greenland). None of the PGEs or REEs indicate a perturbation coinciding with this NH_4 peak. In fact, REEs are noticeably flat during this period, as is Ir. Pt appears to record an excursion within 6 months before the event, displaying a peak with 224% the concentration of surrounding samples. It is possible this excursion records the impact event within age uncertainty of the samples, but unlikely given the precision of layer counting at this depth.

Ir fluxes for this period span a broader range than the Tambora period, recording values between 0.70-29.79 fg $cm^{-2}a^{-1}$, while Pt fluxes record 161.65-789.3 fg $cm^{-2}a^{-1}$. Ir/Pt ratios are comparable to the Tambora period but exhibit greater variance, averaging 0.019 (SD = 0.016). **Figure 1.13** depicts histogram distributions of all Hf, Lu, Pt and Ir concentrations measured throughout the entire study: Hf peaks in the 1.7 x 104 – 3.3 x 104 fg/g window, Lu peaks in the

83.9-109.9 fg/g window, Pt peaks in the 11.4-14.1 fg/g window, and Ir peaks in the 0.13-0.24 fg/g window.

1.4.4 *Strong vs. Weak Acid Digestion Comparison*

Procedural error during blank preparation for digestion comparison experiments, illustrated in **Figure 1.15** , introduced unintended Ir contamination, resulting in large uncertainties in Ir comparisons. REE and Pt comparisons were largely unaffected by this laboratory error. Strong digestions reported higher concentrations for 10/12 Hf replicates, 11/12 Lu replicates, 10/ 12 Pt replicates and 9/12 Ir replicates. The relative difference between strong and weak digestion concentrations spans a broad range for all species. Strong digests are on average 41.7% higher for Lu (SD = 25.3%), 44.2% higher for Hf (SD = 42.8%), and 45.4% higher for Pt (SD = 35.1%). In Pt, the relative difference between digests range from -8.34% (higher for weak digest) to 92.7% (higher for strong digest). Ir comparisons are difficult due to the large uncertainties, but 9 samples record 91.0% (SD = 20.6%) higher average concentrations in strong digests. The other 3 samples record 72.5% higher concentrations on average in weak digests.

There does not appear to be a strong difference between 1% HNO3 digestion and 50% HNO_3 digestion methods, based on a small sample size (8 vs 4 samples, respectively). Among PGEs, samples that record higher concentrations in weak digests are not the same: weak digests record higher Pt concentrations in 1825 and 1833, but higher Ir concentrations in 1827, 1828, and 1835. REE's are more comparable: weak digests record slightly higher Hf concentrations in 1830 and 1835, and barely slightly higher Lu concentrations in 1835 (In 1830, strong and weak digestions are almost identical for Lu).

1.5 DISCUSSION

1.5.1 Background Seasonality of PGEs in Polar Ice

Seasonal variability in extraterrestrial PGE deposition to ice sheets is possible, though not necessarily likely. Atmospheric models based on satellite measurements and ground-based LiDAR indicate that density of neutral metal atom and ion layers of Na and Fe at 85-105 km altitude (which are formed from the ablation of meteors, and representative of MSP parental material) vary considerably with season at high latitudes. Both metal layers indicate a clear minimum density profile near the summer solstice, followed by a 3x increase near the winter solstice at high latitudes, largely attributed to seasonal temperatures that change O_3 reservoirs available for chemical reactions and condensation rate of polar mesospheric clouds (Fan et al., 2007; Gardner et al., 2011). The assertion by Gabrielli et al (2004) that seasonal MSPs are concentrated in polar regions due to mesospheric circulation from summer pole to winter pole implies a similar winter concentration of MSPs in the stratosphere. Actual *deposition* onto ice sheets may not occur until spring or early summer, when tropopause folding events exchange air from the stratosphere to the troposphere (Hsu et al., 2005). Whether or not this tropopause folding occurs in time to mix elevated concentrated winter MSPs from the stratosphere remains unclear. Furthermore, any potential terrestrial source of PGEs would likely maximize in late winter and early spring months, closely following the Ca record of terrestrial dust input. Larger IDPs probably exhibit no seasonal pattern because they spend so little time in the atmosphere and enter at an approximately constant rate. If any seasonal pattern exists in PGE deposition

(from MSP or terrestrial sources), it is not unreasonable to predict peak distribution anywhere between mid-winter and early summer.

High resolution measurements from ice cores in previous studies do not appear to record obvious seasonal signals in PGEs (Gabrielli et al., 2008), though a slight Ir uptick in spring and summer may exist. Our measurements of Ir and Pt during seasonal background periods similarly indicate that there is no clear seasonal pattern to PGE deposition, within measurement constraints. No correlation whatsoever (positive or negative) exists between Ir or Pt values and corresponding Ca values, which are known to record clear seasonal patterns (which also indicates minimal terrestrial contribution of PGEs in our records). However, we recognize that seasonal signals are difficult to observe given the resolution of our measurements (4 measurements per year). Between the years 1922 and 1926 (which have the largest measurement uncertainties) the highest Ir concentration by far is always recorded in either the 2nd or 3rd quarter of the year. This pattern exists, though muted, from 1918-1922 and 1916 as well. Plotted together in **Figure 1.16**, samples through the entire study period record a slightly higher mean Ir concentration in spring and summer quarters (0.77 fg/g and 0.75 fg/g, respectively) than in winter and fall quarters (0.28 fg/g and 0.48 fg/g, respectively). Pt concentrations remain relatively stable throughout the year (16.5 fg/g in winter, 17.3 fg/g in spring, 16.2 fg/g in summer and 19.1 fg/g in fall). Individual years also indicate greater summer deposition of Ir than winter deposition for 9 of 12 years (**Figure 1.17**). The overall picture here indicates that if any seasonal signal is present in the seasonal records, spring and summer quarters exhibit slightly amplified Ir deposition. These patterns do not exist in the Pt record, which displays far more erratic behavior, potentially as a result of large uncertainties produced during early method development.

Gabrielli et al. (2008) Pt and Ir signals from Greenland snowpits exhibit behavior remarkably similar to ours in a record that spans a shorter time period (1991-1994) at a higher resolution (~12 measurements per year). They record highly variable background concentrations of Ir and Pt that rise mainly in summer periods. However, the atmosphere at this time was heavily influenced by the large eruption of Mt. Pinatubo in 1991, so this summer deposition may not be measuring a true "background" signal of PGEs. Excluding 1993 and 1991 summer measurements from the record (when the volcanic PGE signal is assumed to be highest), Ir and Pt exhibit minimal seasonal variability in their data, much like our record. Ir/Pt ratios on the other hand, do show higher values during summer periods. However, a study of source region air masses during the period indicate a potential large anthropogenic input from highly industrialized Eurasian regions (Kahl et al., 1997), potentially interfering with their signal. Our record (1920's) likely came before significant anthropogenic sources of PGEs existed. Despite data from our study and Gabrielli et al. (2008) hinting at amplified spring and summer signals, both studies have clear limitations from sample resolution and volcanic and anthropogenic contamination, respectively. Further research is necessary to accurately constrain the natural seasonal variability of PGE deposition in ice.

1.5.2 *PGEs as Volcanic Tracers*

We conclude that a moderate peak of Pt (38 fg/g) , and small jump in Ir (0.54 fg/g) concentrations in the second half of 1815 represent deposition of fallout material from the Tambora eruption of 1815 (VEI = 7) based on the following lines of evidence: (1) The magnitude of measured concentrations in 1815 Q3 sample (depth 66.79 - 66.85 m) represent 271% and 225% the preceding background signals for Pt and Ir, respectively. (2) The timing of this major Pt

peak lies directly between spikes in other volcanic tracers: an initial spike in S and particulate content at 1814.24 (depths 66.87-66.95m), and a delayed, long lasting peak in S from 1815.93-1817.92 (depths 66.75 - 66.35 m). (3) Smaller, secondary spikes from Pt and Ir, as well as pronounced peaks in REE elements in 1816 Q2 sample (depth 66.61 - 66.67 m) overlap with the delayed S signal. (4) No change in ice accumulation rate is observed in samples with elevated PGE concentrations, ruling out amplified wet deposition or reduced accumulation as explanations for these signatures.

The small magnitude of PGE spikes, particularly in Ir, is somewhat unexpected given the enormity of the eruption event. Gabrielli et al. (2008) records volcanic fallout from the Hekla 1991 stratovolcano eruption in Summit snowpits, measuring an Ir peak of 30 fg/g and a Pt peak of 59 fg/g , each representing 2307% and 1639% of preceding background signals, respectively. While the Icelandic eruption had a low VEI of 3, its much closer proximity to Summit, Greenland (~1300 km) within the same polar vortex as the depositional environment, likely led to a much stronger signal. However, it is critical to compare the eruptions based on their respective tectonic settings. Hekla is a mid-ocean ridge volcano that sits on a divergent boundary, indicating that a greater proportion of its source material was likely from the upper mantle. Tambora is a stratovolcano that sits on a convergent boundary, which means that a greater portion of its source material was from recycled crustal slab material. The relative siderophile enrichment of the upper mantle, compared to the siderophile-depleted continental crust (Arculus & Delano, 1981), would predict greater proportion of Ir and Pt emissions from a Hekla eruption than from a Tambora eruption. A notable similarity between their Hekla record our Tambora record is the presence of a robust Pt signal (spanning ~4 samples) and a short-lived Ir signal (in a single sample).

Perhaps a better analog to the 1815 Tambora eruption, both in geographic and tectonic setting, was the similarly distant (>10,000 km) Pinatubo eruption of 1991 in the Philippines (Stratovolcano, VEI = 6). Gabrielli et al. (2008) attribute the multi-year atmospheric perturbation from this eruption to amplified deposition of PGEs in summer, 1993 snowpit samples. Peak concentrations in summer snow reach 8.7 fg/g Ir and 9.5 fg/g Pt, representing 669% and 264% of preceding background concentrations, respectively. These relative increases in concentration are much closer to those we observe in Tambora ice samples. There is also a notable lag between the eruption (June, 1991) and the peak signal (Summer, 1993), though it is much longer than our observed lag (April, 1815 eruption – 1815 Q3 peak signal). Direct comparison of fallout signals and their respective atmospheric transport conditions is difficult due to the limited volcanic observation technology available in 1815. Measurable differences between the eruptions include their respective VEIs, latitude positions (Tambora: 8.3°S, Pinatubo: 15.1°N), and Northern Hemisphere temperature anomalies attributed to each eruption, estimated from boreal tree ring properties (Tambora: -0.51°C, Pinatubo: -0.30°C; (Briffa et al., 1998) This comparison may also be flawed because the referenced snowpit samples may be recording a significant anthropogenic signal. Gabrielli et al. (2008) note that their median snowpit values of Ir and Pt concentrations are a factor of 5 and 8 higher than Holocene ice (Gabrielle et al., 2004), respectively.

The only other reference for comparison of volcanic aerosol fallout comes from Soyol-Erdene et al. (2011) PGE records in East Antarctic snowpits, which over a 50 year span incorporate several volcanic perturbations. While none of the recorded eruptions exceed a VEI of 5, the relative magnitude of their peak/background signals are quite similar to ours (**Table 1.3**). Using the same 1% nitric acid method established by Gabrielli et al.(2004) they record peak/background

signals from Cerro Hudson, 1991 (727% Ir, 156% Pt), El Chichon, 1982 (121% Pt), Ngauruhoe, 1974 (197% Pt), Deception Island, 1967 (127% Ir, 419% Pt), and Agung, 1963 (309% Ir, 342% Pt). Temporal resolution is not sufficient to precisely gauge the timing of each signal with respect to eruption events. While most of these eruptions take place with much closer proximity to the depositional (Antarctic) environment, the magnitude of their peak signals compared to preceding background signals is comparable to those measured through Tambora in Summit.

Volcanic aerosol emissions are relatively well constrained for Hawaiian hotspot volcanoes like Kilauea (Zoller et al., 1983), Indian Ocean hotspot volcanoes like Piton de la Fournaise (Toutain & Meyer, 1989), and Plinean Kamchatkan eruptions (Felitsyn & Vaganov, 1988), among others. Volcanic Ir and Pt anomalies appear characteristic in a number of polar (Gabrielli et al., 2008, Soyol-Erdene et al., 2011) and sedimentary (Tankersley et al., 2018) archives, but further investigation of PGE content and mass ratios in volcanic aerosols would help to quantify their volcanic budgets. Though a difficult undertaking, it might provide another chronostratigraphic tool in archives with otherwise limited chronometric control.

1.5.3 PGEs as Impact Tracers

Ice measurements indicate no PGE response to the Tambora impact of 1908. Given the modeled size of the impactor, a strong signal might not necessarily be expected for this event, but the infrequent nature of impact events means there is scarce opportunity to measure these impact tracers elsewhere. The only tracer that may be recording a response in the ice core is NH_4, which displays a very subtle excursion (>0.7µM, seasonal peaks rarely breached 0.45µM in this timeframe, but elsewhere in the core reach as high as 1.6 µM). A controversial Melott et al.

(2010) study records a much larger NH_4 spike in the GISP2 ice core in late 1908-early 1909. The relative magnitude of this excursion appears to be much greater (approaching 200 ppb concentration, compared to a background of <10ppb) than ours. They attribute a minor portion of this NH_4 excursion to biomass burning of boreal forests resulting from the Tunguska impact, but theorize that most of it is due to an analogue of the Haber process (combining nitrogen and hydrogen under high pressure) which may have occurred in the shock front of a water-bearing impactor (in this case, a comet). It is worth noting they also observe a similar, significant NH_4 spike at the onset of the Younger Dryas.

Other studies have also not found Ir excursions during the Tunguska event. (K. L. Rasmussen et al., 1995) used neutron activation analysis to measure dust layers in shallow Greenland ice cores, with no deviation from background variability recorded around 1815. Based on the combined estimates of the energy released during the impact and mechanisms of atmospheric transport, Rasmussen suggests the absence of Ir anomalies in Greenland implies either an impactor of relatively low Ir content, or one with a high geocentric velocity. Later measurements by (K. L. Rasmussen et al., 1999) from peat cores at the Tunguska impact site predict an impactor with high C/Ir content, consistent with a cometary like object rather than an asteroid like object. Eyewitness reports following the impact event indicate the likely presence of noctilucent clouds that induced “bright night skies” in the days following the impact. (Kelley et al., 2009) liken these clouds to those produced by space shuttle water vapor plumes of 2003 and 2005, suggesting a likely cometary body for the 1908 impact event. The absence of an Ir anomaly in our data distal from impact location, missing crater and possibly achondritic composition of the impactor generally support the hypothesis of a cometary body triggering an air blast at the

impact site. A stony meteorite entering at low velocity or an oblique angle, preventing the injection large amounts of ablated material into the stratosphere, is also a consistent possible cause of the event.

The proposed impact at the onset of the Younger Dryas shares many of the perplexing qualities of the Tunguska impact event. As of yet no impact crater is connected to the onset of the period, the hypothetical composition of the impactor appears achondritic with low Ir (Petaev et al., 2013), and an anomalous NH_4 values are recorded in Greenland ice cores. While our results do little to support or deny the findings of Petaev et al. (2013), they indicate that the aggressive digestion methods they used are viable, and that the very high Pt concentrations they record are striking in magnitude. Considering our laboratory setting suffers from far less environmental control than theirs, it is fair to say that the elevated Pt levels they record (in 5 adjacent samples) are likely not the result of accidental contamination. A further investigation of Greenland ice during the Younger Dryas transition should be conducted using aggressive HF digestion methods, which we have found to be more than adequate for this type of measurement. Replicate measurements over the YD transition and further atmospheric entry modeling of the unusual Tunguska impactor could help further assess the controversial YD impact theory, and better constrain the perturbations impact events have on global PGE budgets.

1.5.4 Strong vs. Weak Digestion Methods & Implications for MSP Formation

Greater PGE concentrations among samples that underwent strong digestion procedures using Petaev et al. (2013) methods compared to Gabrielli et al. (2004) methods support the assertion by Petaev et al. that previous methods did not capture the entire PGE signal. The

magnitude of the discrepancy between our samples, however, is not sufficient to explain their astonishing PGE concentrations, which even during background periods tend to be at least 10x greater than those found in any other ice samples (**Table 1.4**). A contributing factor may be that Petaev et al. samples incorporate greater proportions of terrestrial dust. Based on GISP2 records from Summit, our depth range (~40-70 m) has 1.2 - 30 µg/kg of Ca^{2+}, whereas samples from the Petaev. Depth range (1709-1720m) has ~20 - 100+ µg/kg of Ca^{2+} (Mayewski, 1999). In theory, the weak 1% HNO_3 digestion should target only MSPs and small volcanic aerosols that require little to no chemical breakdown compared to larger IDPs and terrestrial dust particles. In contrast, the strong HF + HNO_3 digestion, followed by suspension in aqua regia is targeted at breaking down silicate minerals, recording a signal that includes PGES from MSPs, larger micrometeorites and all terrestrial dust. Based on results from their respective studies, this seemed true to an inexplicable extent. During the LGA- Holocene transition (spanning the Younger Dryas) Gabrielli et al. (2004) records concentrations of Ir in the range of 0.1-5.0 fg/g and Pt in the range of 0.4-7.0 fg/g (terrestrial correction of ~2% for Ir and 7% for Pt), whereas through the same period, Petaev et al. (2013) recorded concentrations of Ir in the range of 22-137 fg/g Ir, and Pt in the range of 38-82,200 fg/g (without terrestrial correction). Direct comparison of these values would suggest that only about ~5.5% of Ir and ~0.7% of Pt in ice are either deposited by MSPs or volcanic aerosols of a similar size fraction, with the rest coming from larger terrestrial dust particles or IDPs and micrometeorites. Our direct comparison of the two methods from nearly identical ice samples, which yield very similar results (**Figure 1.15**), indicate the exact opposite, that most PGEs are deposited in the form of MSPs or volcanic aerosols.

Our understanding of IDP entry processes and terrestrial PGE abundance, along with the results from this study, indicate that those inputs to the ice reservoir are highly unlikely. Terrestrial dust PGE corrections are negligible for the Petaev et al. record (based on their Al measurements, and crustal abundances of 8.23 $x10^{-4}$ ppm for Al, 5 $x10^{-4}$ ppm for Pt and 1 $x10^{-4}$ ppm for Ir; Haynes et al., 2016), indicating that the vast majority of their measured PGEs are extraterrestrial in origin. If that is the case, then it suggests over 90% of the PGEs deposited on Greenland during this time were in the form of large IDPs, and less than 10% were deposited as MSPs. In contrast, atmospheric models and micrometeorite studies suggest that approximately 90% of IDP material is ablated upon entry (some of which re-condenses into MSPs), and only 10% of material survives as micrometeorites (Taylor et al., 1998; Vondrak et al., 2008). Our data fit this prediction more closely, though not perfectly. Weak digestions represent anywhere from 7% - 108% (mean: 54.6%) of the strong digestion signal for Pt, and excluding outliers and negative values, 2% - 239% (mean: 72.82%) of the strong digestion signal for Ir. Replicate measurements for samples with such low area•time products are inevitably subject to noise (theoretically it should be impossible for a weak digestion to yield a greater signal than a strong digestion when measuring truly identical samples), but the mean signal ratios we record indicate that at least a 50% of PGE signals are likely coming from small MSP or aerosol particles, rather than those bound within silicate minerals. The only way to improve this estimate is to perform more digestion comparison experiments on replicate samples of large volume, to reduce signal-to-noise ratio.

These results make the very high Petaev et al. PGE signals (both background and peak values) more perplexing. It is possible that slight differences in our methodologies, discussed in the *Methods* section, are responsible for the dramatic differences in our measured

concentrations. Perhaps our decision to digest samples for 3 days on a hotplate, rather than for 5 days and nights in an oven, did not allow for silicates to fully digest. It is critical to recognize that their samples span a notoriously dusty Younger Dryas climate interval (Mayewski et al., 1994) with up to 5-100x more terrestrial dust, so direct comparison between records is misleading. Their samples were also drilled a very long time ago (1992-1993) using drilling fluid, and were handled by members of other labs for laser dust measurements (Ram & Koenig, 1997), which are all possible sources of contamination. The wider body of scientific literature suggests that the background PGE concentrations they record, and the total IDP flux they necessitate, are much higher than others have predicted.

1.5.5 PGE Concentrations Compared to Other Ice Core Studies

Figure 1.18 and **Table 1.4** depict how the PGE concentrations recorded in this study compare to those from other ice core studies. Our measurements tend to fall in the range of those reported by other studies that used 1% HNO_3 digestions (Gabrielli et al., 2004, 2006, 2008, Soyol-Erdene et al., 2011). Other measurements from Summit, Greenland during the Holocene or modern period offer the best direct comparison. Our average Ir concentration of 0.40 fg/g (range: 0.027 - 3.79 fg/g) is quite similar to the 0.30 fg/g average (range: 0.1 - 0.58 fg/g) reported by Gabrielli et al. (2004) from Summit Holocene ice. Pt concentrations are not quite as similar, with our measurements averaging 15.7 fg/g (range: 6.78 - 15.78 fg/g) compared to their 0.6 fg/g average (range: 0.4 - 0.9 fg/g). Gabrielli et al. (2008) snowpit records from Summit likely suffer from anthropogenic input, but report averages of 1.60 fg/g Ir (range: 0.4 - 8.7 fg/g) and 5.6 fg/g (range: 2.5 – 90.0 fg/g). The general agreement between our measured concentrations those

reported from the same study site suggest that our methods are likely recording a reasonably accurate signal. The Petaev et al. (2013) record is also from Summit, but records dramatically higher concentrations, averaging 36 fg/g Ir (range: 22.0- 1 37 fg/g) and 419 fg/g Pt (range: 38 – 82,200 fg/g). A graphic comparison of our PGE results to selected Gabrielli and Petaev records is presented in **Figure 1.19**.

In theory, Ir and Pt mass ratios can assist in determining the origins of deposited PGEs, with values near or above chondritic values suggesting dominant extraterrestrial or explosive volcanic input. Two distinct categories seem to emerge when classifying reported Ir/Pt ratios from studies in **Table 1.4**: three that report Ir/Pt ratios near or above the chondritic ratio of 0.49 (Gabrielli et al., 2004, 2006, 2008), and three that report distinctly lower Pt/Ir ratios at or below the crustal ratios (Haynes et al., 2016) of ~0.1 - 0.2 (Soyol-Erdene et al., 2011, Petaev et al., 2013, and this study). Soyol-Erdene et al. report ratios between 0.002- 0.01 (mean: 0.008), we report ratios between 0.0018 – 0.058 (mean: 0.019) , and Petaev et al. reports ratios between 0.0007 – 0.76 (mean: 0.191), though their large Pt anomaly drives the lower range estimate down significantly). Petaev et al. data come from a notoriously dusty Younger Dryas climate interval (Mayewski et al., 1994), so their aggressive digestion procedure is likely picking up a dominant proportion of wind-blown terrestrial dust. An Ir/Pt ratio consistent with crustal ratios is unsurprising if most of the PGE-bearing material in their ice was in fact terrestrially sourced. It is also possible, based on these ratios and high Pt concentrations, that strong digestion methods may preferentially extract greater amounts of Pt than Ir, driving these ratios down, though a comparison of our strong and weak digestions report no difference in Ir/Pt ratios (both are 0.05 on average). It is important to recognize, however, that our ice is from a period of significantly

lower dust deposition (possibly by as much as 100x, Mayewski et al, 1994), so it is unlikely that a large portion our PGEs are from terrestrial dust. The methodological difference also does not explain the extremely low ratios reported by Soyol-Erdene in Antarctic snowpits. It is feasible that some studies record predominantly IDP signals, while others more heavily record volcanic signals. Soyol Erdene et al. (2011) , this study, and Gabrielli et al. (2008; albeit with likely anthropogenic input) deliberately measure during periods of known volcanic activity. New research on siderophile element abundance (including Ir and Pt) and Os isotopes from Hall's cave in Texas suggests that the Pt anomaly identified by Petaev et al. at the onset of the Younger Dryas is most likely volcanic in origin (Sun et al., 2020). If this is the case, volcanic portions of the PGE signal may be skewing towards lower Ir/Pt ratios in these particular records (though in the case of Soyol-Erdene at al. and this study, probably not by an enormous 0.4 or more). The cause of such variable Ir/Pt ratios measured in ice cores remains an open question. A better characterization of PGEs in the atmosphere and in volcanic emissions could help explain what controls these ratios in ice.

1.5.6 IDP Mass Flux Calculations in Context

Reported Ir concentrations and fluxes in ice core samples can be multiplied by chondritic Ir mass concentration (481 ppb; Anders & Grevesse, 1989) to estimate the total IDP mass flux to earth over measured time intervals. A selection of various IDP mass flux estimates is provided in **Table 1.5**. Estimates of IDP flux from measurements the very top or above Earth's atmosphere range from 10-270 (metric) tons/day. Estimates for the flux of these particles in the atmosphere, based primarily on telescope and satellite data, range from 5-104 tons per day. Estimates based on terrestrial collection vary considerably, ranging from 1.74 – 4,473 tons/day. However,

excluding the highest and lowest estimates (Petaev et al., 2013 and Soyol-Erdene et al., 2011 which are almost a factor of ~10 higher or lower than the nearest in terms of magnitude) and the record with known anthropogenic PGE input from Gabrielli et al. (2008), this range shrinks to 10.96- 217 tons per day, far more consistent with atmospheric and extraterrestrial predictions.

Precisely dated Ir records from this study were converted to fluxes, and multiplied by the meteoric mass ratio of Ir (481 ppb) to calculate the total mass of IDP material deposited on earth on an average day, which in our case returned 217 tons/day. Following the logic proposed by Gabrielli et al. (2004, 2006), which asserts that MSPs are not universally deposited, but amplified in the winter polar vortex by a factor of ~5, we divide our estimate by 5 to obtain a lower limit. Our calculated result thus ranges from 43.5 - 217 tons/day of IDP material deposited to the surface. This aligns quite well the Gabrielli et al. (2004) estimate from Summit Holocene ice: 38.35- 214 (±82) tons/day. It also falls comfortably between magnetic estimates from Greenland and Antarctic ice cores which report 175 ± 68 tons / day and 15 ± 5 tons/day respectively (Lanci & Kent, 2006, Lanci et al., 2007). Magnetic estimates are limited to just MSP size fractions, but due to the unique magnetic properties of MSPs, there is very little question as to where the signal originates, making them possibly the most accurate estimate of MSP abundance in ice. The compilation of fluxes also points towards a consistently higher IDP flux estimates from Greenland ice (this study included) than from Antarctic ice, which may hold important information regarding the atmospheric transport of MSPs and their wet and dry depositional processes. The similarities between our estimates and those from other physical methods gives confidence that our methods are detecting a relatively accurate signal of Ir, and that IDPs play a large role in the Earth's surface PGE budget.

1.5.7 Interpretation of REE Measurements

As previously noted in *Methods*, we record Hf concentrations in ice that surpass those recorded by Petaev et al. (2013). Their average reported Lu and Hf concentrations averaged 128fg/g ppt (range: 3 – 390 fg/g) and 974 (range: 200 – 3210 fg/g), respectively. Our study reports averages of 170 fg/g Lu (range: 50 – 817 ppt) and 43,800 ppt Hf (range: 6,210 – 269,570 fg/g). In comparison, our moderately high Lu and strikingly high Hf concentrations, paired with significantly lower PGE concentrations, made the oxide corrections in our study a significantly larger portion of the measured signal. LuO and HfO contributed to 70.88% of signal for Ir and 89.2% of signal for Pt, on average, compared to < 5% for both elements in the Petaev et al. study. Measured REE concentrations were not reported for Gabrielli et al. studies, but they report oxide interferences < 3% on measured PGEs (implying Hf concentrations rarely exceeded 5.0 ppt). The high abundance of Hf is particularly puzzling, considering that our samples were deposited well before industrial processes that may emit Hf (primarily commercial extraction of Zr) were developed. Laboratory or collection contamination of samples should not be entirely ruled out, our procedural blanks do little to control for any surficial contamination of ice when it was cut or transported. All samples were scraped thoroughly prior to melting with an acid-cleaned ceramic knife however, making this an unlikely source of Hf contamination. A critical variable might be the material of the knife itself: We used a WACOOL brand knife with a blade composed of ZrO_2. The chemistry of Hf and Zr are nearly identical, making them difficult to separate, and most natural Hf is present in Zr ores (Larsen et al., 1943). It is feasible that some Hf is present in our ZrO_2 blade, and our scraping procedure may have served to introduce excess Hf onto the surface

of ice samples. If nothing else, our REE records indicate that concentrations of Lu and Hf can be quite variable from archive to archive, and should always be reported alongside trace PGE measurements from ICP-MS instruments.

1.5.8 Assessment of Methods and Future Work

We believe the methods used in this study to be sound based on acceptable procedural blanks, the PGE concentrations and IDP flux estimates reported in the context of other studies and the similarities between our methods and other published work. This method, with a few minor improvements, could be used to measure Greenland ice samples that span the Younger Dryas boundary, in order to corroborate the unusual results presented by Petaev et al. (2013) and contribute to the debate surrounding the YD impact hypothesis. The first research priority should be to determine the origin of our elevated Hf values, and to eliminate the source of Hf contamination, if present. To further improve this method and continue performing ultra-trace level PGE analysis in ice cores, we suggest to test the following: 1) Performing all laboratory procedures in a class 1000 clean room or under a class 100 clean bench, to reduce any existing laboratory contamination, 2) conducting digestions in round-bottom digestion vessels to possibly improve sample yield (this study uses conical bottom digestion vessels), 3) extending the digestion period to 5 continuous days (overnight) to determine if full digestion is achieved 4) if permitted, using a stronger rinse solution (10% aqua regia) during ICP-MS analysis immediately after Hf standards and oxide-check solutions are measured, to prevent Hf cross contamination into samples, 5) standardizing the sample scraping technique (using a non-ceramic blade) to "chisel" away exactly 1 cm (or similar) of outermost ice edges without gloved handling, or melting

outer layers with Milli-Q and 6) adding Al or another terrestrial tracer to the pool of measured isotopes to better constrain terrestrial PGE input. Combining these improvements with the existing methods should produce future records with better confidence intervals and improved precision.

Future work should focus on improving our interpretation of Ir and Pt in ice cores and on Earth, to better constrain the relative inputs of IDPs (MSPs and micrometeorites), terrestrial dust, volcanic aerosols, and anthropogenic emissions. Efforts should be made to continue (strong vs. weak) digestion-comparison experiments on a greater number of very large ice samples to improve signal-to-noise ratio and provide more data to constrain MSP vs. micrometeorite deposition of IDP material in Earth's surface. In addition, further emphasis should be placed on finding a column chemistry technique that adequately separates REEs from PGEs in trace concentrations, to improve accuracy of measurements in Hf-rich samples. Constraining PGE abundance directly from volcanic emissions and aerosols could vastly improve our estimate of the volcanic PGE flux, which is currently very limited. All methods of IDP study in terrestrial archives, the atmosphere, and outer space should continue in order to narrow our constraints on the total IDP mass flux to Earth, which has important implications for our understanding of bioavailable Fe in the oceans, particles involved in the stratospheric O_3 cycle, as well as broader applications in in long distance space missions along with our knowledge of early solar system materials and the building blocks of our planet. Finally, continued research into PGEs in ice cores and other archives through known impact and volcanic events is necessary to develop these tracers as a widespread stratigraphic marker in archives that are otherwise challenging to interpret temporally.

1.6 SUMMARY & CONCLUSIONS

We have developed a method to measure total concentrations of Ir and Pt in ice core samples at the sub-ppq level using ICP-MS instrumentation at Oregon State University. This method was applied to precisely dated ice core samples from Summit, Greenland to produce seasonal-resolution records of PGEs that span the Tambora volcanic eruption of 1815, and the Tunguska impact event of 1908. The Pt signal appears to record a clear response to the Tambora eruption, with concentrations rising to 271% of preceding background levels (225% for Ir) shortly after the event. No other significant PGE signal was detected during or after these events, and no particular seasonal signal was identified in these records. A very subtle NH_4 spike was recorded around the time of the Tunguska impact, which could potentially be attributed to an analogue of the Haber process, caused by the extreme temperature and pressure caused by a water- bearing (cometary) impactor's atmospheric entry. A comparison of 2 established digestion methods (1% HNO_3 suspension vs. concentrated HF + HNO_3) likely indicates that over 50% of extraterrestrial Pt and Ir are deposited in the form of nano-meter sized meteoric smoke particles, as opposed to larger micrometeorites.

Our samples contained Lu and Hf in very high abundance compared other studies and compared to PGEs, which could not be removed using established column chemistry techniques. As a result, PGE measurements suffered from large oxide interference mass corrections caused by the production of LuO and HfO during analysis, resulting in larger than anticipated calculated uncertainties. Nonetheless our Ir and Pt concentration measurements across all samples, averaging 0.4 fg/g and 15.7 fg/g, respectively, fall well within the range of those recorded in other

ice core studies. Furthermore, our estimate of Earth's IDP mass flux (based on Ir measurements) of 43.5 - 217 tons/ day depending on depositional processes, is very similar to those reported by other studies using satellite, radar, and terrestrial collection methods. The study on which our methods were based (Petaev et al., 2013) records an anomalous spike in Pt during the onset of the Younger Dryas, which they attribute to a Pt-rich impactor. We propose the methods we employed here (with some modification) be used to replicate measurements over the same period, to further assess the validity of their unusually high PGE measurements, and the wider validity of the Younger Dryas impact hypothesis.

FIGURES & TABLES

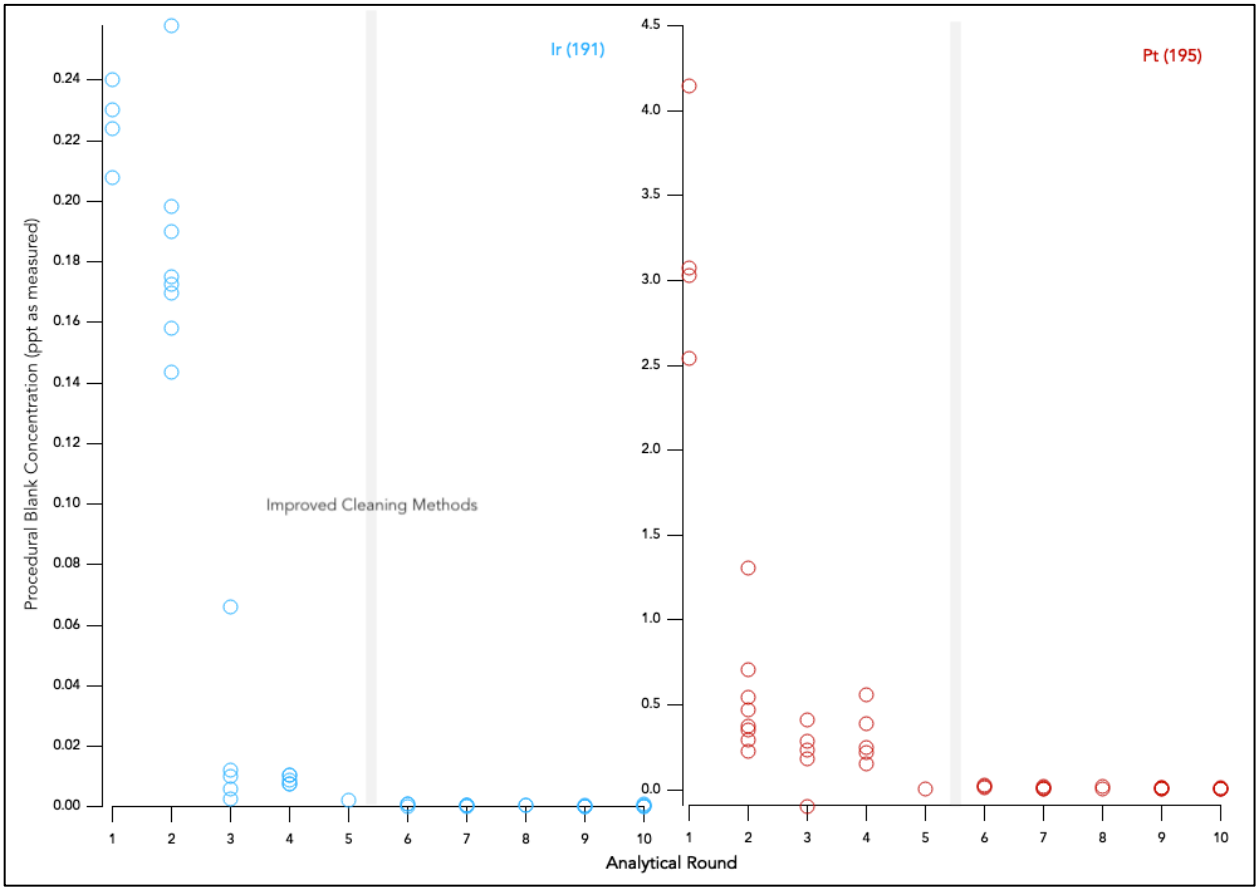

Figure 1.1: Procedural blank concentrations of Ir (left) and Pt (right) in ppt for each individual analytical round (concentrations reported in solutions measured, not digestion products). Each analytical round represents a separate date of ICP-MS measurement. We attribute reduction of procedural blanks in round 3 to the addition of a laminar flow hood during sample dry down post-digestion. We attribute reduction of blanks in round 5 to the addition of HF acid in analytical solutions and longer, stronger washing procedures of ICP-MS autosampler between samples. In round 6, new Teflon cleaning methods were introduced (See "Reducing Blanks & Teflon Digestion Vessel Cleaning Procedures).

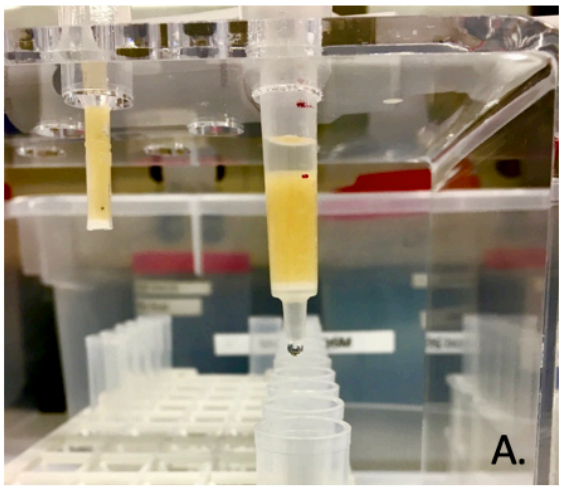

Tube #	Acid	Volume (mL)	Purpose
-	-	0.5	Load resin
-	6M HCl	0.5 x 3	Clean resin
-	MQ	0.5 x 3	Condition resin
-	0.5 M HCl	1 x 2	Condition resin
1	0.5 M HCl + sample	Sample + 935uL	Load sample
2	0.5 M HCl	1mL	Rinse sample teflon
			Rinse sample teflon
			PGE's
3		1mL	
4	1 M HCl	1mL	
5		1mL	
6	2M HCl	1mL	
7		1mL	
8	3M HCl	1mL	
9		1mL	

With column volumes: 0.5 cc & 0.25 cc
Total of 18 tubes.

B.

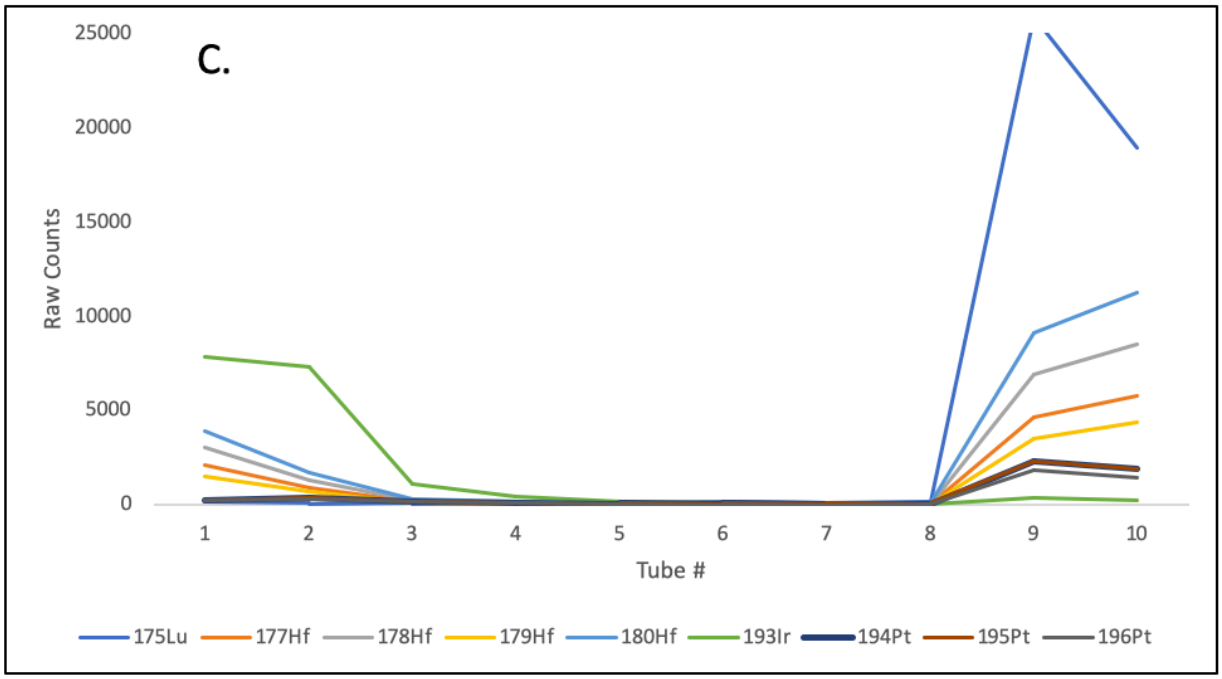

Figure 1.2: A. cation exchange columns were tested using "dummy" solutions to determine if columns were capable of removing Hf and Lu from samples. B. Column chemistry "recipe": first resin is loaded, cleaned, and conditioned. Subsequent steps ("tube #") begin when the sample is added, and progressively stronger acids are used to rinse materials through the resin. Tubes 3-9 introduced strong HCl acid to the column, with the intention to flush all remaining ions from the column. C. Real time measurements of sample collections from each tube were measured as they came off the column. Results indicate that while Ir comes off the column almost completely in the first 4 steps, most of the Pt only comes off with REEs during a 3M HCl rinse.

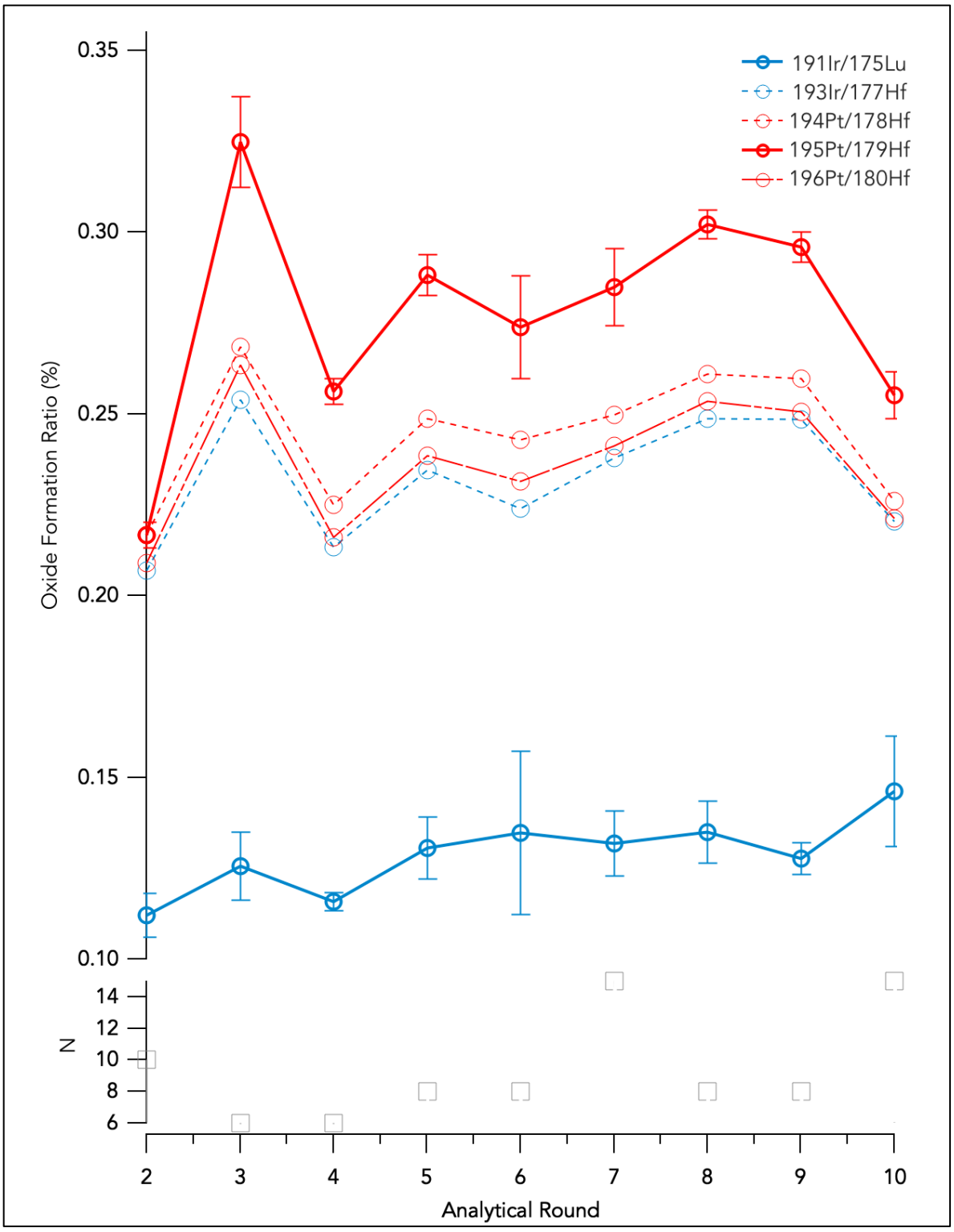

Figure 1.3: % of oxide interferences formed by a 2.5ppt Lu, 250ppt Hf "oxide check" solution in each analytical round. N represents the number of times the oxide check solution was run on a given day (sample size). Ir-191 and Pt-195 were used to calculate Ir and Pt concentrations in ice samples.

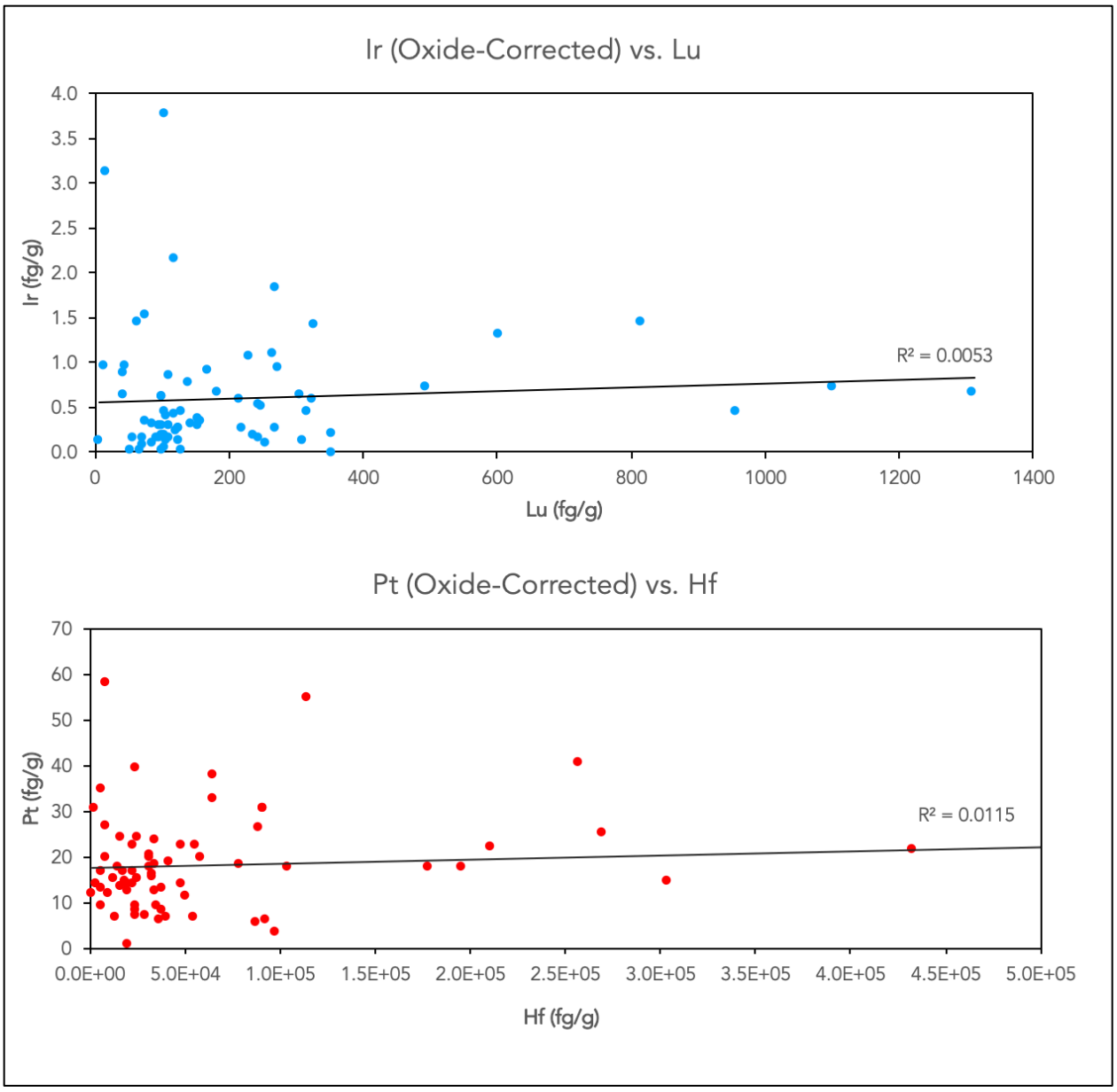

Figure 1.4: Scatterplots of oxide-corrected PGE measurements and accompanying measurements from interfering REE species. No correlation between corrected Ir and Lu measurements or Pt and Hf measurements indicate that oxide corrections adequately remove oxide interferences from raw data produced by the mass spectrometer.

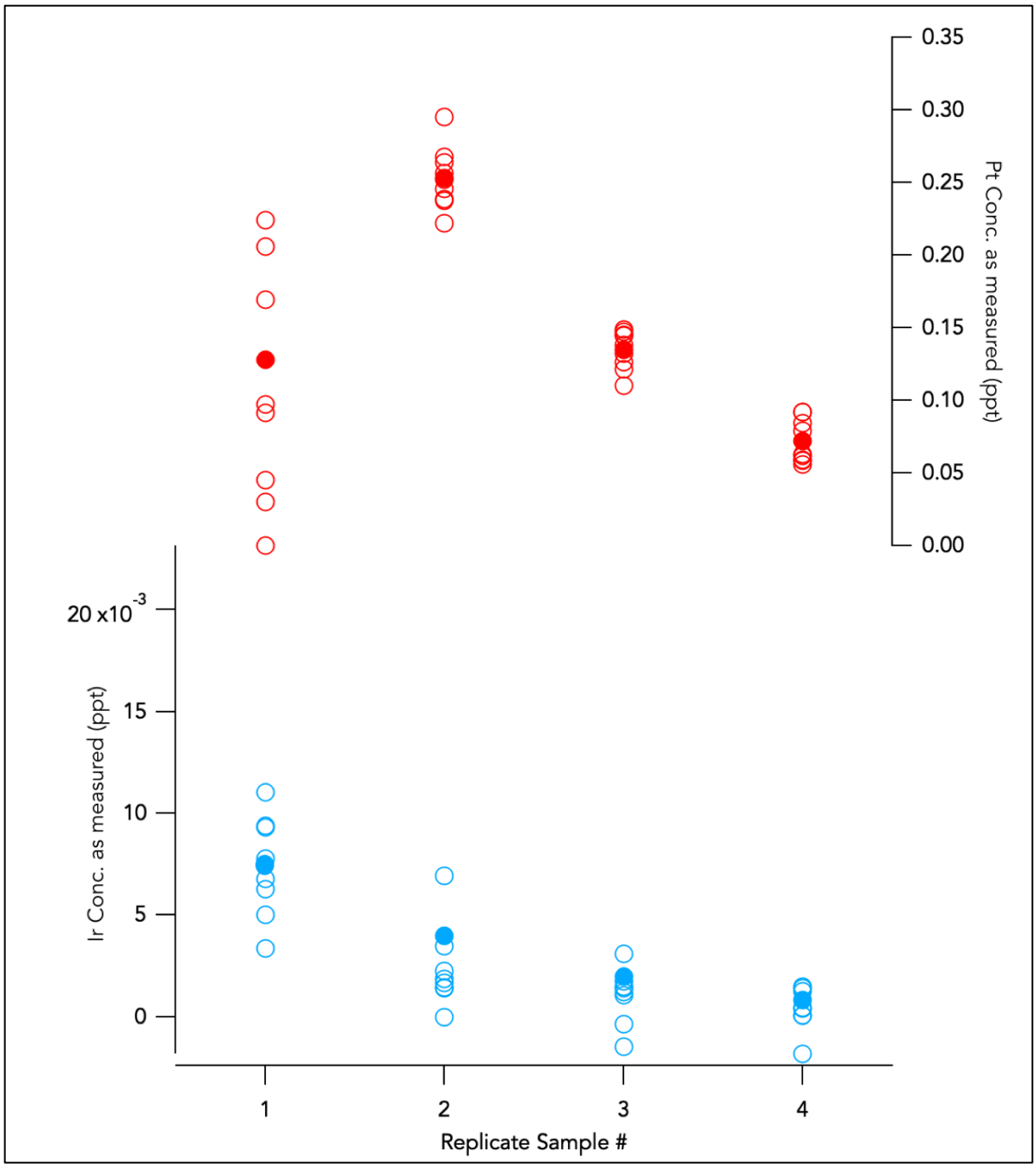

Figure 1.5: 4 digested samples (1917 Q4, 1917 Q3, 1919 Q2, and 1918 Q3) were preserved and measured in every analytical round to in an attempt to determine small signal reproducibility. Open circles represent individual remeasurements of the sample, and closed circles represent the mean from all measured rounds. % Relative standard deviations from measurements are represented in Table 1.

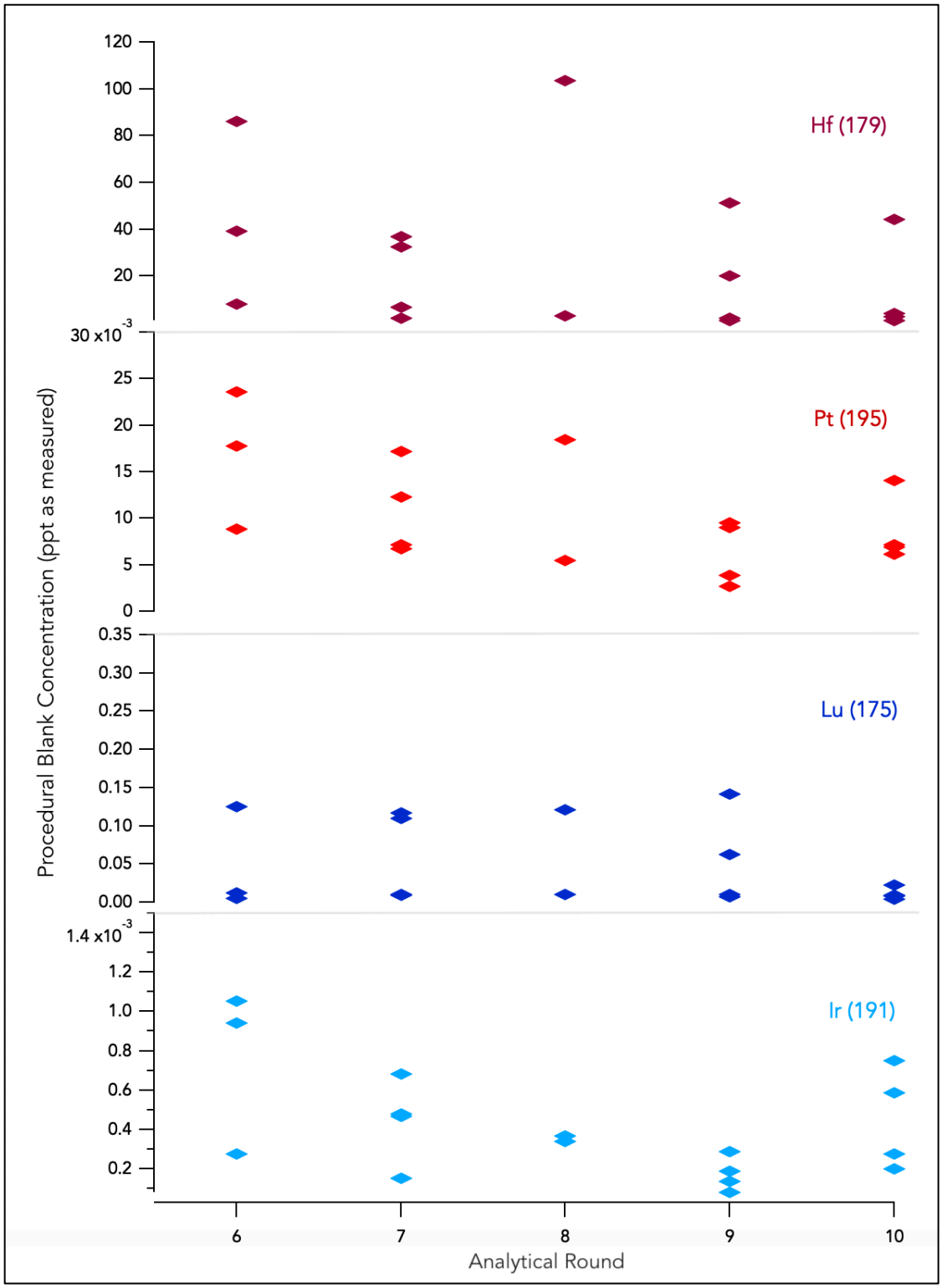

Figure 1.6: Procedural blank measurements remained low, with low variability once laboratory and analytical methods were finalized in analytical rounds 6-10. All Tambora, Tunguska, and digest comparison samples were analyzed in round 6 or later.

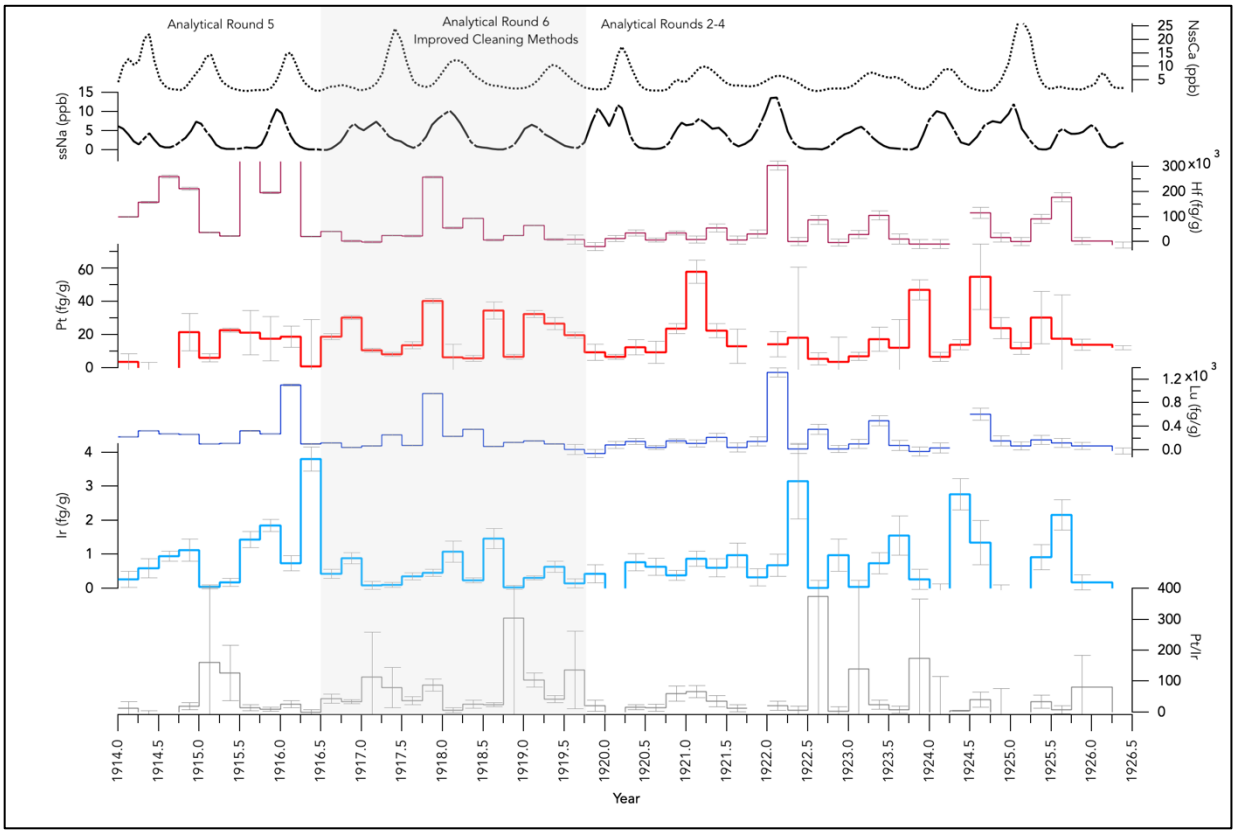

Figure 1.7: Seasonal background signals among Na, Ca, Hf, Pt, Lu and Pt from Summit ice. No clear seasonal signal is observed in REEs or PGEs. Samples from 1920-1926 were measured first in analytical rounds 2-4 and they have the largest error bars. Samples from 1914-1916.5 were processed in analytical round 5, when analytical methods were altered, resulting in reduced uncertainties. Samples from 1916.5-1919.5 were measured in round 6, once finalized Teflon cleaning methods were introduced, resulting in the smallest calculated uncertainties. Methods from this round were maintained throughout the remainder of the project.

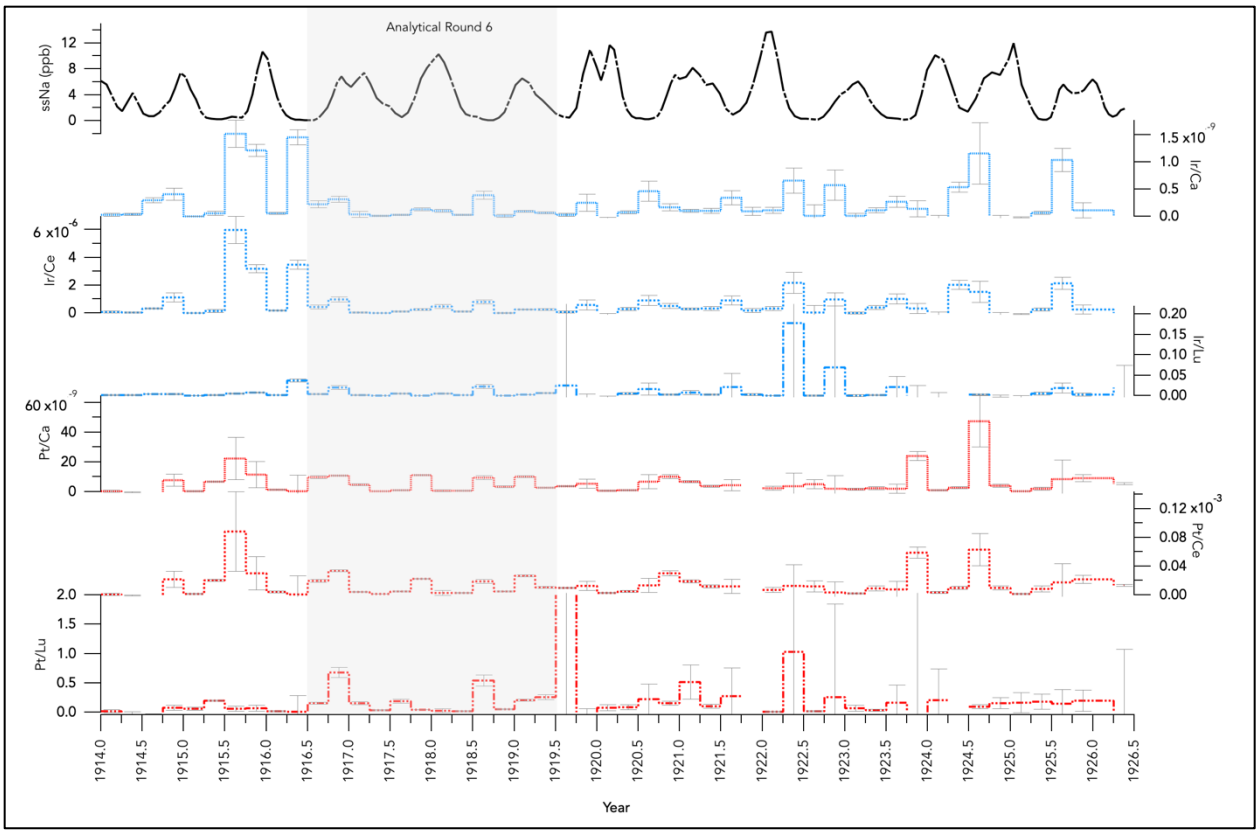

Figure 1.8: Seasonal background signals of Ir and Pt normalized to Ca, Ce, and Lu records (intended to track terrestrial dust signals). Seasonal Ca and Ce records were derived from continuous flow measurements performed at DRI. The normalized records indicate no clear seasonal signal in extraterrestrial PGE deposition.

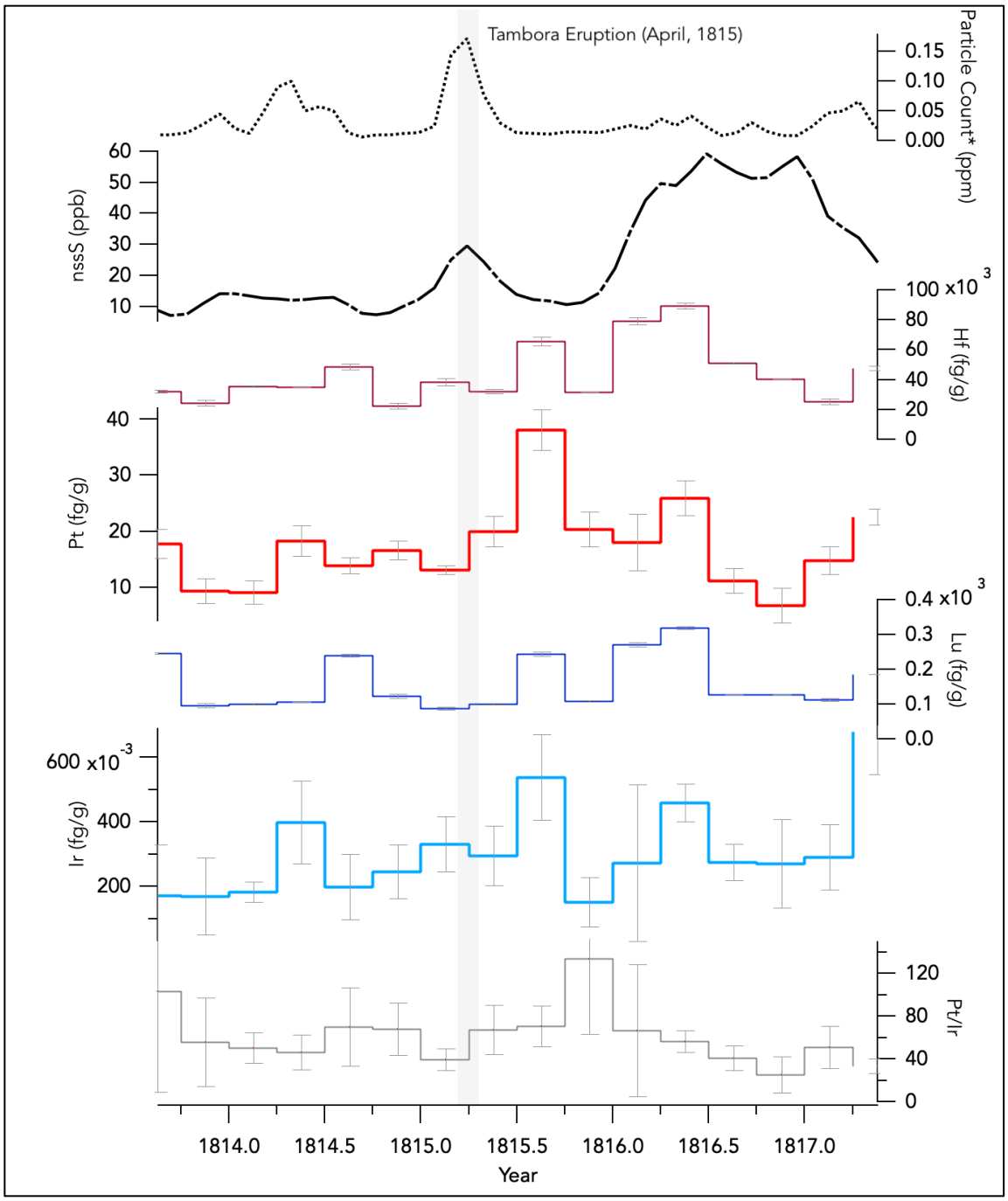

Figure 1.9: Summit ice records of particulate content, S, Hf, Pt, Lu and Ir across the Tambora eruption of 1815 (precise timing of the event is marked). Particulate content jumps immediately during the event. Sulfur experiences a small immediate jump, followed by a larger, delayed peak 1.5 years later. Pt exhibits a clear maximum within a year of the event. Ir displays a much smaller potential peak within a year of the event.

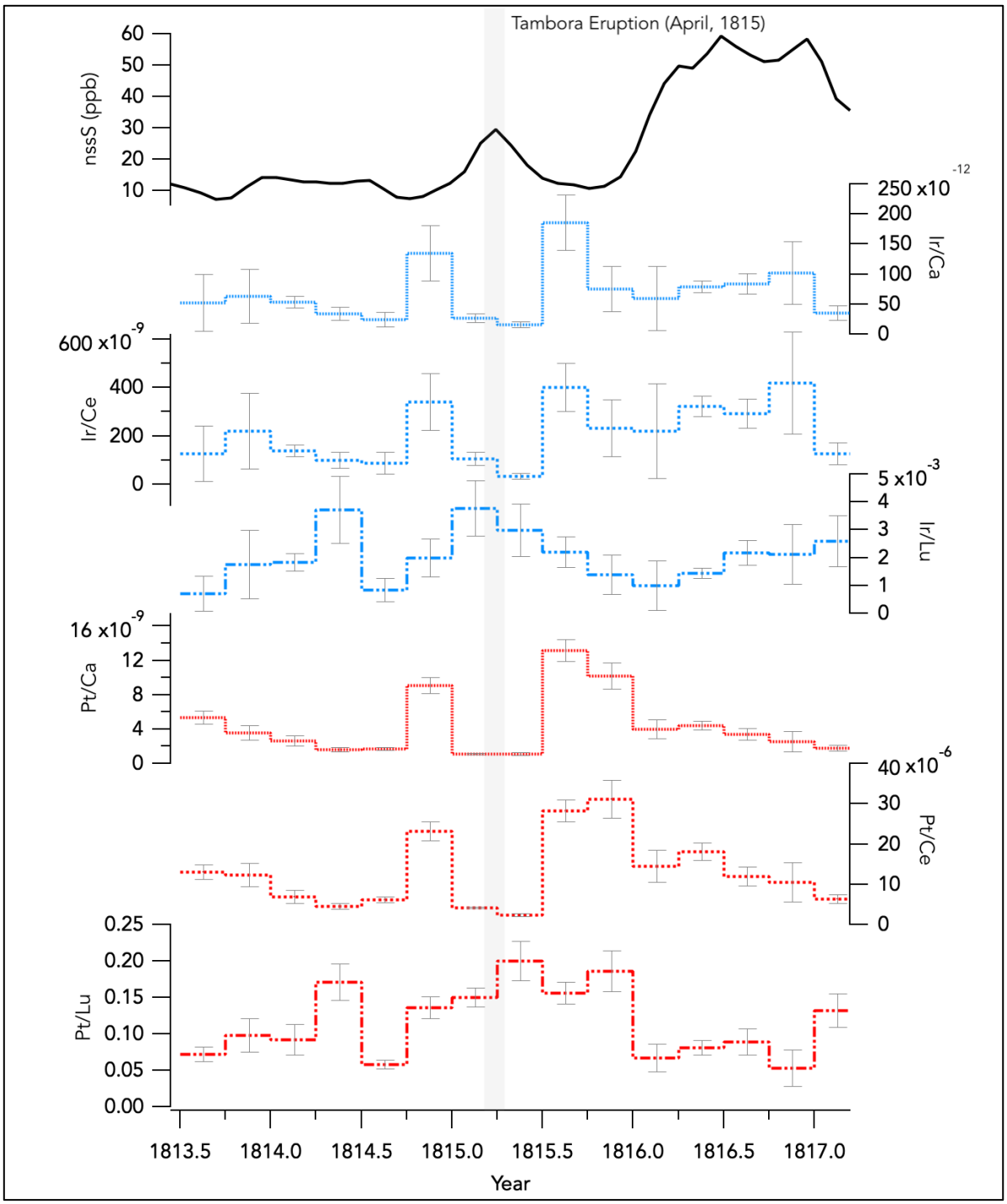

Figure 1.10: Ir and Pt signals from the Tambora sample period, normalized to Ca, Ce, and Lu records (intended to track terrestrial dust signals). Normalized records still indicate a large extraterrestrial Pt anomaly following the eruption event, as well as a smaller extraterrestrial Ir spike.

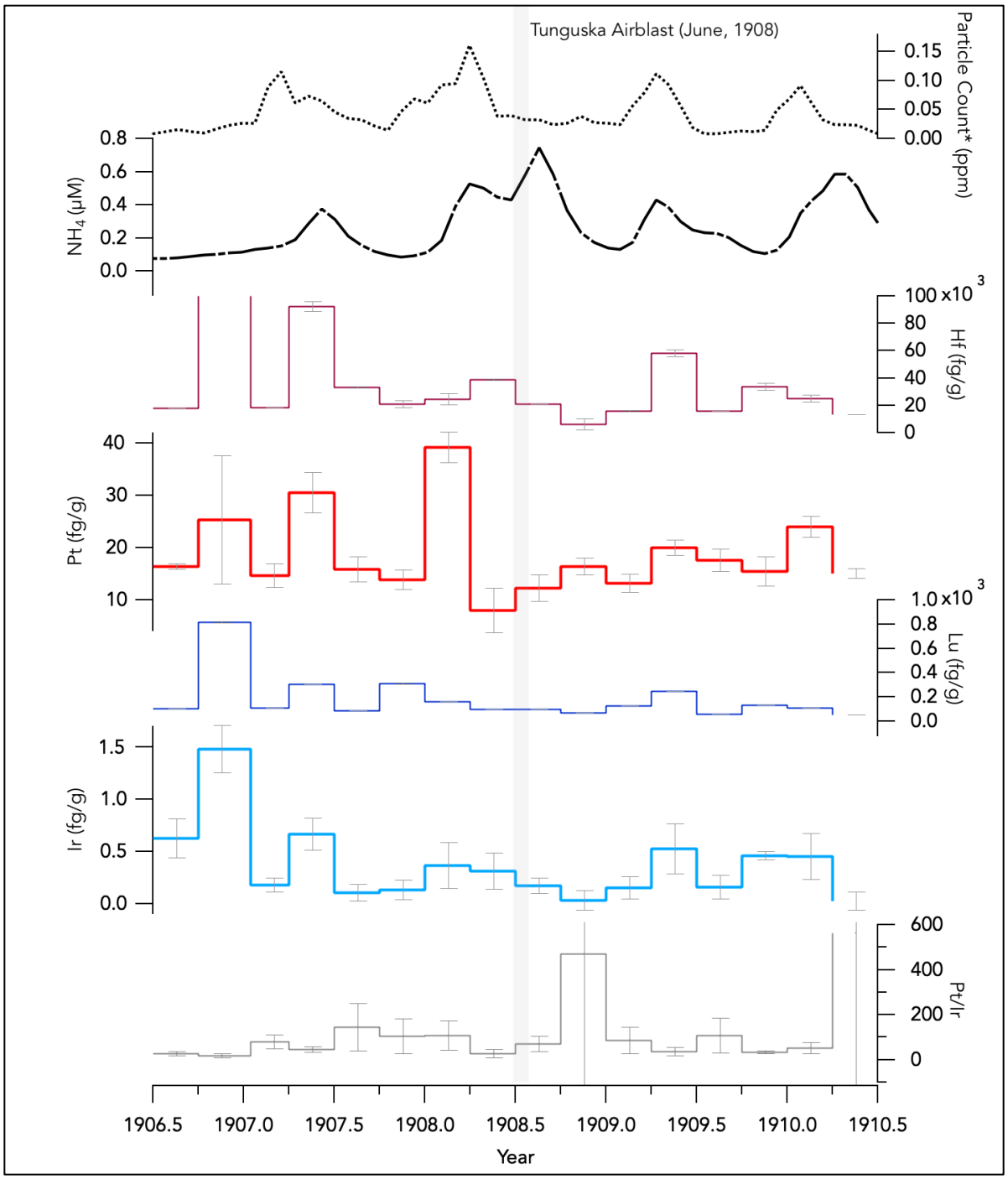

Figure 1.11: Summit ice records of particulate content, NH_4, Hf, Pt, Lu and Ir across the Tunguska air blast of 1908. The only tracer that may pick up a signal is NH_4 (a signal that is also picked up by Melott et al., 2010) , which peaks immediately after the event. A PGE response was not necessarily expected for an impactor of this size, at this distance from the Greenland Ice Sheet.

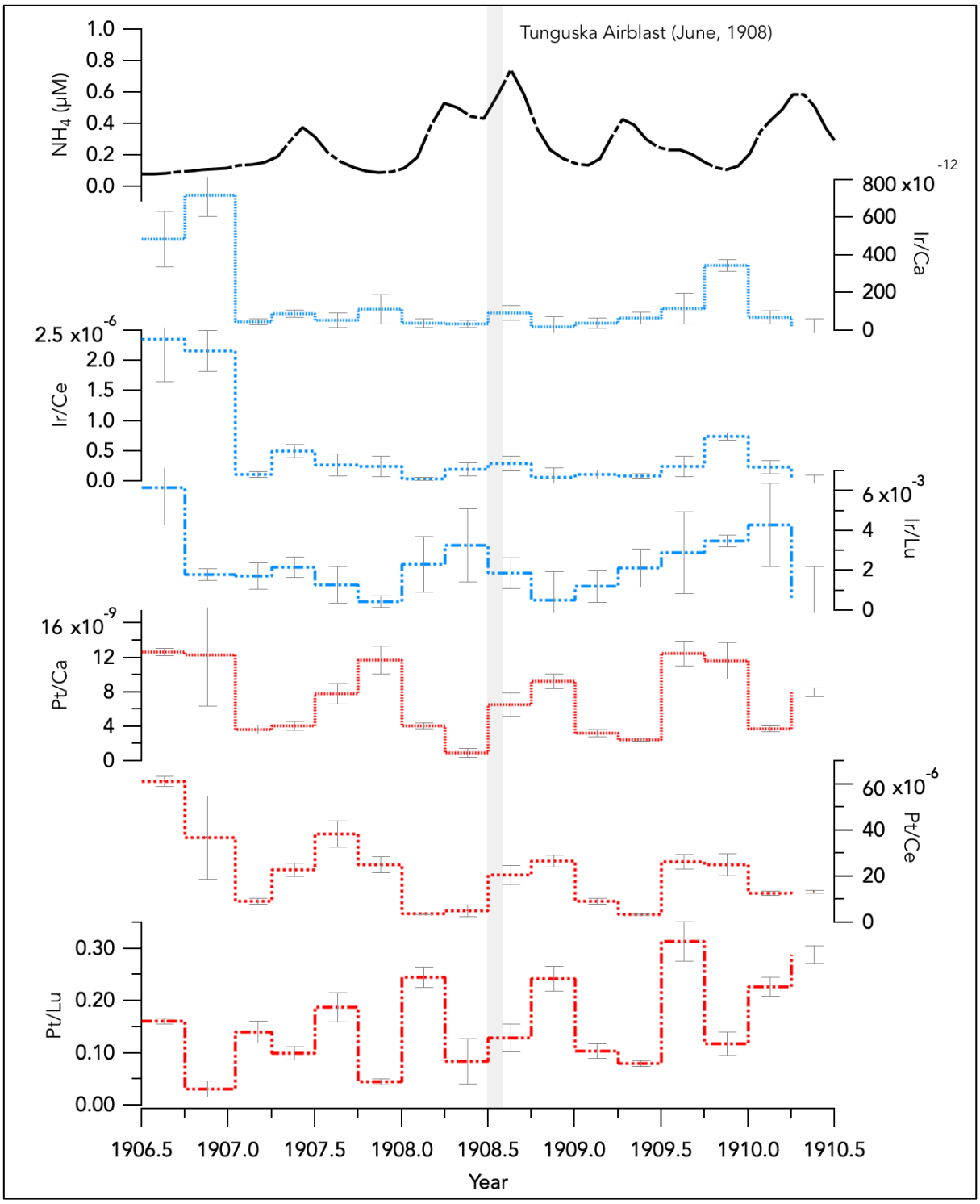

Figure 1.12: Ir and Pt signals from the Tunguska sample period, normalized to Ca, Ce, and Lu records (intended to track terrestrial dust signals). Normalized records still indicate no extraterrestrial PGE anomalies corresponding to the impact event.

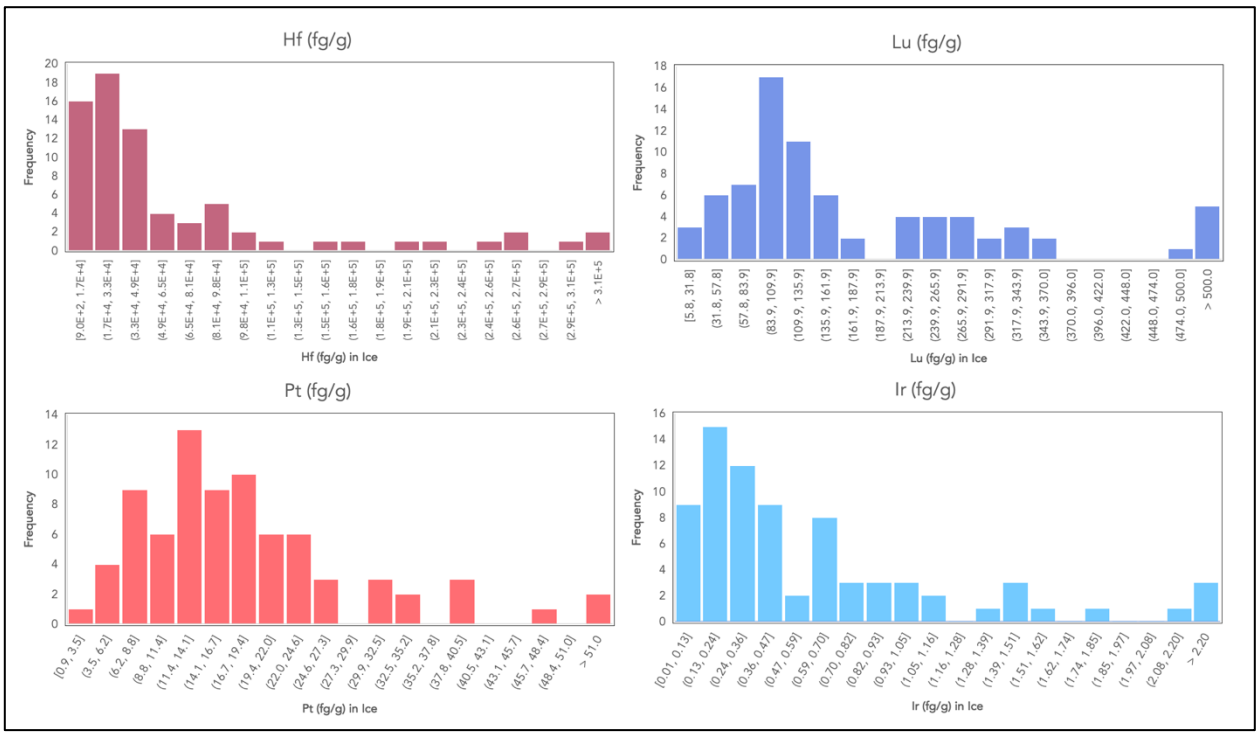

Figure 1.13: Comprehensive histograms of all corrected Hf, Lu, Pt, and Ir concentrations in ice samples (measured in fg/g) from the entire study. Hf peaks in the 1.7 x 10^4 – 3.3 x 10^4 fg/g window, Lu peaks in the 83.9-109.9 fg/g window, Pt peaks in the 11.4-14.1 fg/g window, and Ir peaks in the 0.13-0.24 fg/g window.

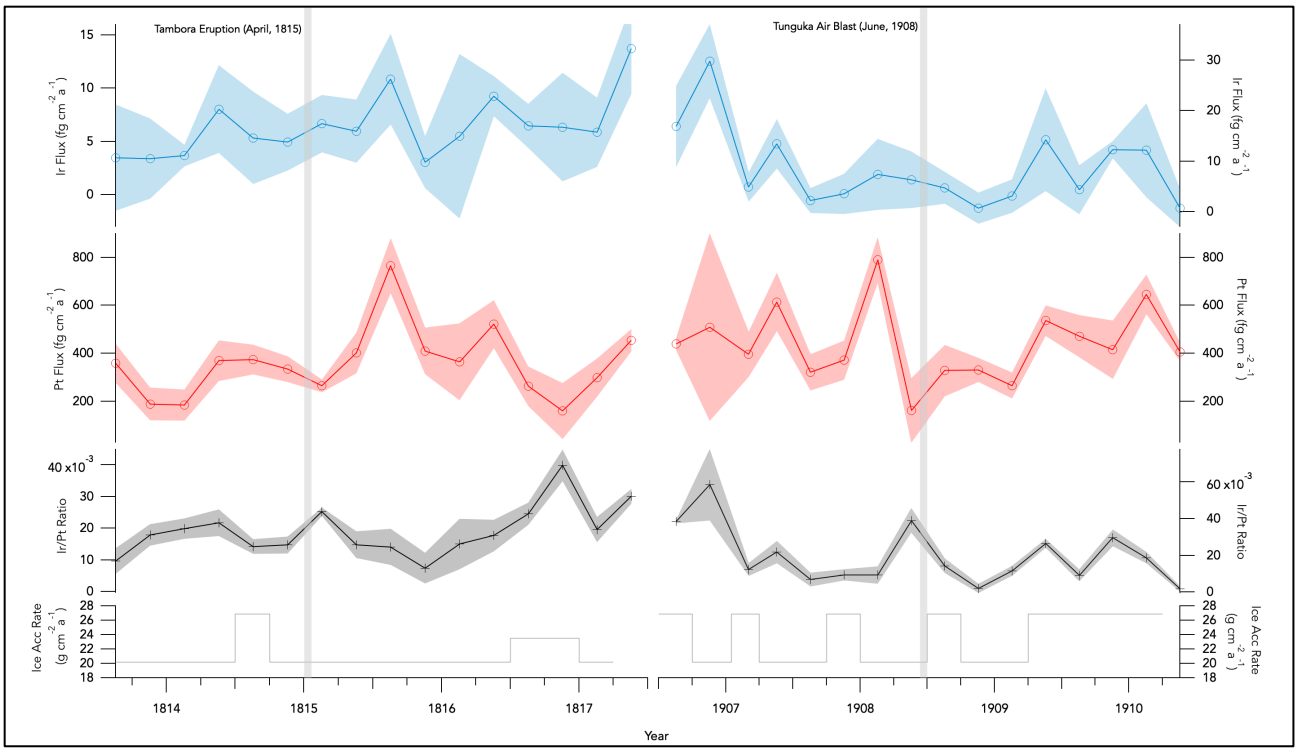

Figure 1.14: Ir and Pt records from Tambora and Tunguska converted to flux measurements. Because each sample was cut to represent the same amount of time (3 months), flux records look very similar to concentration records from Figures 7 & 8. Ir/Pt ratios do not exhibit any clear response to either event, and remain quite low compared to similar studies (Gabrielli et al., 2004, 2006, 2008). Ice accumulation rates for each sample, converted to g cm^2 a^{-1} in water equivalent, are represented at the bottom.

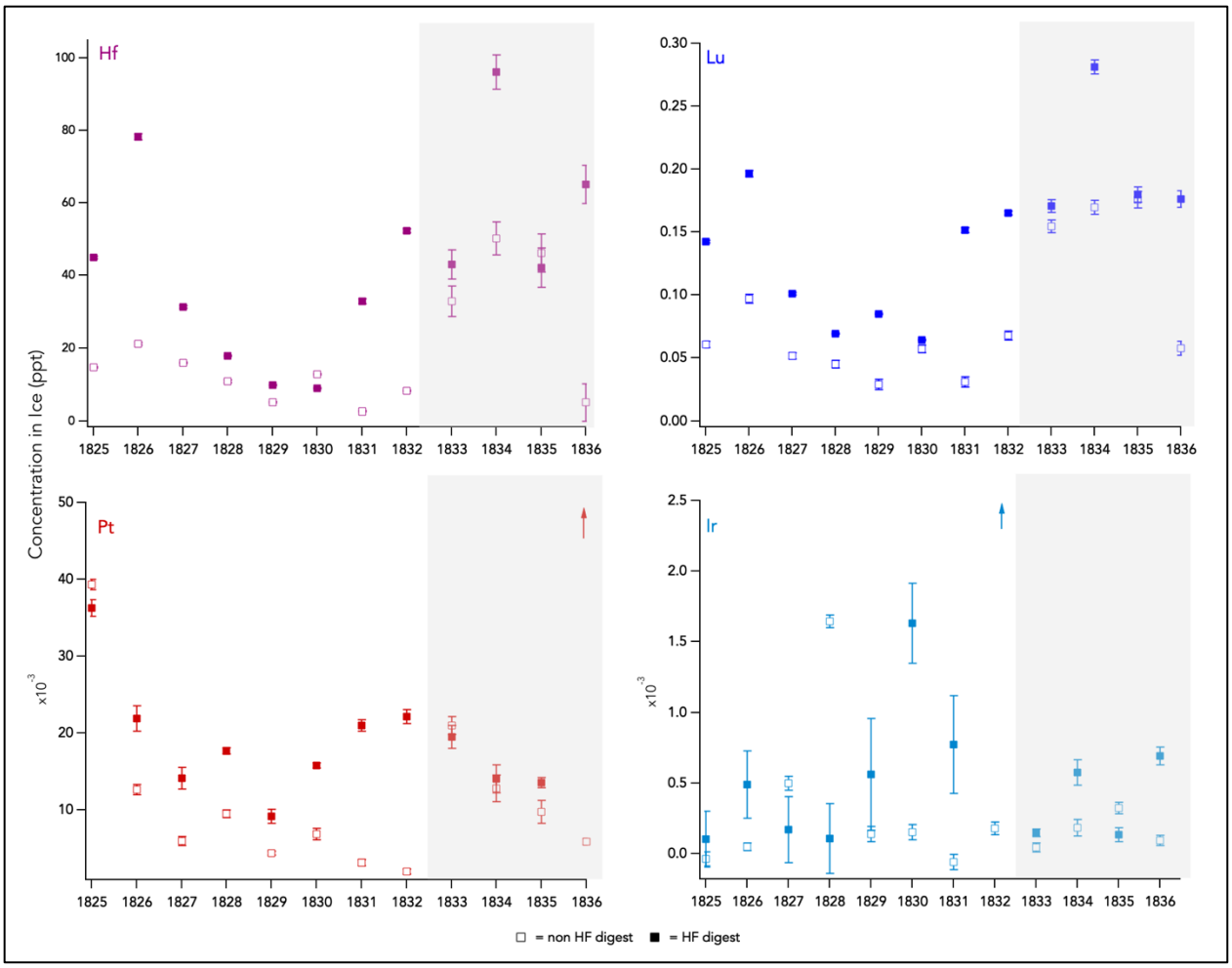

Figure 1.15: Comparisons between "strong" HF digestion methods (adapted from Petaev et al., 2013) and "weak" HNO_3 digests (adapted from Gabrielli et al., 2004), for Hf, Lu, Pt and Ir. Shaded areas represent non-HF digests that used 50% HNO_3, compared to unshaded areas which used 1% HNO_3. HF digests consistently measure slightly higher concentrations in all 4 species of interest. Procedural blanks recorded very strange, anomalously high Ir concentrations, contributing to larger error bars.

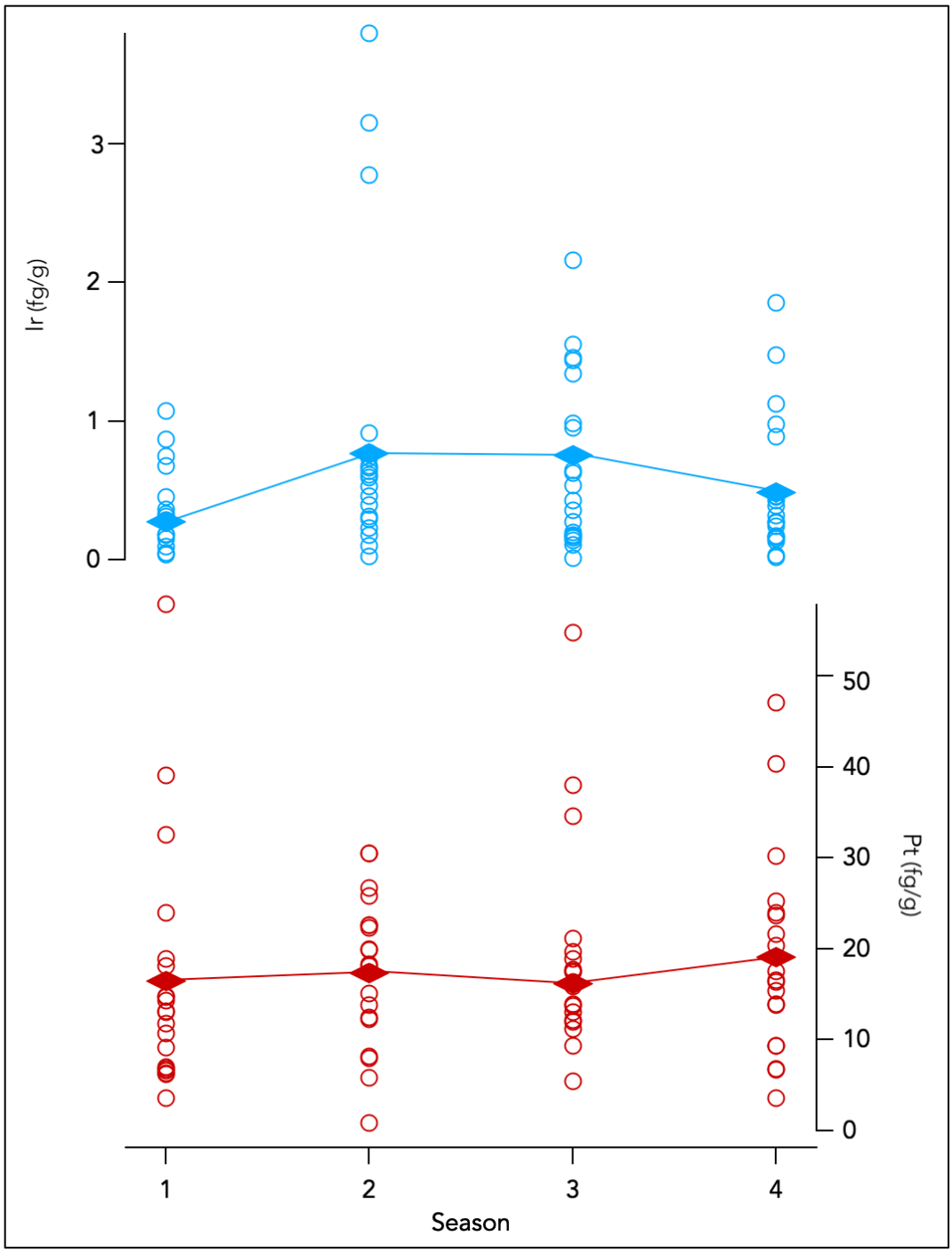

Figure 1.16: Pt and Ir concentrations in ice plotted together by season/ annual quarter (1 = Winter, 2 = Spring, 3 = Summer, 4 = Fall). Open circles represent individual measurements, and shaded diamonds represent population averages. Ir displays slightly increased deposition in spring and summer quarters. Pt does not display any obvious seasonal signal.

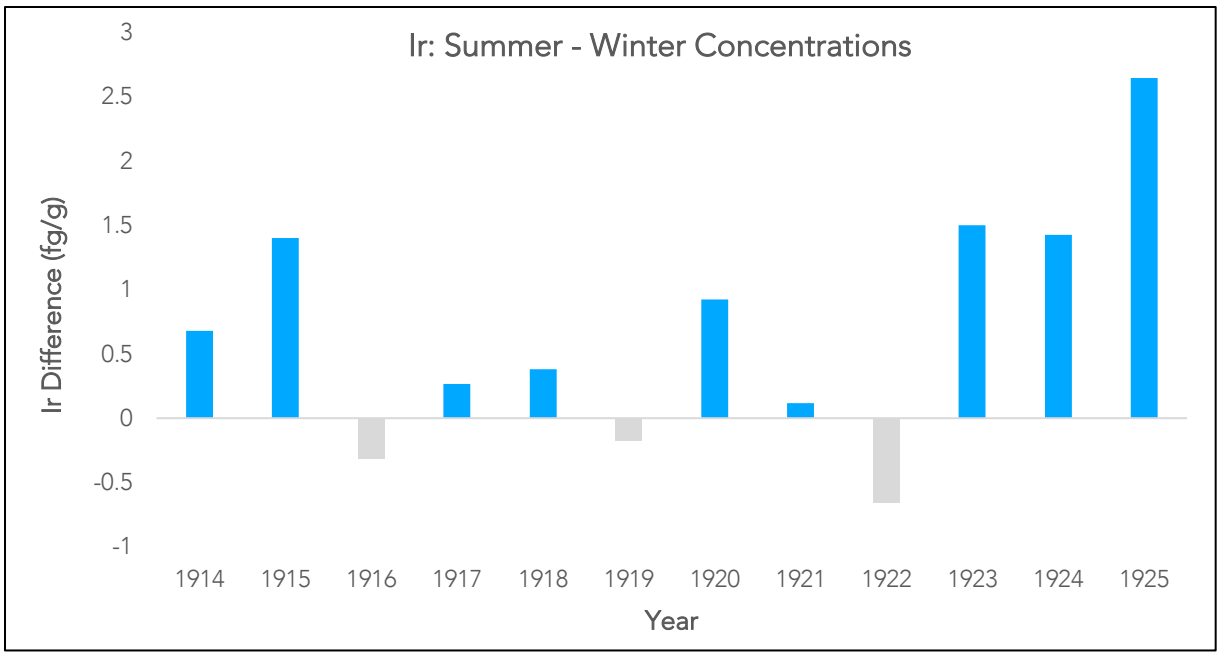

Figure 1.17: Reported differences in Ir deposition for summer vs. winter seasons, in the years 1914-1925. 9 of 12 years report greater Ir deposition in summer months, consistent with a hypothesis of increased terrestrial deposition to the Greenland ice sheet in Spring and Summer months. The same procedure was performed for Pt measurements but no trend was observed.

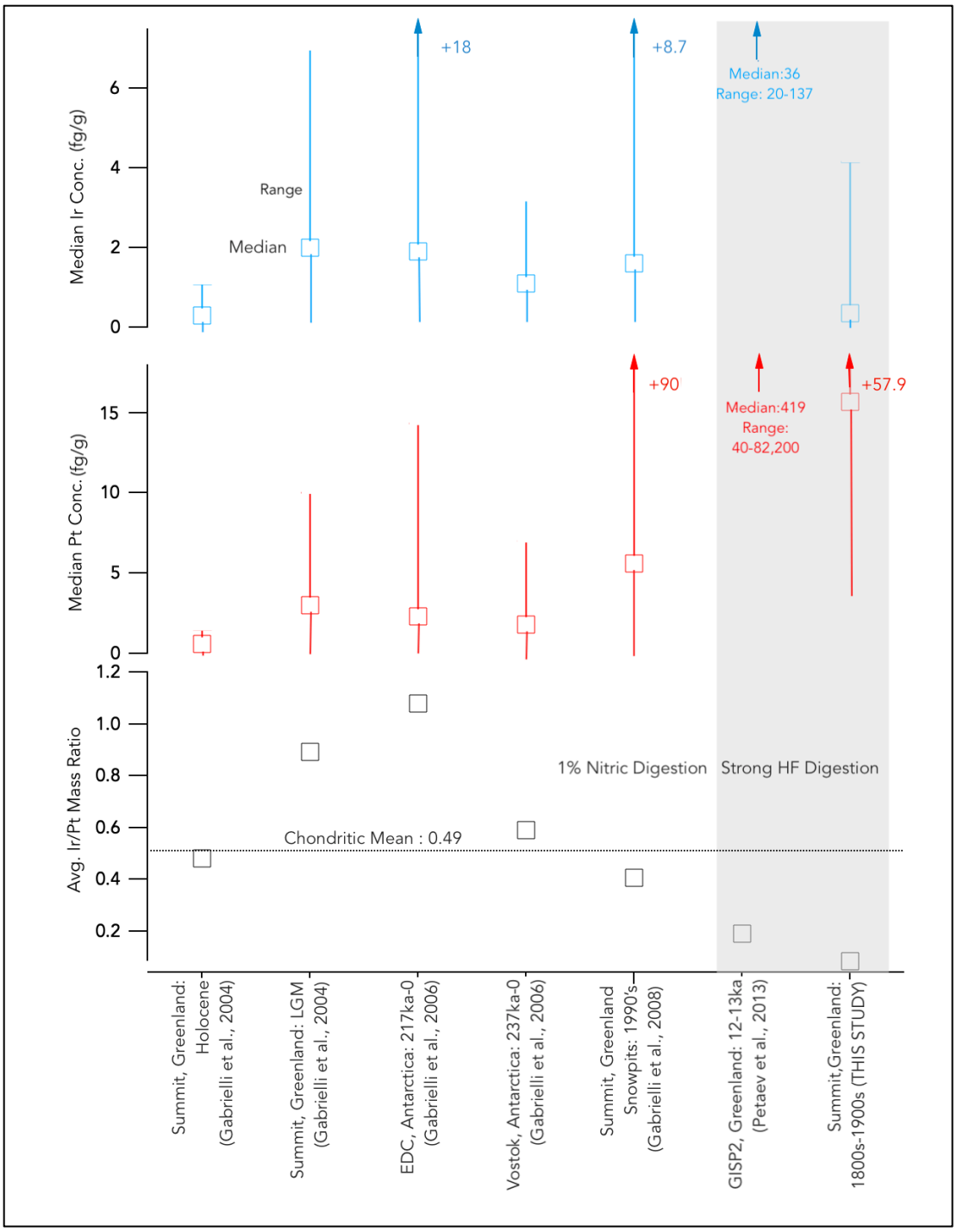

Figure 1.18: Reported median PGE concentrations from selected ice core studies. Our samples appear to have relatively low Ir, high Pt, and very low Ir/Pt ratios. Specific values are reported in Table 4. Vertical bars represent the range of concentrations recorded for each study. Vertical arrows indicate outliers that do not fit on axes along with the median and maximum (+#) recorded values for the study.

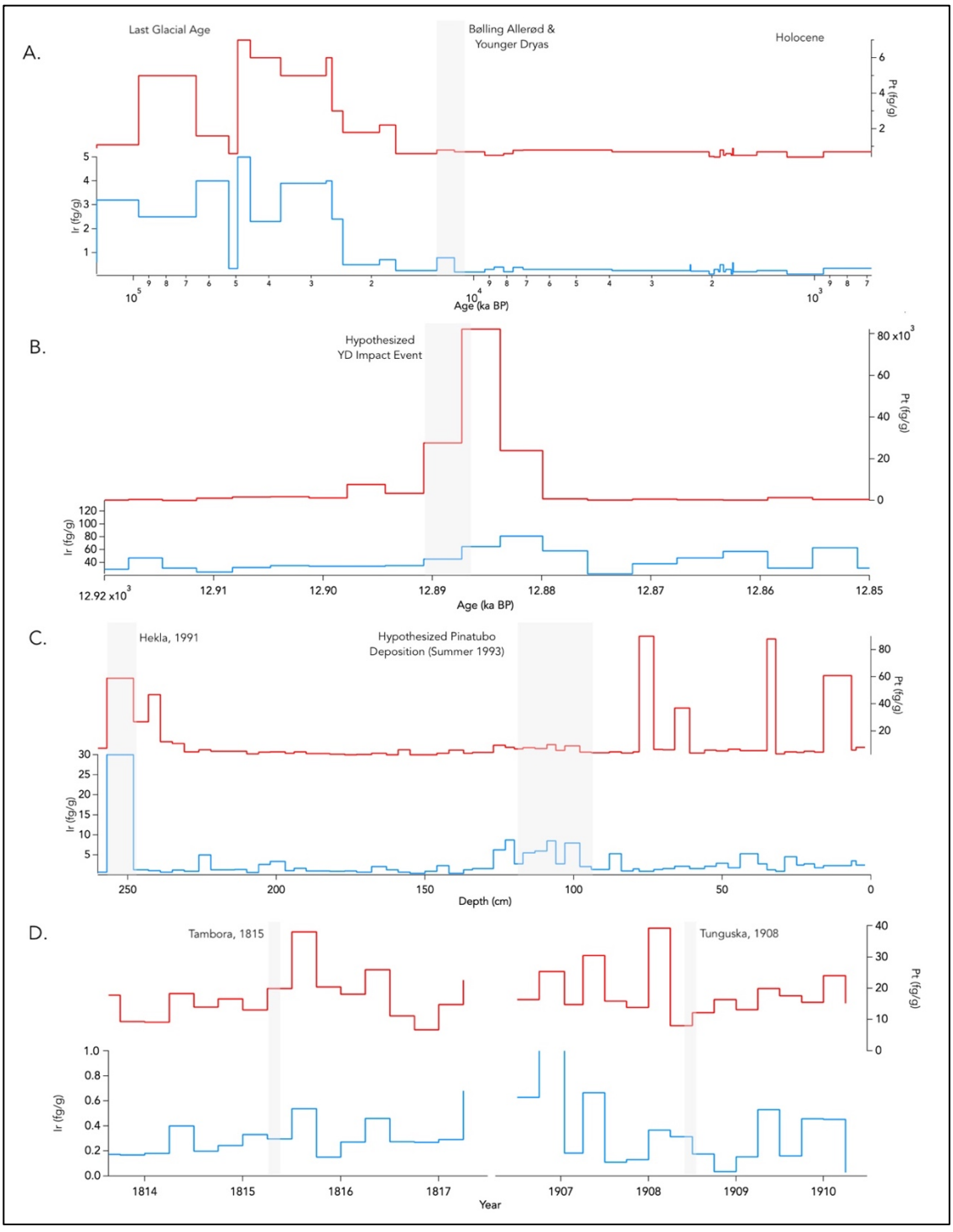

Figure 1.19: Selected Ir and Pt records in Greenland ice and snow from (A.) Gabrielli et al. (2004) depicting the glacial-interglacial variability in PGE tracers, (B.) Petaev et al. (2013) depicting a Pt anomaly at the onset of the Younger Dryas, (C.) Gabrielli et al. (2008) depicting PGE responses to the Hekla eruption (1991) and Pinatubo volcanic deposition (Summer, 1993), and (D.) This study, depicting PGE response to the Tambora and Tunguska events.

Table 1.1: Replicate sample measurements. Four samples were kept and measured each analytical round to determine the relative standard deviation between measurements days. Calibrations are performed each day to adjust for instrumental parameters, but this result indicates that something changed in sample reservoirs once they were first opened for initial analysis, leading to large variability between runs.

Sample	Ir Range* (ppt as measured)	Pt Range* (ppt as measured)	Ir %RSD	Pt %RSD
1 (1917 Q4)	3.3 - 11.0 x 10^{-3}	0.03 - 0.22	34.14	62.36
2 (1917 Q3)	1.4 - 6.9 x 10^{-3}	0.22 - 0.30	72.64	9.77
3 (1919 Q2)	1.1 - 3.1 x 10^{-3}	0.12- 0.15	44.46	7.99
4 (1918 Q3)	0.3 – 4.2 x 10^{-3}	0.06 – 0.09	92.01	21.97

*Oxide corrected ppt as measured

Table 1.2: Methodological improvements. Various improvements in early analytical rounds, such as adding small volumes of HF to analytical solutions, adding more aggressive autosampler wash procedures between samples (both introduced round 5) and switching to a more aggressive Teflon cleaning method (introduced round 6) helped bring down calculated uncertainty and improve confidence in sample measurements. * Blank ranges as measured are extrapolated to fit a standard, 250g sample for easier comparison.

Round	**Record Trait**	**Ir** (fg/g)	**Pt** (fg/g)	**Lu** (fg/g)	**Hf** (fg/g)
Analytical Rounds 2-4 N= 25	Blank Range*:	0.8-8.8	21-55	3.0-14	24-75
	Mean sample	0.706	18.6	171	41,725
	Samples SD	0.905	14.6	277.9	71,655
	Mean Uncertainty	**0.405**	**17.9**	113.2	25,215
Analytical Round 5 N=10	Blank Range*:	0.31	7.7	10.1	67.31
	Mean sample	1.10	8.90	333.7	256,258
	Samples SD	1.11	13.8	879.2	6,947
	Mean Uncertainty	**0.341**	**9.81**	7.3	8,736
Analytical Round 6 N= 13	Blank Range*:	0.0037-0.12	1.2-3.2	0.6-16.6	10.8-52.7
	Mean sample	0.479	19.6	204.5	47,747
	Samples SD	0.431	12.1	242.9	68,475
	Mean Uncertainty	**0.220**	**3.98**	6.55	4,583

Table 1.3: Volcanic response. Results from other ice core PGE studies that tracked volcanic signals. "Background" Ir and Pt signals (reported as concentrations in fg/g) are reported as an average of signals just before the volcanic event (the length of this preceding period is subjective, but generally concentrations are relatively stable prior to the recorded events). "Peak" Ir and Pt are recorded as the maximum value recorded that was attributed to the denoted volcanic event. The relative size of peak signal to background signals is reported in %. Our samples record a moderate peak in Pt, and a small peak in Ir.

Study	Eruption (VEI)	Background Ir (fg/g)	Background Pt (fg/g)	Peak Ir (fg/g)	Peak Pt (fg/g)	Ir Peak/ Background	Pt Peak/ Background
Gabrielli, 2008	Hekla, 1991 (3)	1.3	3.6	30	59	2307%	1639%
	Pinatubo, 1991 (6)	1.3	3.6	8.7	9.5	669%	264%
T.Soyol-Erdene, 2011	Cerro Hudson, 1991 (5+) Pit B	0.11	*17.5*	0.8	27.3	727%	156%
	El Chichon, 1982 (5) Pit A	0.11	*11.7*	NR	14.15	NR	121%
	Ngauruhoe, 1974 (3) Pit B	0.11	*11.7*	0.11	23	100%	197%
	Deception Island, 1967 (3) Pit A	0.11	11.7	0.14	49	127%	419%
	Agung, 1963 (5) Pit A	0.11	11.7	0.34	40	309%	342%
This Study, 2020	Tambora, 1815 (7)	0.24	14	0.54	38	**225%**	**271%**

Table 1.4: Ir and Pt signals compared to other studies. Average Ir and Pt concentrations (reported as fg/g) from our study compared to those from 5 other selected ice core studies. Ir concentrations for our study are relatively low, Pt concentrations are relatively high, and Ir/Pt ratios are relatively low. Chondritic Ratios: 0.49 (Anders & Grevesse, 1989). Crustal Ratios: ~0.2 (Wedepohl, 1995).

Study	Location & Period	Ir fg/g	Ir Range	Pt fg/g	Pt Range	Mean Ir/Pt Ratio	Ir/Pt Range
Gabrielli, 2004	SUMMIT Holocene	0.30	0.1-0.58	0.6	0.4-0.9	0.482	0.2-0.8
	SUMMIT LGM	2.00	0.34-5.0	3.0	0.6-7.0	0.891	0.28-2.9
Gabrielli, 2006	EDC-217ka	1.90	0.4-18.0	2.3	0.2-12.0	1.080	0.2-3.3
	Vostok-237ka	1.10	0.3-2.1	1.8	0.7-5.2	0.591	0.28-1.1
Gabrielli, 2008	SUMMIT snowpit 90s	1.60	0.4-8.7	5.6	2.5-90.0	0.406	0.1-1.1
T.Soyol-Erdene, 2011	E. Ant snowpit Pre-1980	0.09	0.052-0.34	11.7	6.3-57.0	0.008	0.002-0.01
	E. Ant snowpit Post-1980	0.11	0.05-0.34	26.2	5.8-76.0	0.003	0.002-0.01
Petaev, 2013	GISP2 12-13ka	36.0	22.0-137	419.0	38.0-82200.0	0.191	0.0007-0.76
This Study, 2020	SUMMIT 18th 19th C	0.4	0.027-3.79	15.7	6.78-57.9	0.019	0.0018-0.058
					Chondritic Ratio: 0.49		

Table 1.5: Total IDP flux estimates from selected studies. Total Ir and Pt mass fluxes are calculated using known accumulation rates and estimated density of ice or firn samples for Gabrielli et al. (2008), Petaev et al. (2013) and this study. *Average meteoric Ir concentrations (481 ppb; Anders and Grevesse, 1989) were used to convert Ir fluxes to total IDP mass fluxes, reported in Metric tons/day. Parentheses indicate estimates if no polar amplification is present, and top numbers represent estimates if stratospheric transport preferentially directs MSPs to winter poles for amplified deposition (proposed by Gabrielli et al., 2004). Because our IDP flux estimates of 43.5-217 tons/day are not corrected for terrestrial input of PGEs, they should be considered upper limits.

Category	Study	Technique/Location	Ir Flux (fg cm^{-2} a^{-1})	Pt Flux (fg cm^{-2} a^{-1})	Estimated IDP mass flux (tons/day)
Extraterrestrial	Nesvorny et al. (2009)	Zodiacal Dust Modeling			270
	Love and Brownlee (1993)	LDEF			110 ± 55
Atmospheric	Matthews et al. (2001)	Atmospheric Radar			5 ± 2
	Plane (2004)	Na Layer Modeling			20 ± 10
	Gardner et al. (2011)	Fe Layer Modeling			6
	Czisco et al. (2001)	Fe/Mg Stratospheric Sulphate Layer			22 - 104
	Hervig et al. (2009)	Satellite Optics			10 - 40
Terrestrial Collection	Lanci & Kent (2006)	Fe in Greenland ice (Magnetics)			175 ± 68
	Lanci et al. (2007)	Ge in Antarctic Ice (Magnetics)			15 ± 5
	Peuker-Ehrenbrink (1996)	Os in Marine Sediments			101 ± 36
(Polar Ice-Chemistry)	Gabrielli et al. (2004)	Summit Ice Core Ir, Pt	8	15	38.35 ± 13.7 (214 ± 82)
	Gabrielli et al. (2006)	EDC + Vostok Ice Cores Ir, Pt	2-4	4	10.96 ± 3.8 (57.5 ± 19.2)
	Gabrielli et al. (2008)	Summit snowpit Ir, Pt	64.5	225.8	*Ir: 371.8 (1859.1)
	T. Soyol Erdene et al. (2011)	E. Antarcric Snowpit Ir, Pt	0.3	50	*Ir: 1.74 (8.71)
	Petaev et al. (2013)	Summit Ice Core Ir, Pt	154.4	915.4	*Ir: 894.7 (4473)
	This Study (2020)	Summit Ice Core Ir, Pt	7.48	397.4	*Ir: 43.5 (217)
Parenthesis indicate universal distribution model (no amplified polar deposition)					

REFERENCES

Alvarez, L. W., Alvarez, W., Asaro, F., & Michel, H. v. (1980). Extraterrestrial cause for the Cretaceous-Tertiary extinction. *Science*, *208*(4448), 1095–1108. http://science.sciencemag.org/content/208/4448/1095.long

Anders, E. (1989). Pre-biotic organic matter from comets and asteroids. *Nature*, *342*(6247), 255–257. https://doi.org/10.1038/342255a0

Anders, E., & Grevesse, N. (1989). Abundances of the elements: Meteoritic and solar. *Geochimica Et Cosmochimica Acta*, *53*(1), 197–214.

Arculus, R. J., & Delano, J. W. (1981). Siderophile element abundances in the upper mantle: evidence for a sulfide signature and equilibrium with the core. *Geochimica et Cosmochimica Acta*, *45*(8), 1331–1343. https://doi.org/https://doi.org/10.1016/0016-7037(81)90226-X

Baales, M., Jöris, O., Street, M., Bittmann, F., Weninger, B., & Wiethold, J. (2002). Impact of the Late Glacial Eruption of the Laacher See Volcano, Central Rhineland, Germany. *Quaternary Research*, *58*(3), 273–288. https://doi.org/DOI: 10.1006/qres.2002.2379

Balcerzak, M. (2009). Methods of Elimination of Hafnium Interference in the Determination of Platinum in Environmental Samples by ICP-MS Technique. *Chemia Analityczna*, *54*, 135–149.

Barbante, C., Boutron, C., Morel, C., Ferrari, C., Jaffrezo, J. L., Cozzi, G., Gaspari, V., & Cescon, P. (2003). Seasonal variations of heavy metals in central Greenland snow deposited from 1991 to 1995. *J. Environ. Monit.*, *5*(2), 328–335. https://doi.org/10.1039/B210460A

Barbante, C., Schwikowski, M., Döring, T., Gäggeler, H. W., Schotterer, U., Tobler, L., van de Velde, K., Ferrari, C., Cozzi, G., & Turetta, A. (2004). Historical record of European emissions of heavy metals to the atmosphere since the 1650s from Alpine snow/ice cores drilled near Monte Rosa. *Environmental Science & Technology*, *38*(15), 4085–4090.

Barbante, C., Veysseyre, A., Ferrari, C., van de Velde, K., Morel, C., Capodaglio, G., Cescon, P., Scarponi, G., & Boutron, C. (2001). Greenland Snow Evidence of Large Scale Atmospheric Contamination for Platinum, Palladium, and Rhodium. *Environmental Science & Technology*, *35*(5), 835–839. https://doi.org/10.1021/es000146y

Borovička, J., Spurný, P., Brown, P., Wiegert, P., Kalenda, P., Clark, D., & Shrbený, L. (2013). The trajectory, structure and origin of the Chelyabinsk asteroidal impactor. *Nature*, *503*(7475), 235–237. https://doi.org/10.1038/nature12671

Briffa, K. R., Jones, P. D., Schweingruber, F. H., & Osborn, T. J. (1998). Influence of volcanic eruptions on Northern Hemisphere summer temperature over the past 600 years. *Nature*, *393*(6684), 450–455. https://doi.org/10.1038/30943

Broecker, W. S. (2006). Was the Younger Dryas Triggered by a Flood? *Science*, *312*(5777), 1146 LP – 1148. https://doi.org/10.1126/science.1123253

Broecker, W. S., Denton, G. H., Edwards, R. L., Cheng, H., Alley, R. B., & Putnam, A. E. (2010). Putting the Younger Dryas cold event into context. *Quaternary Science Reviews*, *29*(9), 1078–1081. https://doi.org/https://doi.org/10.1016/j.quascirev.2010.02.019

Brownlee, D. E. (1985). Cosmic Dust - Collection and Research. *Annual Review of Earth and Planetary Sciences*, *13*, 147–173. https://doi.org/DOI 10.1146/annurev.ea.13.050185.001051

Brownlee, D. E. (2016). Cosmic Dust: Building Blocks of Planets Falling from the sky. *Elements*, *12*(3), 165–170. https://doi.org/10.2113/gselements.12.3.165

Buizert, C., Gkinis, V., Severinghaus, J. P., He, F., Lecavalier, B. S., Kindler, P., Leuenberger, M., Carlson, A. E., Vinther, B., Masson-Delmotte, V., White, J. W. C., Liu, Z., Otto-Bliesner, B., & Brook, E. J. (2014). Greenland temperature response to climate forcing during the last deglaciation. *Science*, *345*(6201), 1177 LP – 1180. https://doi.org/10.1126/science.1254961

Bunch, T. E., Hermes, R. E., Moore, A. M. T., Kennett, D. J., Weaver, J. C., Wittke, J. H., DeCarli, P. S., Bischoff, J. L., Hillman, G. C., Howard, G. A., Kimbel, D. R., Kletetschka, G., Lipo, C. P., Sakai, S., Revay, Z., West, A., Firestone, R. B., & Kennett, J. P. (2012). Very high-temperature impact melt products as evidence for cosmic airbursts and impacts 12,900 years ago. *Proceedings of the National Academy of Sciences*, *109*(28), E1903 LP-E1912. https://doi.org/10.1073/pnas.1204453109

Chyba, C. F., Thomas, P. J., & Zahnle, K. J. (1993). The 1908 Tunguska explosion: atmospheric disruption of a stony asteroid. *Nature*, *361*(6407), 40–44. https://doi.org/10.1038/361040a0

Cole-Dai, J., Mosley-Thompson, E., & Thompson, L. G. (1997). Annually resolved southern hemisphere volcanic history from two Antarctic ice cores. *Journal of Geophysical Research: Atmospheres*, *102*(D14), 16761–16771. https://doi.org/10.1029/97JD01394

Curtius, J., Weigel, R., Vössing, H.-J., Wernli, H., Werner, A., Volk, C.-M., Konopka, P., Krebsbach, M., Schiller, C., Roiger, A., Schlager, H., Dreiling, V., & Borrmann, S. (2005). Observations of meteoric material and implications for aerosol nucleation in the winter Arctic lower stratosphere derived from in situ particle measurements. *Atmos. Chem. Phys.*, *5*(11), 3053–3069. https://doi.org/10.5194/acp-5-3053-2005

Dai, J., Mosley-Thompson, E., & Thompson, L. G. (1991). Ice core evidence for an explosive tropical volcanic eruption 6 years preceding Tambora. *Journal of Geophysical Research: Atmospheres*, *96*(D9), 17361–17366. https://doi.org/10.1029/91JD01634

Fan, Z. Y., Plane, J. M. C., Gumbel, J., Stegman, J., & Llewellyn, E. J. (2007). Satellite measurements of the global mesospheric sodium layer. *Atmospheric Chemistry and Physics*, *7*(15), 4107–4115. https://doi.org/10.5194/acp-7-4107-2007

Felitsyn, S. B., & Vaganov, P. A. (1988). IRIDIUM IN THE ASH OF KAMCHATKAN VOLCANOES. *International Geology Review*, *30*(12), 1288–1291. https://doi.org/10.1080/00206818809466110

Firestone, R. B., West, A., Kennett, J. P., Becker, L., Bunch, T. E., Revay, Z. S., Schultz, P. H., Belgya, T., Kennett, D. J., & Erlandson, J. M. (2007). Evidence for an extraterrestrial impact 12,900 years ago that contributed to the megafaunal extinctions and the Younger Dryas cooling. *Proceedings of the National Academy of Sciences*, *104*(41), 16016–16021.

Gabrielli, P, Barbante, C., Plane, J. M. C., Boutron, C. F., Jaffrezo, J. L., Mather, T. A., Stenni, B., Gaspari, V., Cozzi, G., Ferrari, C., & Cescon, P. (2008). Siderophile metal fallout to Greenland from the 1991 winter eruption of Hekla (Iceland) and during the global atmospheric perturbation of Pinatubo. *Chemical Geology*, *255*(1–2), 78–86. https://doi.org/10.1016/j.chemgeo.2008.06.012

Gabrielli, P, Plane, J. M. C., Boutron, C. F., Hong, S. M., Cozzi, G., Cescon, P., Ferrari, C., Crutzen, P. J., Petit, J. R., Lipenkov, V. Y., & Barbante, C. (2006). A climatic control on the accretion

of meteoric and super-chondritic iridium-platinum to the Antarctic ice cap. *Earth and Planetary Science Letters*, *250*(3–4), 459–469. https://doi.org/10.1016/j.epsl.2006.08.015

Gabrielli, Paolo, Barbante, C., Plane, J. M. C., Varga, A., Hong, S., Cozzi, G., Gaspari, V., Planchon, F. A. M., Cairns, W., & Ferrari, C. (2004). Meteoric smoke fallout over the Holocene epoch revealed by iridium and platinum in Greenland ice. *Nature*, *432*(7020), 1011.

Gabrielli, Paolo, Varga, A., Barbante, C., Boutron, C., Cozzi, G., Gaspari, V., Planchon, F., Cairns, W., Hong, S., & Ferrari, C. (2004). Determination of Ir and Pt down to the sub-femtogram per gram level in polar ice by ICP-SFMS using preconcentration and a desolvation system. *Journal of Analytical Atomic Spectrometry*, *19*(7), 831–837.

Gardner, C. S., Chu, X., Espy, P. J., Plane, J. M. C., Marsh, D. R., & Janches, D. (2011). Seasonal variations of the mesospheric Fe layer at Rothera, Antarctica (67.5°S, 68.0°W). *Journal of Geophysical Research: Atmospheres*, *116*(D2). https://doi.org/10.1029/2010JD014655

Gupta, S., Zhao, D., & Rai, S. S. (2009). Seismic imaging of the upper mantle under the Erebus hotspot in Antarctica. *Gondwana Research*, *16*(1), 109–118. https://doi.org/https://doi.org/10.1016/j.gr.2009.01.004

Hammer, C. U. (1977). Past volcanism revealed by Greenland Ice Sheet impurities. *Nature*, *270*(5637), 482–486. https://doi.org/10.1038/270482a0

Hans Wedepohl, K. (1995). The composition of the continental crust. *Geochimica et Cosmochimica Acta*, *59*(7), 1217–1232. https://doi.org/https://doi.org/10.1016/0016-7037(95)00038-2

Haynes, W. M., Lide, D. R., & Bruno, T. J. (2016). *CRC handbook of chemistry and physics : a ready-reference book of chemical and physical data.*

Hou, Q. L., Ma, P. X., & Kolesnikov, E. M. (1998). Discovery of iridium and other element anomalies near the 1908 Tunguska explosion site. *Planetary and Space Science*, *46*(2), 179–188. https://doi.org/https://doi.org/10.1016/S0032-0633(97)00174-8

Hsu, J., Prather, M. J., & Wild, O. (2005). Diagnosing the stratosphere-to-troposphere flux of ozone in a chemistry transport model. *Journal of Geophysical Research: Atmospheres*, *110*(D19). https://doi.org/10.1029/2005JD006045

Janches, D., Heinselman, C. J., Chau, J. L., Chandran, A., & Woodman, R. (2006). Modeling the global micrometeor input function in the upper atmosphere observed by high power and large aperture radars. *Journal of Geophysical Research: Space Physics*, *111*(A7). https://doi.org/10.1029/2006JA011628

Jarvis, I., Totland, M. M., & Jarvis, K. E. (1997). Determination of the platinum-group elements in geological materials by ICP-MS using microwave digestion, alkali fusion and cation-exchange chromatography. *Chemical Geology*, *143*(1), 27–42. https://doi.org/https://doi.org/10.1016/S0009-2541(97)00098-3

Kahl, J. D. W., Martinez, D. A., Kuhns, H., Davidson, C. I., Jaffrezo, J.-L., & Harris, J. M. (1997). Air mass trajectories to Summit, Greenland: A 44-year climatology and some episodic events. *Journal of Geophysical Research: Oceans*, *102*(C12), 26861–26875. https://doi.org/10.1029/97JC00296

Karner, D. B., Levine, J., Muller, R. A., Asaro, F., Ram, M., & Stolz, M. R. (2003). Extraterrestrial accretion from the GISP2 ice core. *Geochimica Et Cosmochimica Acta*, *67*(4), 751–763.

Kelley, M. C., Seyler, C. E., & Larsen, M. F. (2009). Two-dimensional turbulence, space shuttle plume transport in the thermosphere, and a possible relation to the Great Siberian Impact Event. *Geophysical Research Letters*, *36*(14). https://doi.org/10.1029/2009GL038362

Kennett, D. J., Kennett, J. P., West, A., Mercer, C., Hee, S. S. Q., Bement, L., Bunch, T. E., Sellers, M., & Wolbach, W. S. (2009). Nanodiamonds in the Younger Dryas boundary sediment layer. *Science*, *323*(5910), 94.

Kennett, D. J., Kennett, J. P., West, A., West, G. J., Bunch, T. E., Culleton, B. J., Erlandson, J. M., Hee, S. S. Q., Johnson, J. R., & Mercer, C. (2009). Shock-synthesized hexagonal diamonds in Younger Dryas boundary sediments. *Proceedings of the National Academy of Sciences*, *106*(31), 12623–12628.

Kjær, K. H., Larsen, N. K., Binder, T., Bjørk, A. A., Eisen, O., Fahnestock, M. A., Funder, S., Garde, A. A., Haack, H., Helm, V., Houmark-Nielsen, M., Kjeldsen, K. K., Khan, S. A., Machguth, H., McDonald, I., Morlighem, M., Mouginot, J., Paden, J. D., Waight, T. E., … MacGregor, J. A. (2018). A large impact crater beneath Hiawatha Glacier in northwest Greenland. *Science Advances*, *4*(11), eaar8173. https://doi.org/10.1126/sciadv.aar8173

Koeberl, C. (1989). Iridium enrichment in volcanic dust from blue ice fields, Antarctica, and possible relevance to the K/T boundary event. *Earth and Planetary Science Letters*, *92*(3), 317–322. https://doi.org/https://doi.org/10.1016/0012-821X(89)90056-3

Kvasnytsya, V., Wirth, R., Dobrzhinetskaya, L., Matzel, J., Jacobsen, B., Hutcheon, I., Tappero, R., & Kovalyukh, M. (2013). New evidence of meteoritic origin of the Tunguska cosmic body. *Planetary and Space Science*, *84*, 131–140. https://doi.org/https://doi.org/10.1016/j.pss.2013.05.003

Lanci, L, Delmonte, B., Kent, D. v, Maggi, V., Biscaye, P. E., & Petit, J.-R. (2012). Magnetization of polar ice: a measurement of terrestrial dust and extraterrestrial fallout. *Quaternary Science Reviews*, *33*, 20–31. https://doi.org/https://doi.org/10.1016/j.quascirev.2011.11.023

Lanci, L, & Kent, D. v. (2006). Meteoric smoke fallout revealed by superparamagnetism in Greenland ice. *Geophysical Research Letters*, *33*(13). https://doi.org/10.1029/2006GL026480

Lanci, Luca, Kent, D. v, & Biscaye, P. E. (2007). Meteoric smoke concentration in the Vostok ice core estimated from superparamagnetic relaxation and some consequences for estimates of Earth accretion rate. *Geophysical Research Letters*, *34*(10).

Larsen, E., Fernelius, W. C., & Quill, L. (1943). Concentration of Hafnium. Preparation of Hafnium-Free Zirconia. *Industrial & Engineering Chemistry Analytical Edition*, *15*(8), 512–515. https://doi.org/10.1021/i560120a015

Legrand, M., & Mayewski, P. (1997). Glaciochemistry of polar ice cores: A review. *Reviews of Geophysics*, *35*(3), 219–243. https://doi.org/10.1029/96RG03527

Love, S. G., & Brownlee, D. E. (1993). A direct measurement of the terrestrial mass accretion rate of cosmic dust. *Science*, *262*(5133), 550–553.

Lyne, J. E., & Tauber, M. (1995). Origin of the Tunguska event. *Nature*, *375*(6533), 638–639. https://doi.org/10.1038/375638a0

Mathews, J. D., Janches, D., Meisel, D. D., & Zhou, Q.-H. (2001). The micrometeoroid mass flux into the upper atmosphere: Arecibo results and a comparison with prior estimates. *Geophysical Research Letters*, *28*(10), 1929–1932. https://doi.org/10.1029/2000GL012621

Matsumoto, A., & Hinkley, T. K. (2001). Trace metal suites in Antarctic pre-industrial ice are consistent with emissions from quiescent degassing of volcanoes worldwide. *Earth and Planetary Science Letters*, *186*(1), 33–43. https://doi.org/https://doi.org/10.1016/S0012-821X(01)00228-X

Mayewski, P A, Meeker, L. D., Whitlow, S., Twickler, M. S., Morrison, M. C., Bloomfield, P., Bond, G. C., Alley, R. B., Gow, A. J., Meese, D. A., Grootes, P. M., Ram, M., Taylor, K. C., & Wumkes, W. (1994). Changes in Atmospheric Circulation and Ocean Ice Cover over the North Atlantic During the Last 41,000 Years. *Science*, *263*(5154), 1747–1751. https://doi.org/10.1126/science.263.5154.1747

Mayewski, Paul Andrew. (1999). *GISP2 Ions: Deep (D) Core (Detailed)*. PANGAEA. https://doi.org/10.1594/PANGAEA.55533

McConnell, J. R., Edwards, R., & Banta, R. (2005). A novel method for high-resolution, broad spectrum ice core analyses using ICP-OES and dual HR-ICP-MS. *Geophys. Res. Abstr*, *7*(10,713).

McCormick, M. P., Thomason, L. W., & Trepte, C. R. (1995). Atmospheric effects of the Mt Pinatubo eruption. *Nature*, *373*(6513), 399–404. https://doi.org/10.1038/373399a0

McDonough, W. F., & Sun, S.-S. (1995). The composition of the Earth. *Chemical Geology*, *120*(3–4), 223–253.

Meija, J., Coplen, T. B., Berglund, M., Brand, W. A., Bièvre, P. de, Gröning, M., Holden, N. E., Irrgeher, J., Loss, R. D., Walczyk, T., & Prohaska, T. (2016). Isotopic compositions of the elements 2013 (IUPAC Technical Report). *Pure and Applied Chemistry*, *88*(3), 293–306. https://doi.org/https://doi.org/10.1515/pac-2015-0503

Melott, A. L., Thomas, B. C., Dreschhoff, G., & Johnson, C. K. (2010). Cometary airbursts and atmospheric chemistry: Tunguska and a candidate Younger Dryas event. *Geology*, *38*(4), 355–358. https://doi.org/10.1130/G30508.1

Murrell, M. T., Davis, P. A., Nishiizumi, K., & Millard, H. T. (1980). Deep-sea spherules from Pacific clay: mass distribution and influx rate. *Geochimica et Cosmochimica Acta*, *44*(12), 2067–2074. https://doi.org/https://doi.org/10.1016/0016-7037(80)90204-5

Oppenheimer, C. (2003). Climatic, environmental and human consequences of the largest known historic eruption: Tambora volcano (Indonesia) 1815. *Progress in Physical Geography: Earth and Environment*, *27*(2), 230–259. https://doi.org/10.1191/0309133303pp379ra

Pearson, D. G., & Woodland, S. J. (2000). Solvent extraction/anion exchange separation and determination of PGEs (Os, Ir, Pt, Pd, Ru) and Re–Os isotopes in geological samples by isotope dilution ICP-MS. *Chemical Geology*, *165*(1–2), 87–107.

Petaev, M. I., Huang, S., Jacobsen, S. B., & Zindler, A. (2013). Large Pt anomaly in the Greenland ice core points to a cataclysm at the onset of Younger Dryas. *Proceedings of the National Academy of Sciences*, *110*(32), 12917–12920.

Pino, M., Abarzúa, A. M., Astorga, G., Martel-Cea, A., Cossio-Montecinos, N., Navarro, R. X., Lira, M. P., Labarca, R., LeCompte, M. A., Adedeji, V., Moore, C. R., Bunch, T. E., Mooney, C., Wolbach, W. S., West, A., & Kennett, J. P. (2019). Sedimentary record from Patagonia, southern Chile supports cosmic-impact triggering of biomass burning, climate change, and megafaunal extinctions at 12.8 ka. *Scientific Reports*, *9*(1), 4413. https://doi.org/10.1038/s41598-018-38089-y

Pinter, N., Scott, A. C., Daulton, T. L., Podoll, A., Koeberl, C., Anderson, R. S., & Ishman, S. E. (2011). The Younger Dryas impact hypothesis: A requiem. *Earth-Science Reviews*, *106*(3), 247–264.

Plane, J. M. C. (2003). Atmospheric chemistry of meteoric metals. *Chemical Reviews*, *103*(12), 4963–4984.

Plane, J. M. C. (2012). Cosmic dust in the Earth's atmosphere. *Chemical Society Reviews*, *41*(19), 6507–6518.

Ram, M., & Koenig, G. (1997). Continuous dust concentration profile of pre-Holocene ice from the Greenland Ice Sheet Project 2 ice core: Dust stadials, interstadials, and the Eemian. *Journal of Geophysical Research: Oceans*, *102*(C12), 26641–26648. https://doi.org/10.1029/96JC03548

Rasmussen, K. L., Clausen, H. B., & Kallemeyn, G. W. (1995). No iridium anomaly after the 1908 Tunguska impact: Evidence from a Greenland ice core. *Meteoritics*, *30*(6), 634–638.

Rasmussen, K. L., Olsen, H. J. F., Gwozdz, R., & Kolesnikov, E. M. (1999). Evidence for a very high carbon/iridium ratio in the Tunguska impactor. *Meteoritics & Planetary Science*, *34*(6), 891–895.

Rasmussen, S. O., Andersen, K. K., Svensson, A. M., Steffensen, J. P., Vinther, B. M., Clausen, H. B., Siggaard-Andersen, M.-L., Johnsen, S. J., Larsen, L. B., Dahl-Jensen, D., Bigler, M., RöThlisberger, R., Fischer, H., Goto-Azuma, K., Hansson, M. E., & Ruth, U. (2006). A new Greenland ice core chronology for the last glacial termination. *Journal of Geophysical Research (Atmospheres)*, *111*, D06102. https://doi.org/10.1029/2005JD006079

Saunders, R W, Dhomse, S., Tian, W. S., Chipperfield, M. P., & Plane, J. M. C. (2012). Interactions of meteoric smoke particles with sulphuric acid in the Earth's stratosphere. *Atmos. Chem. Phys.*, *12*(10), 4387–4398. https://doi.org/10.5194/acp-12-4387-2012

Saunders, Russell W, & Plane, J. M. C. (2011). A photo-chemical method for the production of olivine nanoparticles as cosmic dust analogues. *Icarus*, *212*(1), 373–382. https://doi.org/https://doi.org/10.1016/j.icarus.2010.12.019

Sengupta, A., Airan, Y., Thulasidas, S. K., & Natarajan, V. (2015). Evaluation of Spectral Interference of Lutetium on Analytes Including Specified Rare Earth Elements Using a CCD Detector-based ICP-AES. *Atomic Spectroscopy*, *36*, 82–95.

Soyol-Erdene, T.-O., Huh, Y., Hong, S., & Hur, S. do. (2011). A 50-year record of platinum, iridium, and rhodium in Antarctic snow: volcanic and anthropogenic sources. *Environmental Science & Technology*, *45*(14), 5929–5935.

Stothers, R. B. (1984). The Great Tambora Eruption in 1815 and Its Aftermath. *Science*, *224*(4654), 1191 LP – 1198. https://doi.org/10.1126/science.224.4654.1191

Suavet, C., Rochette, P., Gattacceca, J., & Folco, L. (2008). Micrometeorites: A possible bias on the sedimentary magnetic record. *Geochemistry, Geophysics, Geosystems*, *9*(11). https://doi.org/10.1029/2008GC002160

Sun, N., Brandon, A. D., Forman, S. L., Waters, M. R., & Befus, K. S. (2020). Volcanic origin for Younger Dryas geochemical anomalies ca. 12,900 cal B.P. *Science Advances*, *6*(31), eaax8587. https://doi.org/10.1126/sciadv.aax8587

Tankersley, K. B., Dunning, N. P., Owen, L. A., Huff, W. D., Park, J. H., Kim, C., Lentz, D. L., & Sparks-Stokes, D. (2018). Positive Platinum anomalies at three late Holocene high

magnitude volcanic events in Western Hemisphere sediments. *Scientific Reports*, *8*(1), 11298. https://doi.org/10.1038/s41598-018-29741-8

Taylor, S., Lever, J. H., & Harvey, R. P. (1998). Accretion rate of cosmic spherules measured at the South Pole. *Nature*, *392*(6679), 899–903. https://doi.org/10.1038/31894

Toutain, J.-P., & Meyer, G. (1989). Iridium-bearing sublimates at a hot-spot volcano (Piton De La Fournaise, Indian Ocean). *Geophysical Research Letters*, *16*(12), 1391–1394. https://doi.org/10.1029/GL016i012p01391

Tseren-Ochir, S.-E., Huh, Y., Hong, S.-M., Hwang, H., & Hur, S. do. (2011). Quantification of Ultra-Trace Levels of Pt, Ir and Rh in Polar Snow and Ice Using ICP-SFMS Coupled with a Pre-Concentration and Desolvation Nebulization System. *Bulletin of the Korean Chemical Society*, *32*, 2105–2108. https://doi.org/10.5012/bkcs.2011.32.6.2105

US Ice Drilling Program. (2019). *Blue Ice Drill Operations and Maintenance Manual*.

Vondrak, T., Plane, J. M. C., Broadley, S., & Janches, D. (2008). A chemical model of meteoric ablation. *Atmos. Chem. Phys.*, *8*(23), 7015–7031. https://doi.org/10.5194/acp-8-7015-2008

Wasson, J. T. (1999). Trapped melt in IIIAB irons; solid/liquid elemental partitioning during the fractionation of the IIIAB magma. *Geochimica et Cosmochimica Acta*, *63*, 2875–2889. https://doi.org/10.1016/S0016-7037(99)00283-5

Wasson, J. T., & Choe, W.-H. (2009). The IIG iron meteorites: Probable formation in the IIAB core. *Geochimica et Cosmochimica Acta*, *73*(16), 4879–4890. https://doi.org/https://doi.org/10.1016/j.gca.2009.05.062

Watson, A. J., Bakker, D. C. E., Ridgwell, A. J., Boyd, P. W., & Law, C. S. (2000). Effect of iron supply on Southern Ocean CO2 uptake and implications for glacial atmospheric CO2. *Nature*, *407*(6805), 730–733. https://doi.org/10.1038/35037561

WDOWIAK, T. J., ARMENDAREZ, L. P., AGRESTI, D. G., WADE, M. L., WDOWIAK, S. Y., CLAEYS, P., & IZETT, G. (2001). Presence of an iron-rich nanophase material in the upper layer of the Cretaceous-Tertiary boundary clay. *Meteoritics & Planetary Science*, *36*(1), 123–133. https://doi.org/10.1111/j.1945-5100.2001.tb01814.x

ZOLLER, W. H., PARRINGTON, J. R., & KOTRA, J. M. P. (1983). Iridium Enrichment in Airborne Particles from Kilauea Volcano: January 1983. *Science*, *222*(4628), 1118 LP – 1121. https://doi.org/10.1126/science.222.4628.1118

Zreda-Gostynska, G., Kyle, P. R., Finnegan, D., & Prestbo, K. M. (1997). Volcanic gas emissions from Mount Erebus and their impact on the Antarctic environment. *Journal of Geophysical Research: Solid Earth*, *102*(B7), 15039–15055. https://doi.org/10.1029/97JB00155

Chapter 2

CONCENTRATIONS OF ^{3}HE AND PROPERTIES OF ^{3}HE-BEARING INTERPLANETARY DUST PARTICLES IN ANTARCTIC ICE CORES

2.1 ABSTRACT

^{3}He is highly enriched in extraterrestrial material, and can be used to trace its input to terrestrial archives. As such, the flux of ^{3}He in these archives may be of interest to identify major solar system events that impact the flux of extraterrestrial dust, or to calculate sediment or ice accumulation rates. Given the rare nature of interplanetary dust particles, sufficiently large samples must be used to measure ^{3}He concentrations with high reproducibility. Previous work on ice core samples suggests that the presence of rare, large ^{3}He-rich 'nugget' particles can significantly skew measured ^{3}He concentrations, and contribute to large variability in replicate samples. We present new ^{3}He concentrations in very large ice (~3kg) samples from Taylor Glacier, Antarctica, and report an average concentration among 7 samples of 5.32 x 10^{-17} ccSTP/g (SD: 2.1 x 10^{-17} ccSTP/g), with an average ^{3}He/^{4}He ratio of 98.8 R_A (SD: 34.4 R_A) . Size fraction experiments likely experience input from a 20+ μm 'nugget' particle, but otherwise suggest that most ^{3}He present in ice is delivered by particles in the 0.45- 5 μm size range, consistent with previous results. Magnetic separation experiments indicate no clear difference in ^{3}He concentrations between magnetic and non-magnetic fractions, also consistent with previous results. A third experiment to test the use of ^{3}He concentrations as a rudimentary proxy for ice accumulation rates provided mixed results, with high accumulation rate samples exhibiting greater ^{3}He concentrations than low accumulation rate samples.

2.2 INTRODUCTION

^{3}He is an attractive tracer of extraterrestrial (ET) input in ice cores because the vast majority of ^{3}He in filtered particles is extraterrestrial (Brook et al., 2000, 2009), and the risks of

sample contamination are quite low. ^{3}He is also present in a unique size fraction (~5-20 μm) compared to terrestrial dust in ice cores (~1-2 μm; Brook et al., 2009). However, using ^{3}He as an extraterrestrial (ET) tracer is somewhat problematic because the average number of ^{3}He bearing particles in a conventional ice core sample (usually well below 1 kg) is believed to be quite low (Brook et al., 2009; Farley et al., 1997). Low particle numbers lead to large flux uncertainties, which grow as sample size decreases. Because of this, flux estimates based on existing ice core data are uncertain by at least a factor of ~2, making it difficult to establish the true natural variability. For example, it is unclear if there are significant variations in ^{3}He flux due to solar variability, volcanic eruptions, or impact events, or redistributions of deposited ^{3}He based on local pressure and precipitation patterns.

2.2.1 Investigation and Previous Use in Sediment Cores

It is argued that ^{3}He flux from interplanetary dust particles (IDPs) is relatively constant on long timescales, and can be used as a constant flux proxy in marine sediment cores to accurately estimate sediment accumulation rates. The two primary sources of He in sediment archives include old continental material rich in radiogenic ^{4}He from the decay of U and Th ($R < 0.015R_A$; $R = {}^{3}He/{}^{4}He$ ratio in sample / ^{3}He/^{4}He ratio in atmosphere, R_A = the atmospheric ^{3}He/^{4}He ratio of 1.39×10^{-6}) and ^{3}He rich interplanetary dust particles (IDPs, $R_A > 150$; Ozima et al., 1984). It is worth noting that ^{3}He/^{4}He ratios in most mantle-derived MORB materials are estimated to range from 6.2 - 14 R_A (Graham et al., 2001, 2014), significantly greater than most old continental rocks, but well below estimates for IDPs which can be > 100 R_A. By using continental and IDP ^{3}He/^{4}He values as endmembers, a mixing model can be used to estimate the relative contribution of each

component to a single He sample using the equation: $\left[\,{}^{3}He_{ET}\right] = \left(\frac{1-\frac{{}^{3}He/{}^{4}He_{TERR}}{{}^{3}He/{}^{4}He_{meas}}}{1-\frac{{}^{3}He/{}^{4}He_{TERR}}{{}^{3}He/{}^{4}He_{IDP}}}\right) \cdot [{}^{3}He_{meas}]$.

Fallout of ET material as a continuous source of ^{3}He to marine sediments was reintroduced by Ozima et al (1984), and later corroborated by (Takayanagi & Ozima, 1987) who calculated a relatively constant ^{3}He flux of 1.5 ± 1 x 10^{-15} $cm^{3}STPcm^{2}a^{-1}$ based on a collection of samples spanning 40 Ma in the Atlantic, Pacific and Japan Sea**.** Farley (1995) demonstrated that sediment samples retain their $^{3}He_{ET}$ very well over long periods (>70 Myr), and that significant changes in ^{3}He flux to earth have occurred since the start of the Cenozoic (likely as a result of local asteroidal breakup events and passage of comets through the inner solar system). On shorter timescales (<1 Myr), the flux appears to be constant enough to utilize as a constant-flux proxy for calculating sediment accumulation rates (Farley & Eltgroth, 2003; Marcantonio et al., 1996; Mukhopadhyay et al., 2001) and this conclusion is corroborated by independent 230Th normalization (Marcantonio et al., 1995). This approach permits sediment flux estimates at sub-orbital resolution that are independent from age model errors and changes in carbonate preservation.

Excursions in $^{3}He_{ET}$ flux from these archives may indicate the presence of notable celestial events, including earth impacts, collisions within the solar system, and changes to the orbital plane. Mukhopadhyay et al. (2001) identify anomalously high (>200 R_A) ^{3}He concentrations in marine carbonate sediments from Gubbio, Italy at the 65 Ma K-Pg boundary (endmembers of 0.03 R_A and 290 R_A). They observe a near-constant $^{3}He_{ET}$ flux from 63.9 - 65.4 Ma, indicating that the apparent K-Pg bolide was not associated with enhanced solar system dustiness, therefore the impactor could not have been a member of a comet shower. In addition, their $^{3}He_{ET}$ flux measurements imply that the K-Pg boundary clays were deposited rapidly over ~10 kyr; an

observation inconsistent with long timescales (>1 Myr) attributed to the Deccan Traps flood basalts, and indicating an extremely fast faunal turnover following an impact event. Farley & Mukhopadhyay (2001) later used low ^{3}He measurements in fullerenes to refute hypotheses by Becker et al. (2001) of a major impact event at the Permian Triassic Boundary (PTB) at 250Ma.

IDPs have also been attributed by some as a potential forcing for 100 kyr glacial-interglacial climate periodicity (Muller & MacDonald, 1995, 1997). According to this inclination hypothesis, oscillations in Earth's orbital inclination cause the planet to periodically pass through a cloud of IDPs, which in turn affects global climate (Muller & MacDonald, 1995, 1997). $^{3}He_{ET}$ has displayed regular 100 kyr cycles in late Pleistocene sediments from several locations, including the North Atlantic (Farley & Patterson, 1995), the Ontong-Java Plateau (Higgins et al., 2002; Patterson & Farley, 1998) and the eastern Equatorial Pacific (Marcantonio et al., 1996). However, measurements from other locations record no 100ka periodicity, and consequently suggest that sediment focusing plays a large role in ^{3}He deposition in sediment (Marcantonio et al., 1999; Winckler et al., 2004). Nonetheless, the relatively stable ^{3}He fluxes reported in various sediment archives around the world continue to support the use of $^{3}He_{ET}$ as a constant flux proxy for sediment accumulation rates well into the Mesozoic. The question remains as to whether this tracer might be of use in other climate archives, such as polar ice.

Perhaps the most critical parameter for determining potential uses of [^{3}He] in any matrix is the *area•time product* of samples. This is the ratio between sample mass and accumulation rate, which is proportional to the total number of IDPs delivered over a particular "area" over a particular "time" period. A sample with a larger area•time product should contain more IDPs, a higher [^{3}He] per gram of sample, and better sample reproducibility (Torfstein, 2012). Previous ice

core studies use samples with area•time products between 0.04 and 0.06 m^2a (Brook et al., 2009), whereas samples from this study span approximate area•time products between 0.05 and 0.2 m^2a in most samples. *This project aims to constrain the variability of ^3He on comparatively short timescales in ice cores, in an effort to identify smaller scale events and/or track ice accumulation rates in polar archives. It is still unclear if samples with relatively small area•time products are capable of providing a robust record of $^3He_{ET}$ influx.*

2.2.2 Origins, Collection in Space & Size and Entry Heating

External to their apparent applications in paleoclimate research, the physical and chemical properties of IDPs may uncover information about early solar system dynamics and accretional material. IDPs originate as asteroid and comet collisional material, though the relative contribution from each source remains poorly constrained. IDPs are primarily composed of porous silicate minerals and carbonaceous chondritic material (Nier & Schlutter, 1990), with a peak mass flux above Earth's atmosphere at an average diameter of ~200 µm (Love & Brownlee, 1993) and average density of 2 g/cm^3 (Range: 1-6 g/cm^3; Love et al., 1994). Nesvorný et al. (2010) suggest that comets within the Jupiter family are the most important source of IDPs within 5 AU of Earth. As IDPs travel through the solar system, they are bombarded by ^{3}He-enriched solar wind (SW, $^3He/^4He$ ratio=4.48 x 10^{-4}; ~322 R_A ; Nier & Schlutter, 1990), implanting the particles with He ratios near that of SW. The majority of particles collected in the upper stratosphere have $^3He/^4He$ ratios of only ~2.0 - 2.7 x 10^{-4} (~194 R_A ; Nier & Schlutter, 1990), suggesting a partial loss of SW He during atmospheric entry heating.

This hypothesis was supported by the Farley, Love & Patterson (1997) entry heating and He retentivity model, which concludes only 0.5% of the mass and ~4% of the surface area of infalling dust transmits through the atmosphere below 600°C (threshold for He release; Hiyagon, 1994). Size-dependent heating causes those particles which retain He to be far smaller than those in the parental IDP population. Competition between melting induced by frictional drag in larger particles and diffusional loss of He in small particles results in particle size distributions with most of the He-bearing IDP mass delivered by ~20 μm diameter particles (Trull, 1990), and most of the He-bearing IDP surface area delivered by ~7 μm diameter particles. Grain size distribution of ^{3}He from numerous terrestrial deposits generally agree with this model (Brook et al., 2009; McGee & Mukhopadhyay, 2013; Mukhopadhyay & Farley, 2006) . However, in archives that integrate over small areas and times, like ice cores and rapidly accumulating marine sediments, concern remains regarding the high degree of variability in replicate He analyses, and a strong tendency to under-sample rare, large, ^{3}He-rich particles (Farley, Love and Patterson, 1997; Brook et al., 2009).

Torfstein (2012) investigated the variability issues further. Their work on pelagic clays further supported the idea that scatter within and between previous data sets may be due to the presence of rare, He-rich particles (referred to as the 'nugget effect'). This study along with others hypothesized that these rare particles may only be present in larger size fractions, and significant improvement in ^{3}He flux measurements could perhaps be made by restricting particle size in filtered material.

2.2.3 Previous ^{3}He Work in Ice Cores

Brook et al. (2000) were the first to make detailed measurements of ^{3}He in particles from ice core samples, observing average ^{3}He flux values from recently deposited samples of 0.62 ± 0.27 x 10^{-12} cm^{3} $STPcm^{-2}$ ka^{-1} from GISP2 (central Greenland) and 0.77 ± 0.25 x 10^{-12} cm^{3} $STPcm^{-2}$ ka^{-1} at Vostok (East Antarctica), using samples primarily <1200 g in Greenland and <300 g in Antarctica. $^{3}He/^{4}He$ ratios of these samples ranged from 0.96 - 42.83 R_A in GISP2, and 90.85-200.05 R_A in Vostok (Brook et al., 2000), high enough to suggest that all of the ^{3}He they contained was extraterrestrial.

Winckler & Fischer (2004) measured 5 kg samples from EPICA Dome C, recording an average ^{3}He flux of 0.76 ± 0.26 x 10^{-12} cm^{3} $STPcm^{-2}$ ka^{-1} , in very close agreement with Brook et al. (2000). However, a later study by Brook et al. (2009) measured 9 replicate samples from Vostok, each 800-1200g, observing an average ^{3}He flux of 1.25 ± 0.37 x 10^{-12} cm^{3} $STPcm^{-2}$ ka^{-1}, higher than any of the previous results. They hypothesized that the large range for the 9 replicates was probably due to the small number of IDPs present in the samples, suggesting that *larger ice samples are required for more precise constraints on temporal variations in the flux.* Following the Torstein (2012) and Brook (2009) studies, we measure ^{3}He fluxes on very large (~3-5 kg) samples, to reduce influence of this potential "nugget effect," and better constrain the variability of ^{3}He flux on short timescales.

2.2.4 Research Significance and Primary Research Goals

Determining the characteristics and accretion rate of ET material to earth is important for developing stratigraphic tools to better understand ice and sediment accumulation rates, and for learning about the composition and dynamics of our solar system. In this work, we present ^{3}He

measurements from large (3-5 kg) ice samples from Taylor Glacier, Antarctica and Vostok, Antarctica. Our primary research goals were to:

1) Develop and improve viable methods of filtering and measuring ^{3}He-bearing IDPs (and separating them based on their size and magnetic characteristics) from large ice samples using facilities at Oregon State University.

2) Determine the short term variability of ^{3}He flux in ice samples with larger area•time products than those previously measured by Brook et al. (2000, 2009) and Winckler & Fischer (2006).

3) Investigate ^{3}He carrier phases by estimating the proportion of magnetic vs. non-magnetic ^{3}He-bearing IDPs, following methods similar to those established by Mukhopadhyay & Farley (2006).

4) Investigate ^{3}He carrier phases by estimating the size distribution of ^{3}He-bearing IDPS, following methods similar to those established by Brook et al. (2009).

5) Test the use of ^{3}He as a rudimentary proxy for ice accumulation rates, by comparing ^{3}He measurements in ice from relatively high accumulation and low accumulation time intervals.

6) Replicate ^{3}He flux measurements made by Brook et al. (2009) in nearly adjacent ice samples from Vostok, Antarctica.

2.3 METHODS

2.3.1 Extraction Line and Filtration Procedure

Figure 2.1 depicts a schematic outlining the samples and experiments performed in this study Twelve large (3-5 kg) ice core samples were collected in 2011 spanning 2.2 - 15.15 m depths from Taylor Glacier, Antarctica (TG). These “bricks,” initially cut to measure in situ ^{14}C by Petrekno et al. (2016), were collected using the high-volume Blue Ice Drill (BID) without drilling fluid and

squared off using an unlubricated chainsaw. Taylor Glacier is located in an ablation zone with very cold and windy conditions, and old ice that resurfaces here is originally sourced by the nearby accumulation zone at Taylor Dome (Bliss et al., 2011). Measured samples span approximately 53-55 ka, extrapolated from Petrenko et al. reported gas age records. Accumulation rates for these samples are not as well constrained, but Taylor Dome likely experienced accumulation rates between 2-4 cm/year (ice equivalent) during this time interval (Petrenko et al., 2016; Steig et al., 2000). In addition, two predicted sample populations spanning the Marine Isotope Stage 5/4 transition were assembled from core sections collected in 2015. "Low accumulation" samples (<1 cm/year from 60 - 70 ka) and "high accumulation" samples (2-4 cm/year from <60 and 70+ ka) were put together using various pieces of ice from TG 5/4 (0 - 20m) and TG 5/4-2 (0 – 20m) core sections. Rough accumulation estimates for these samples were derived from delta-age (difference in gas age vs. ice age) measurements in N_2O profiles (Menking et al., 2019), and are not well constrained. Finally, two adjacent samples from the Vostok BH-5 core drilled in 1991 - 1992 spanning 122 - 123 m were retrieved from the NSF Ice core facility. Depths of Vostok samples were carefully selected for their proximity to samples analyzed in Brook et al. (2009), and used to validate our ^{3}He extraction methods.

Prior to processing, all samples were cut using a bandsaw and exposed surfaces were shaved with a ceramic knife to eliminate surface contamination. Each sample was melted at room temperature in a covered glass beaker, and impurities within the ice became suspended in the sample water. Liquid samples were stirred with a Teflon stirrer to disaggregate particles from beaker surfaces, and samples were poured into a clean stainless-steel funnel feeding into peristaltic pump tubing. The pump pushed sample fluid through a filter cartridge into a vacuum-

backed Erlenmeyer flask. All filtration was performed under a laminar flow hood to minimize particulate additions (**Figure 2.2**).

0.45 µm silver filters (Osmotics-Poretics) were used to collect ice impurities, placed into and retrieved from filter cartridges using acid-cleaned forceps. Once sample filtrations were complete, filters were wrapped in acid-cleaned and sonicated aluminum packets and stored in glass vials until measurement in the OSU Noble Gas Lab.

2.3.2 Analytical Procedure

Packaged samples were loaded into a stainless steel vacuum chamber carousel then dropped vertically and heated individually in a Heine ultra-high vacuum furnace to a temperature of 1450° C. The gas released was directed through an extraction line where reactive gases were removed by SAES gettering and noble gases were cryo-sorbed and then He released at 45 K from a cryotrap. He was separated from other gases by release at 45 K on a cryotrap. He isotope ratios were measured on a Nu Instruments Noblesse mass spectrometer using Helium standard of Japan (HESJ) standards with a precisely known $^{3}He/^{4}He$ ratio of 20.4 R_A (Matsuda et al., 2002). A further description of the analytical process and instrumentation can be found in Graham et al. (2014). 13 ice samples were measured in total: 2 from Vostok and 11 from Taylor Glacier, 3 of which were used for magnetic separation experiments, 1 used for a size separation experiment, and 4 used for an experiment comparing high and low accumulation zones (cut in 2015).

Wet and dry filter blanks were both used for blank correction of ^{3}He concentrations as outlined by Brook at al., (2009). Wet blanks were made using 1 L of Milli-Q deionized water in place of ice sample, and processed using the funnel and foil-packing methods described above.

Dry blanks were taken straight from manufacturer packaging into aluminum foil packets. Line blanks consisted of heating the furnace between samples for the same amount of time prescribed for samples.

2.3.3 Magnetic Separation Experimental Procedure

To separate magnetic and nonmagnetic portions of collected ^{3}He-bearing particles, samples were passed through a constructed "magnetic chamber" surrounding the existing Tygon tubing. The chamber was composed of several Neodymium magnets arranged across a ~15 cm stretch of tubing, designed to trap magnetic particles as they travelled through the line. During the magnetic separation process, samples were passed through the line as usual with the magnetic chamber in place. All samples filtered at this stage were designated "nonmagnetic fractions." In the second stage, the magnetic chamber was removed, and tubing was flushed with 1 L of Milli-Q water. Particles filtered during this stage were designated "magnetic fractions." Three magnetic separations were performed in total.

2.3.4 Size Separation Experimental Procedure

Size separations of samples were performed using nylon mesh of varying opening size. Liquid samples were poured through 20 µm mesh prior to entering the stainless-steel funnel. On the outward flow side of the peristaltic pump, samples traveled through three consecutive filter cartridges containing: 10 µm nylon mesh, 5 µm silver filter, 0.45 µm silver filter. Once the first stage of filtration completed, material on 10 µm and 20 µm mesh liners was individually rinsed back into the funnel and through 0.45 µm silver filters.

2.3.5 Assessment of Blanks, Measurement Uncertainty, and Incremental Step Heating Trials

3 procedural blanks were measured alongside samples, recording total ^{3}He amounts ranging from too small to quantify to 1.53 $x10^{-16}$ ccSTP (mean ^{3}He of procedural blanks was 7.87 x 10^{-17} ccSTP; mean ^{3}He of measured samples was 2.27 x 10^{-13} ccSTP). Procedural blank values represent <0.01% - 2.6 % of measured ^{3}He and 0.3 – 57.2% of measured ^{4}He in individual measured samples. Furnace hot blanks were always performed before sample analysis, representing 0.02% - 11.3% of ^{3}He sample signals and 0.4- 52% of ^{4}He sample signals. Line blank corrections were applied to all samples and to procedural blanks for ^{3}He and ^{4}He. Final, 2-sigma analytical uncertainty intervals are less than or equal to 4% for [^{3}He], 1% for [^{4}He], and 4% for $^{3}He/^{4}He$ ratios

In 2015, two ice sample filters from two 8 kg Taylor glacier samples were incrementally heated, and corresponding [^{3}He] was measured to determine the necessary temperature for complete He release (**Figure 2.3**). Both samples record a rising [^{3}He] by 600°C, a maximum release of ^{3}He by 800-1000°C, and a complete ^{3}He release by 1450°C with released [^{3}He] near zero in the highest temperature step. During our experiment, all samples were furnace heated to 1450°C to ensure complete extraction of He from samples. Our He release profiles in **Figure 2.3** appear very similar to those previously reported from marine sediment cores (McGee & Mukhopadhyay, 2013; Mukhopadhyay & Farley, 2006).

2.3.6 Assessment of Filter Yield: Secondary Filter Test

A simple experiment was conducted to determine if ^{3}He-bearing particles were passing around the 0.45 µm filters, and to ensure our measurements were not missing a significant portion of the ^{3}He signal present in ice. Two identical filters were aligned in series, and "TG # 10" sample water from was passed through the filtration system (similar to the size fraction experiment, but with two 0.45 µm filters). The primary filter recorded an average [^{3}He] in ice of 3.66 x 10^{-17} ccSTP/g, and the secondary filter recorded 7.61 x 10^{-19} ccSTP/g (^{3}He for the highest procedural blank was 8.99 x 10^{-20} ccSTP/g; **Table 2.1**), indicating that only 2.08% of the ^{3}He present passed by or around the initial filter.

2.3.7 Data Processing

Instrument output values for ^{4}He and ^{3}He were corrected by subtracting furnace hot blank values to generate ^{3}He/^{4}He ratios, and were calibrated using mean HESJ standard measurements performed prior to individual sample analysis and size factor corrections (samples were NOT corrected for average filter blanks). Finalized ^{3}He quantities (ccSTP) were calculated by multiplying corrected ^{3}He/^{4}He ratios by ^{4}He measurements. ^{4}He and ^{3}He concentrations in ice were calculated by dividing final volumes by mass of sample ice filtered, producing a final result in ccSTP/g ice. Error bars for samples were generated using 2-sigma (standard deviations) from measured sample ^{3}He/^{4}He ratios plus the uncertainty on HESJ standard calibrations. Standard uncertainty propagation methods were used throughout all calculations. Uncertainties in sample ^{3}He/^{4}He include standard uncertainties propagated in quadrature.

2.4 RESULTS

2.4.1 [^{3}He] and ^{3}He/^{4}He in Taylor Glacier Samples, and 2 Vostok Samples

^{3}He concentrations from ice samples (Reported in **Table 2.1**) were either directly measured, or calculated by combining separate component measurements from the same ice. For example, concentrations from magnetic and non-magnetic portions were added together to produce the [^{3}He] of the parent ice sample. The same was done for [^{4}He], so ^{3}He/^{4}He ratios could be calculated. 7 Taylor Glacier samples spanning 2.2-15.2 m depths record [^{3}He] in ice ranging from 2.74 x 10^{-17} – 8.15 x 10^{-17} ccSTP/g (mean: 5.32 x 10^{-17} ccSTP/g; **Figure 2.4**). ^{3}He/^{4}He ratios in these samples span 58.4 R_A – 136.1 R_A (mean: 98.8 R_A). Using a simple 2 component mixing model (Equation 1 from Patterson & Farley, 1998) with a terrestrial end member of 0.015 R_A and ET end member of 290 R_A (Brook et al., 2000; Patterson & Farley, 1998), we calculate that over 99.8% of ^{3}He in all samples is of ET nature. Even by applying a terrestrial end member of 1.0 R_A (unrealistically high), the calculated proportion of $^3He_{ET}$ remains over 98% for all samples. As a result, we make no terrestrial correction to measured ^{3}He concentrations.

Two Vostok replicate samples from depths of 122.17 – 123 m were also measured, to compare measured [^{3}He] to published Vostok [^{3}He] from similar depths. Replicates measure [^{3}He] of 10.2 x 10^{-16} ccSTP/g ice and 1.05 x 10^{-16} ccSTP/g ice, with dramatically different ^{3}He/^{4}He ratios of 187.8 R_A and 203.2 R_A , respectively. Values previously reported in adjacent samples span 1.4 – 9.6 x 10^{-16} ccSTP/g ice and 136.0 – 206.1 R_A (Brook et al., 2009).

2.4.2 Magnetic and Non-magnetic Fractions

He isotopes from magnetic and non-magnetic dust fractions exhibit inconsistent results. The magnetic fraction records a significantly higher [^{3}He] and ^{3}He/^{4}He ratio in one trial, and the

non-magnetic fraction records significantly higher values for each in the other two trials (**Figure 2.5**). In the first measured pair, the magnetic fraction exceeds the nonmagnetic by ~ 0.5 x 10^{-17} ccSTP/g He_3, and by 80 R_A. In the following pairs, the non-magnetic fraction exceeds the magnetic by ~1.5 x 10^{-17} and 0.6 5 x 10^{-17} ccSTP/g ^{3}He , and ~66 and ~22 R_A, respectively. Averaged among the 3 trials, non-magnetic fractions record a [^{3}He] of 3.10 x 10^{-17} ccSTP/g and an R_A of 90.33, while magnetic fractions record a [^{3}He] of 2.57 x 10^{-17} ccSTP/g and an R_A of 87.65.

2.4.3 Filtered Particle Size Distribution

The four targeted size fractions of 0.45-5 μm, 5-10 μm, 10-20μm and 20+ μm reflect a He-bearing particle size distribution that differs from those presented by Brook et al. (2009), Mukhopadhyay & Farley (2006) and modeled by Farley, Love and Patterson (1997). The four size fractions combine to a total [^{3}He] in ice of 7.83 x 10^{-17} ccSTP/g. The 0.45 - 5 μm component contributes 9.35 x 10^{-18} ccSTP/g (11.95% of the total), the 5-10 μm component contributes 3.19 x 10^{-18} ccSTP/g (4.08% of the total), the 10-20μm component contributes 1.25 x 10^{-18} ccSTP/g (1.59% of the total), and the 20+ μm component contributes 6.45 x 10^{-17} ccSTP/g (82.38% of the total; **Figure 2.6**). The dominance of the largest size fraction is surprising based on previous published results, and suggests a potential input from at least one relatively large, ^{3}He- bearing 'nugget.' If the 20+ μm component is removed from consideration, the total [^{3}He] in ice drops to 1.38 x 10^{-17} ccSTP/g, with 67.81% contribution from the 0-5 μm component, 23.14 % from the 5-10 μm component, and 9.05% from the 10-20μm component. This size distribution is more consistent with published results.

We estimate the concentration of ^{3}He in the hypothesized nugget found in the largest size fraction. Based on a [^{3}He] concentration of 6.45 x 10^{-17} ccSTP/g in the sample and a total ice mass of 5650g, we calculate a total ^{3}He volume in this size fraction of 3.6 x 10^{-13} ccSTP. A spherical interplanetary particle of 10 μm radius would have a volume of 4.19 x 10^{-15} m^3, and assuming a silicate density of 2700kg/m^3, a mass of 1.13 x 10^{-8} g. Dividing the two results yields a total upper estimate IDP [^{3}He] of 3.2x 10^{-5} ccSTP/g, comparable to the highest [^{3}He] measured by Nier & Schlutter (1990) in stratospheric particles. Using a larger particle diameter of 30 μm reduces particle [^{3}He] to 9.4 x 10^{-6} ccSTP/g, though we cannot determine the true diameter of the particle once it has been filtered.

2.4.4 High and Low Accumulation Ice Tests

The comparison of high and low accumulation ice samples did not record higher [^{3}He] in low accumulation ice samples as expected. If the flux of ^{3}He-bearing particles to the ice surface is approximately constant, ice (or sediment) that accumulates more slowly should contain more particles, and higher [^{3}He] and ^{3}He/^{4}He ratios. Accumulation rates for this ice spans <1 cm/yr on average for low accumulation samples and ~3-5 cm/yr on average for high accumulation samples, though these estimates are poorly constrained because samples are composed of several, discontinuous pieces of ice. Among 2 low accumulation samples, [^{3}He] spans 1.79 x 10^{-17} ccSTP/g and 9.76 x 10^{-17} ccSTP/g (separated by a factor of 5), while in 2 high accumulation samples it spans 3.77 x 10^{-17} ccSTP/g and 1.92 x 10^{-16} ccSTP/g (also separated by a factor of 5; **Figure 2.7**). ^{3}He/^{4}He ratios follow a similar pattern, with low accumulation samples measuring 80.4 R_A and 117.0 R_A, while high accumulation samples measure 109.9 R_A and 199.7 R_A. It Is critical to note

that due to the large amount of particulate content present, multiple filters were needed to complete low accumulation ice filtration. Low accumulation sample 1 was composed of 4 separate filter measurements, and low accumulation sample 2 was composed of 3 separate filter measurements. During measurement of the second filter in low accumulation sample #1 the furnace failed at 1400° C, and the result should be treated as a lower boundary estimate for this portion of the sample. We do not believe this significantly affects the composite measurement of low accumulation sample #1.

2.4.5 Mixing Model to Determine Likely Terrestrial and Extraterrestrial End Members

Three mixing models were constructed to determine if our data from Taylor Glacier are consistent with reasonable terrestrial and extraterrestrial end members (**Figure 2.8**). The model parameters were constructed using approximate terrestrial dust concentrations in ice of 0.1 μg/g, 0.4 μg/g and 0.8 μg/g based on historic Taylor Glacier insoluble particle counts (Figure 2 in Menking et al., 2019). Terrestrial dust inputs with $^3He/^4He$ ratios of 0.015 R_A 0.1 R_A and 1.0 R_A in rock were used. Note that due to the very low ^3He content of terrestrial dust, shifting this parameter does not significantly alter model results. ET endmembers of 173 R_A, 200 R_A and 280 R_A in rock were used. Of the 3 models, the one best fit to our dataset uses a dust concentration of 0.4 μg/g in ice, a terrestrial dust $^3He/^4He$ ratio of 0.1 R_A, and an ET dust $^3He/^4He$ ratio of 200 R_A. Results indicate that 20 - 80% of all He in samples is extraterrestrial in origin. Agreement between models with reasonable endmembers and measured results point towards minimal ^3He contamination or loss during the extraction procedure.

2.5 DISCUSSION

2.5.1 Vostok Replicate Sample Measurements, in Context

Vostok sample depths were strategically selected to span depths near those measured by Brook et al. (2000, 2009), in an attempt to provide method validation for our new extraction procedures. An overview of the relevant measurements from all 3 studies, which span depths of 110-123m from the Vostok drill site, is provided in **Table 2.3**. While all 3 studies share similar mean [^{3}He] values of 3.83 x 10^{-16} ccSTP/g ice (Brook et al., 2000), 6.25 x 10^{-16} ccSTP/g ice (Brook et al., 2009), and 5.60 x 10^{-16} ccSTP/g ice (This Study), our ^{3}He measurements among only 2 samples span the widest range (**Figure 2.9**). In fact, one of our Vostok replicates measures a [^{3}He] higher than anything previously recorded in Holocene Ice (10.2 x 10^{-16} ccSTP/g ice), while the other is lower than any previous measurement from this Vostok core section (1.05 x 10^{-16} ccSTP/g ice).

This is an unexpected result, particularly given the very large size of our ice samples (2826-3070 g) which was predicted to increase the total number of IDPs in each sample and reduce the signal variability of [^{3}He] in replicates (Brook et al., 2009). However, 2 samples the smallest possible number to include replicates within a single study, and it is possible that our upper-range sample contained one or more large, ^{3}He-rich "nugget" IDPs, significantly increasing the recorded [^{3}He] in ice. It is reasonable to assume that significantly increasing sample size also increases the potential to capture these rare particles. It is worth noting that 3 Vostok samples (~200g) from the last glacial period measured by Brook et al. (2000) record [^{3}He] values much higher than ours (128.3 x 10^{-16}, 99.6 x 10^{-16} and 15.1 x 10^{-16} ccSTP/g ice), which were also attributed to rare, "nugget" IDPs. The wide spread between our 2 Vostok replicates, even in ~3 kg ice samples,

indicates that applying ^{3}He as a proxy for ice accumulation rates may be more difficult than previously anticipated.

In terms of method validation, our upper-range sample records only 6.1% higher [^{3}He] than the next highest from Brook et al. (2009; 9.61 x 10^{-16} ccSTP/g ice). Our lower-range sample records only 18.1% lower [^{3}He] than the next lowest sample from Brook et al. (2009; 1.38 x 10^{-16} ccSTP/g ice). $^{3}He/^{4}He$ ratios in our samples are also quite similar to those previously recorded. The close proximity of these measurements to previous results provides confidence that our extraction procedure is in fact collecting a majority of the ^{3}He-bearing IDPs present in ice.

2.5.2 Ice Core ^{3}He Record from Taylor Glacier and Other Ice Cores

^{3}He concentrations from 10 Taylor Glacier samples (plus one sample filtered at 5 μm) generally fall within the range of expected values for this study site. On average, samples have higher [^{3}He] than those from 0.4 - 0.42 ka GISP2 samples in Greenland (Brook et al., 2000; **Figure 2.9**), which is consistent with this site's higher accumulation rate (22.4 g/cm^{2}a) compared to estimated accumulation rates for our site at 53-55ka (~1.8-3.6 g/cm^{2}a). Taylor Glacier also records lower [^{3}He] values than those in Vostok ice from 3.8ka, which experiences slightly lower accumulation rates of about 2.0 g/cm^{2}a. However, the average Taylor Glacier [^{3}He] of 6.53 x10^{-17} ccSTP/g ice, is lower than expected compared to the average Vostok Holocene samples of 6.25 x 10^{-16} ccSTP/g ice reported by Brook et al. (2009). Based purely on accumulation rates (which are poorly constrained in our cores), a value somewhere between to ~ 3 x 10^{-16} and 6 x 10^{-16} ccSTP/g ice was expected, (though if predicting based on Brook et al. (2000) Vostok Holocene data, which reports a lower average [^{3}He], our values are slightly closer to predictions). These results indicate

that accumulation rates in our cores may be higher than previously thought, unless our extraction procedure is missing a significant portion of the ^{3}He signal.

^{3}He/^{4}He ratios from Taylor Glacier are more consistent with these Vostok and GISP2 records. Ratios in our cores average 109.0 R_A (range: 66.76 – 203.23 R_A). Shallow GISP2 Ice records a low average of 17.19 R_A (range: 0.96 - 42.83 R_A), likely driven down by higher terrestrial dust concentrations. Vostok Holocene ratios record averages of 177.9 R_A (range: 136 - 206.1 R_A) from Brook et al. (2009) and 156.9 R_A (range: 139.1-174.1 R_A) from Brook et al. (2000). Plotted together in **Figure 2.10**, samples from these studies lie roughly on a line representing ^{3}He/^{4}He ratios of 2 x 10^{-4} (143.9 R_A). Lower ratios in Taylor Glacier samples suggest either a greater input of terrestrial dust at this site, or a lower flux of ^{3}He-bearing particles at this site and time.

The variability of [^{3}He] among adjacent samples of similar accumulation rate, terrestrial dust deposition and climatic conditions may help assess the potential use of ^{3}He as a proxy for ice accumulation rate. Among our 7 primary Taylor Glacier samples (including one sample filtered at 5 µm), the standard deviation of [^{3}He] is 39.9% of the mean concentration (**Figure 2.4**). Accumulation rates are too poorly constrained in these samples to isolate changes in snow deposition through the period, but it is not unreasonable to assume that accumulation rates remained approximately constant through all 7 samples. To have a standard deviation this large, even among 2-5 kg samples, highlights potential precision issues in the future use of ^{3}He as a proxy for ice accumulation rates.

2.5.3 Use of ^{3}He as a Proxy for Ice Accumulation Rates?

Our high and low accumulation zone ice tests (samples for which can be found in **Table 2.2**) were intended to provide a preliminary demonstration of ^{3}He's utility as a rudimentary proxy for ice accumulation rates. In practice, however, the results of the test indicate that applying [^{3}He] in this regard may be quite difficult to interpret. Based on the predicted accumulation rates for each category (roughly 0.15 cm/yr on average for low accumulation samples and 1.5 cm/yr on average for high accumulation) low accumulation samples were predicted to have higher [^{3}He] by at least a factor of 2. Trial results seem to indicate higher [^{3}He] in high accumulation samples. It is possible, though unlikely, that total $^3He_{ET}$ flux varied across the two sample periods. It is also possible that High-Accumulation Sample #2 possessed a large, ^{3}He-rich "nugget" that elevated its total [^{3}He] and ^{3}He/^{4}He ratio. The existence of these nuggets, as previously discussed by Brook et al. (2009), Torfstein (2012) and Stuart et al. (1999) among others, may contribute to the poor reproducibility of replicate samples, and hinder the interpretation of relative [^{3}He] variations from adjacent ice samples.

Both high and low accumulation rate samples were assembled from the same ice sources, and should be treated as experimental replicates. Individual replicates for low accumulation samples record [^{3}He] of 1.79 x 10^{-17} vs. 9.76 x 10^{-17} ccSTP/g ice, differing by a factor of 5.5. Individual replicates for high accumulation samples record [^{3}He] of 3.78 x 10^{-17} vs. 1.92 x 10^{-16} ccSTP/g ice, differing by a factor of 5.1. The second round of samples does appear systematically higher than the first by a factor of ~5, which may indicate a flaw in the experimental procedure leading to the wide spread. Nonetheless, these results (from 3 kg+ ice samples), along with the wide ranges recorded in our 2 Vostok samples, indicate that any rudimentary proxy of [^{3}He] to predict ice accumulation rates would require even larger ice samples, or several replicate samples

to improve individual sample statistics, in order to function properly. A future test should include several replicates of high accumulation ice and low accumulation ice samples, in order to better identify the reproducibility of relative measurements.

While $^3He_{ET}$ may provide a unique tracer for estimating (notably old) marine sediment accumulation rates, those samples are typically dealing with much higher [^{3}He], in the range of 10^{-12} – 10^{-10} ccSTP/g in sediment (Torfstein, 2012; Patterson & Farley, 1998; Mukhopadhyay & Farley, 2006). These concentrations are 4-7 orders of magnitude greater than we find in our ice samples, meaning that they can be measured in relatively undisturbed, small bulk sediment samples, that do not require extensive cutting or flow through extraction lines and filters, which may cause ice samples to lose relevant IDPs along the way. The relatively poor reproducibility of ^{3}He measurements in ice demonstrated here and in Brook et al. (2000, 2009), indicate that any potential use of ^{3}He would be limited to areas where extremely large ice samples (5 kg+) are possible to collect. This rules out most conventional or deep ice cores, but could still prove useful in areas where ice of interest is available in abundance very close to the surface. For example, ^{3}He may still provide a useful tool for interpreting blue ice areas in Alan Hills, Antarctica, where large portions of stratigraphically disturbed, 1 Ma+ ice is easily accessible near the surface (Higgins et al., 2002). Smaller samples may still be effective if workers exclude particles of larger size fractions (>20 μm) to reduce the 'nugget' effect that contributes to high replicate variability. Polar ice is also still a useful matrix from which to study the characteristics of IDPs, as terrestrial input is relatively low compared to other terrestrial archives.

2.5.4 Magnetic Characteristics of ^{3}He- bearing IDPs

Early studies of ^{3}He in Quaternary sediments suggested that the primary mineral carriers of ^{3}He were magnetite, and a non-magnetic silicate component (Amari & Ozima, 1988; Fukumoto et al., 1986). Magnetite in IDPs is not usually primary, but formed through the oxidation of various minerals upon atmospheric entry (Brownlee, 1985). Because this formation involves high temperatures, breaking of chemical bonds and diffusion of oxygen, significant loss of ^{3}He should be expected (McGee & Mukhopadhyay, 2013). Furthermore, silicate components (mostly olivines and pyroxenes) experience issues with diagenetic alteration on the seafloor, which could significantly alter estimates of [^{3}He] in marine sediments. As a result, polar ice may provide the most accurate terrestrial matrix to assess the carrier phase of ^{3}He.

Our results, which indicate no clear difference in [^{3}He] or $^{3}He/^{4}He$ between magnetic and non-magnetic fractions, generally support those previously reported by Mukhopadhyay & Farley (2006). They too find that similar amounts of ^{3}He are released from magnetic and non-magnetic fractions of old marine sediments. In both cases, it is possible that magnetic separation procedures do not completely separate magnetic and non-magnetic particle fractions. Based on their chemical leaching experiment, Mukhopadhyay and Farley (2006) suggest that about half of the magnetite present in sediments is present in the non-magnetic fraction. One reason may be that a large portion of olivine and pyroxene IDP grains collected in the stratosphere are usually rimmed with a thin layer of magnetite that formed upon atmospheric entry (Sandford & Bradley, 1989) but not enough to exhibit strongly magnetic behavior for separation. The magnetite shells may form an “armor” around the silicate grains to prevent diagenetic alteration on the seafloor, or in our case, increase the helium retentivity of particles. This may be the cause of widespread association of magnetite with $^{3}He_{ET}$.

A direct comparison between our ice core samples and 90 Ma marine sediments is difficult to make, particularly when old sediments undergo significant diagenetic alteration. However, the similar ^{3}He profiles from magnetic and nonmagnetic fractions found in both studies do support the hypotheses that a "true" magnetic separation is likely impossible for IDPs, based on how magnetic minerals may form around silicate grains during atmospheric entry and that the carrier phase of ^{3}He may be magnetic Fe-Ni metals or phases associated with both magnetite and silicate grains. Further chemical investigation of IDPs (preferably directly collected in the stratosphere or in ice water wells) is necessary to better constrain the primary carrier phases of ^{3}He to terrestrial archives.

2.5.5 Size Characteristics of ^{3}He- bearing IDPs

^{3}He-bearing particles appear to exhibit a moderate range of grain size distributions in the established literature. Models by Farley, Love & Patterson (1997) based on surface-area correlated ^{3}He concentrations indicate that the vast majority of IDPs in terrestrial archives should fall between 3-35 µm diameter. The grain size distribution of [^{3}He] in Vostok ice from Brook at al. (2009) resembles their model quite closely. In their study, a vast majority of particles fall within the 5-10 µm diameter size range (**Figure 2.6**). Our size fraction experiment indicates a majority of ^{3}He is deposited by particles greater than 20 µm in diameter. Based on data from the remaining size fractions, it is possible that the 20+ µm size fraction experienced input from one or more rare, ^{3}He-rich "nugget" particles. If the 20+ µm population is removed from the dataset, the majority of ^{3}He is found in particles smaller than 5 µm diameter, a fraction with noticeably low ^{3}He in the Brook et al. (2009) distribution.

Two size fraction distributions from North Pacific marine sediments (Mukhopadhyay & Farley, 2006) and North Atlantic marine sediments (McGee et al., 2010) provide more varying results. The North Pacific distribution indicates nearly equivalent ^{3}He deposition (21-28% of all ^{3}He present) from particles in the <13 µm, 13-37 µm, 37-53 µm and 53+ µm size fractions. Conversely, the North Atlantic distribution records a majority of ^{3}He in <4 µm size fractions, followed closely by 4-20 µm size fractions, with very little ^{3}He present particles >20 µm. The discrepancies between all 4 size distributions may relate to the different area •time products of each matrix (McGee & Mukhopadhyay, 2013), as well as the tendency for marine sediment particles to cement together and form larger aggregate particles. Slow depositing samples, like the red clays from the North Pacific are more likely to collect larger ^{3}He "nugget" particles that drive up the ^{3}He content of larger size fractions compared to faster accumulating North Atlantic sediments.

It is also possible that methodological differences between studies have led to some of the discrepancies. The two marine sediment experiments used gravitational settling to extract particles, Brook et al. (2009) and this study passed samples directly through silver filters, which for larger size fractions, required an intermittent "rinsing" step to remove particles from 10 and 20 µm meshes. The total [^{3}He] from all four size fractions in Brook et al (2009) was 4.21 x 10^{-16} ccSTP/g ice in a 1.5 kg sample, whereas our total amounted to 0.783 10^{-16} ccSTP/g ice in a 5.65 kg sample. This lower than expected [^{3}He] in Taylor Glacier ice resembles the disagreement previously noted that can't be fully explained by accumulation rate (~2.5 – 5.5 g/cm^{2}a in TG samples vs. 1.2-2 g/cm^{2}a in the Vostok BH-5 section). It may be possible that our extraction method is missing a small portion of ^{3}He-bearing particles. We recommend an identical size

fraction experiment be conducted using Taylor Glacier ice, to determine if the 20 μm enriched size fraction we observe is anomalous or characteristic of the particle population.

2.5.6 Estimated Flux of ^{3}He to Earth Surface

Based on an approximate accumulation rate at our Taylor Glacier site of 2-4 cm/year, calculated ^{3}He fluxes from 7 relevant samples approximate 0.96 ± 0.38 - 1.91 ± 0.76 x 10^{-13} ccSTP/cm^2/ka, which is significantly lower than estimates from other ice cores (**Table 2.4**) and marine sediment studies (Brook et al., 2000, 2009; Farley, 1995; Farley & Mukhopadhyay, 2001; S. M. Higgins et al., 2002; F Marcantonio et al., 1995, 1999; Gisela Winckler & Fischer, 2006). Because the ice accumulation rates for our samples are so poorly constrained, our estimates should not be trusted to the same degree as previous studies. The relatively small ^{3}He flux estimates from TG ice suggest that our estimates for ice accumulation rates are lower than their true values. Assuming 100% extraction from our methods, and a true ^{3}He flux close to those reported by other ice core studies (~8 x 10^{-13} ccSTP/cm^2/ka), the accumulation rate for this site would need to be around 15 cm/year, at least 3x our current estimates. It is possible that this accumulation rate is accurate, that our extraction process is missing a portion of ^{3}He-bearing IDPs in ice samples, or a combination of the two factors is present in our results. Nonetheless, our reported upper estimate of 1.91 ± 0.76 x 10^{-13} ccSTP/cm^2/ka nearly overlaps with those reported by Brook et al. (2000) from the GISP2 ice core (6.2 ± 2.7 ccSTP/cm^2/ka) and by Marcantonio et al. (2001) from Arabian sea sediment cores (4.0 ± 2.7 ccSTP/cm^2/ka). We recommend that any future attempt to constrain ^{3}He$_{ET}$ flux in polar ice be conducted using very large ice samples (5 kg+) with precise accumulation rate constraint, in order to compute the most accurate possible flux.

2.6 SUMMARY & CONCLUSIONS

Helium isotopes in dust from 3 kg + ice samples from Taylor Glacier, Antarctica were measured and record values spanning 58 – 203 R_A, consistent with significant extraterrestrial input. Two samples from Vostok, Antarctica were measured and compared to previous study results to ensure the extraction system we developed produces accurate He measurements. Three magnetic separation experiments indicate that magnetic and nonmagnetic portions of IDPs contain approximately the same proportions of ^{3}He. Analysis of ^{3}He content among particles of various size fractions demonstrate the presence of one or more rare, large, 20+ µm ^{3}He-rich "nuggets," which may be one cause for low reproducibility of He measurements in ice core samples. Otherwise, our results suggest that the majority of ^{3}He is present in particles <5 µm in diameter. Attempts to use ^{3}He as a rudimentary proxy to calculate ice accumulation rates provided mixed results, as measured [^{3}He] in ice were greater in high accumulation samples than low accumulation samples. Estimates of the total ^{3}He flux on Earth from our data range from 0.96 ± 0.38 - 1.91 ± 0.76 (x 10^{-13} ccSTP cm^{-2} ka^{-1}), lower than published estimates from other ice cores and marine sediments. Wide variability in measured He between our replicate samples, as well as adjacent ice samples, indicate that either larger ice samples (5 kg+), or samples from lower accumulation rate zones are necessary to measure [^{3}He] with precision and high reproducibility in ice, potentially limiting the applications for which He measurement might be useful in ice cores.

FIGURES AND TABLES (2)

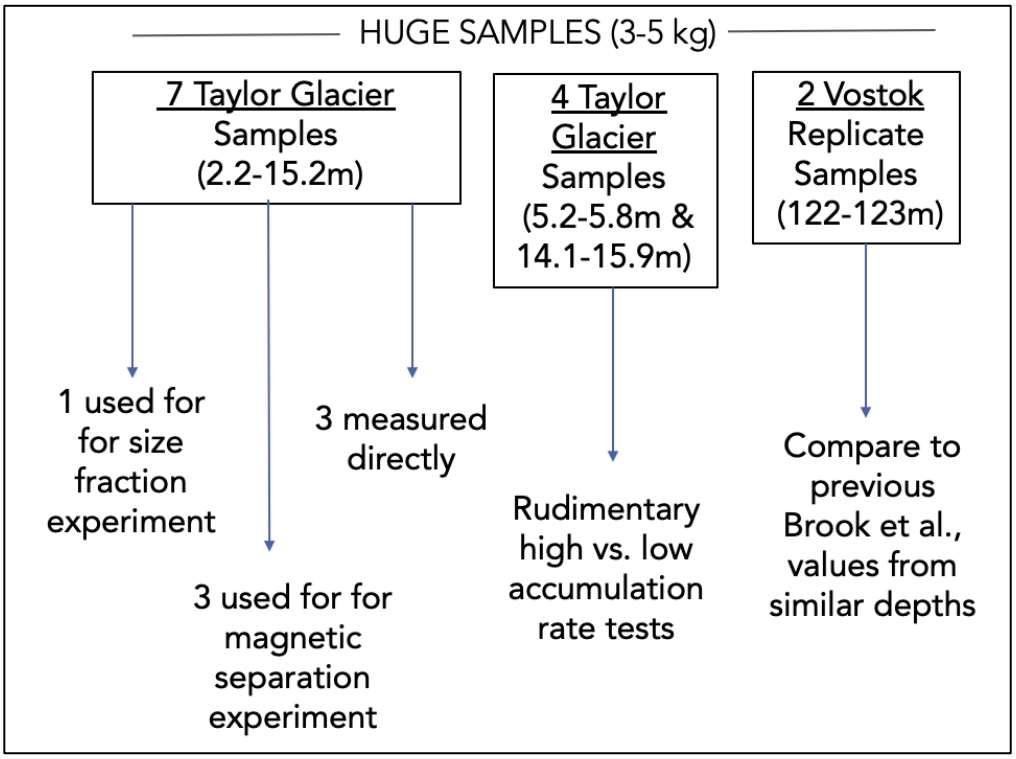

Figure 2.1: Schematic depicting how ice samples were utilized for the ^{3}He study. 7 Taylor Glacier samples were used to generate 1 size fraction experiment, 3 magnetic separation experiments, and 3 were measured directly. 2 sets of 2 replicates from Taylor Glacier (targeted for predicted high and low accumulation rates based on previous work; Menking et al., 2019), were used to attempt rudimentary accumulation proxy tests. Finally, 2 replicate samples from the Vostok ice core were measured to compare with previous Brook et al. (2000, 2009) measurements from adjacent depths.

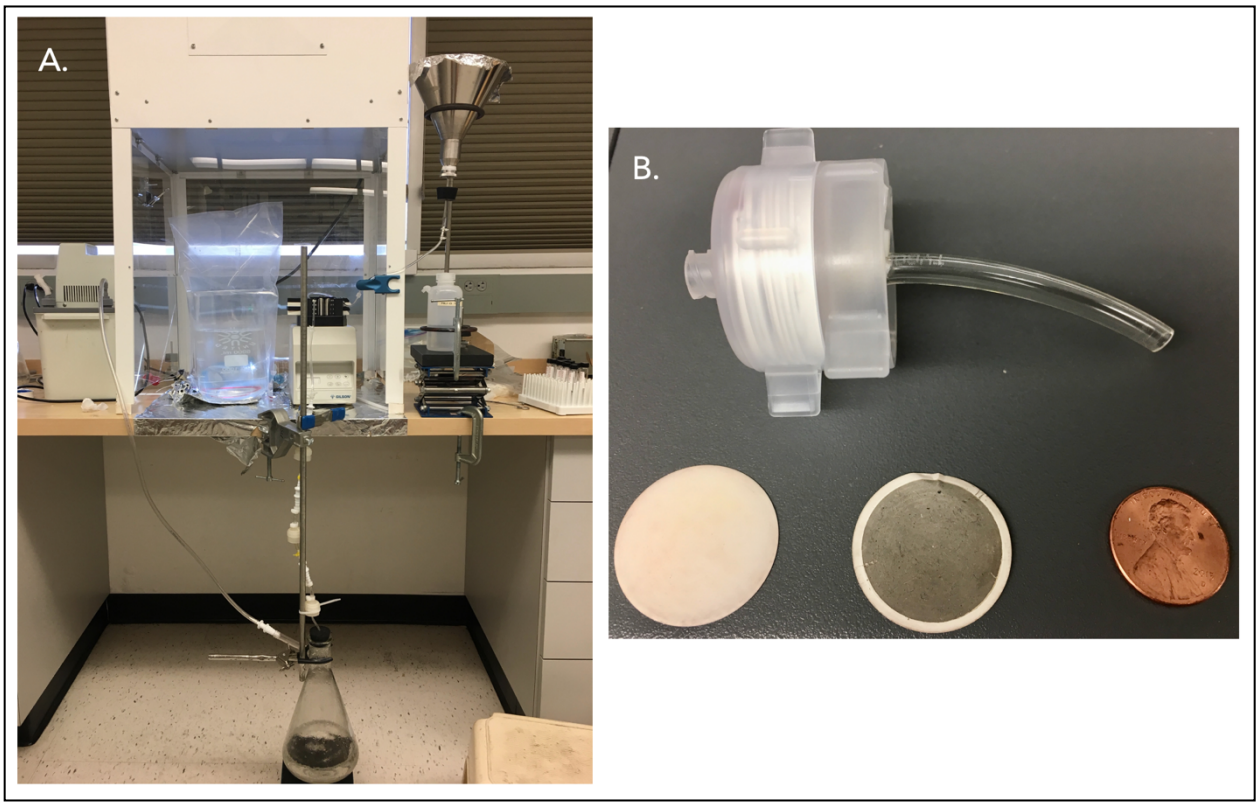

Figure 2.2: A. Experimental setup to filter samples. Sample is placed in clean, stainless steel funnel, and flows through line connected to a peristaltic pump. Behind the pump, samples pass through 1-2 filter holders, which are connected to a vacuum sealed Erlenmeyer flask. All steps of the process are conducted under a laminar flow hood to prevent contamination (the stainless steel funnel and Erlenmeyer flask were moved outside of the hood for this image to clearly represent the process). B. example of In-line filter holder, and 0.45µm filters- one blank and one with filtered contents from scrap ice.

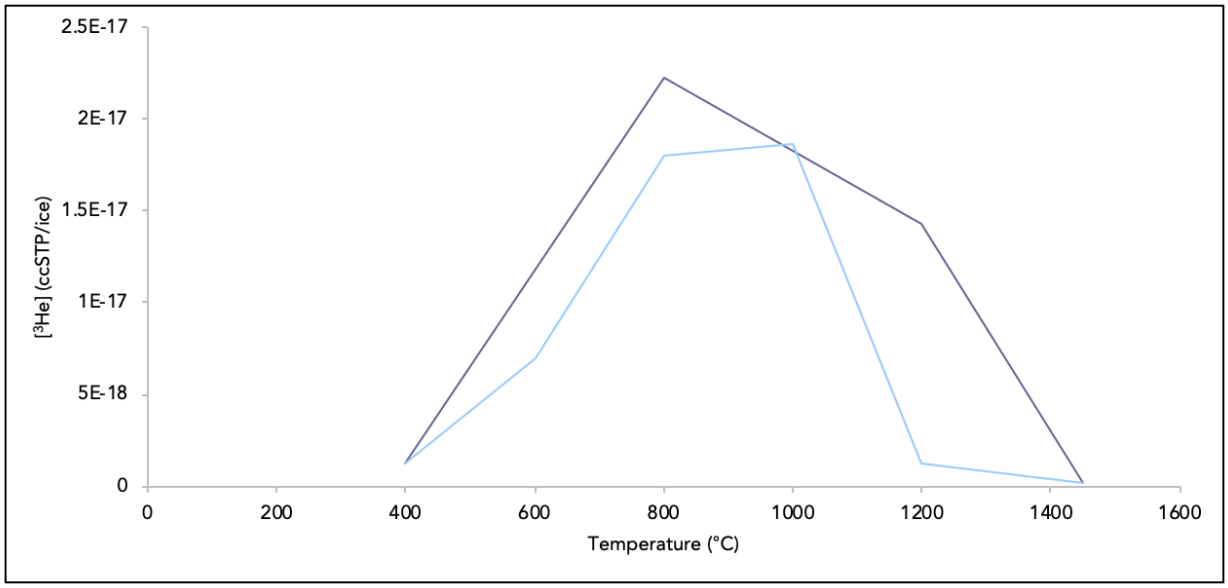

Sample	^{3}He/^{4}He	±	^{4}He, ccSTP	^{3}He, ccSTP	^{4}He, ccSTP/g ice	^{3}He, ccSTP/g ice
TG12-9-10ML2#2-400C	74.820	1.493	9.588E-11	9.900E-15	1.199E-14	1.237E-18
TG12-9-10ML2#2-800C	76.666	1.530	1.681E-09	1.778E-13	2.101E-13	2.223E-17
TG12-9-10ML232-1200C	176.595	3.524	4.687E-10	1.142E-13	5.859E-14	1.428E-17
TG12-9-10ML2#2-1450C	166.700	3.326	7.414E-12	1.706E-15	9.268E-16	2.132E-19
TG12-9-10ML2#1-400C	70.592	1.409	9.817E-11	9.563E-15	1.227E-14	1.195E-18
TG12-9-10ML2#1-600C	52.780	1.054	7.676E-10	5.591E-14	9.595E-14	6.988E-18
TG12-9-10ML2#1-800C	99.844	1.992	1.046E-09	1.442E-13	1.308E-13	1.802E-17
TG12-9-10ML2#1-1000C	186.529	3.722	5.793E-10	1.491E-13	7.241E-14	1.864E-17
TG12-9-10ML2#1-1200C	149.549	2.984	4.782E-11	9.868E-15	5.977E-15	1.234E-18
TG12-9-10ML2#1-1450C	120.072	2.396	1.019E-11	1.688E-15	1.274E-15	2.110E-19
Blank	14.529		2.563E-11	5.139E-16		

Figure 2.3: Step heating trials from a 2015 pilot study. Two 8 kg ice samples from Taylor Glacier are introduced to the furnace crucible and incrementally heated. Released He is measured at each increment. Both tests indicate that most, if not all ^{3}He is released by 1400°C. All samples in the study were heated to 1450°C to ensure full He release.

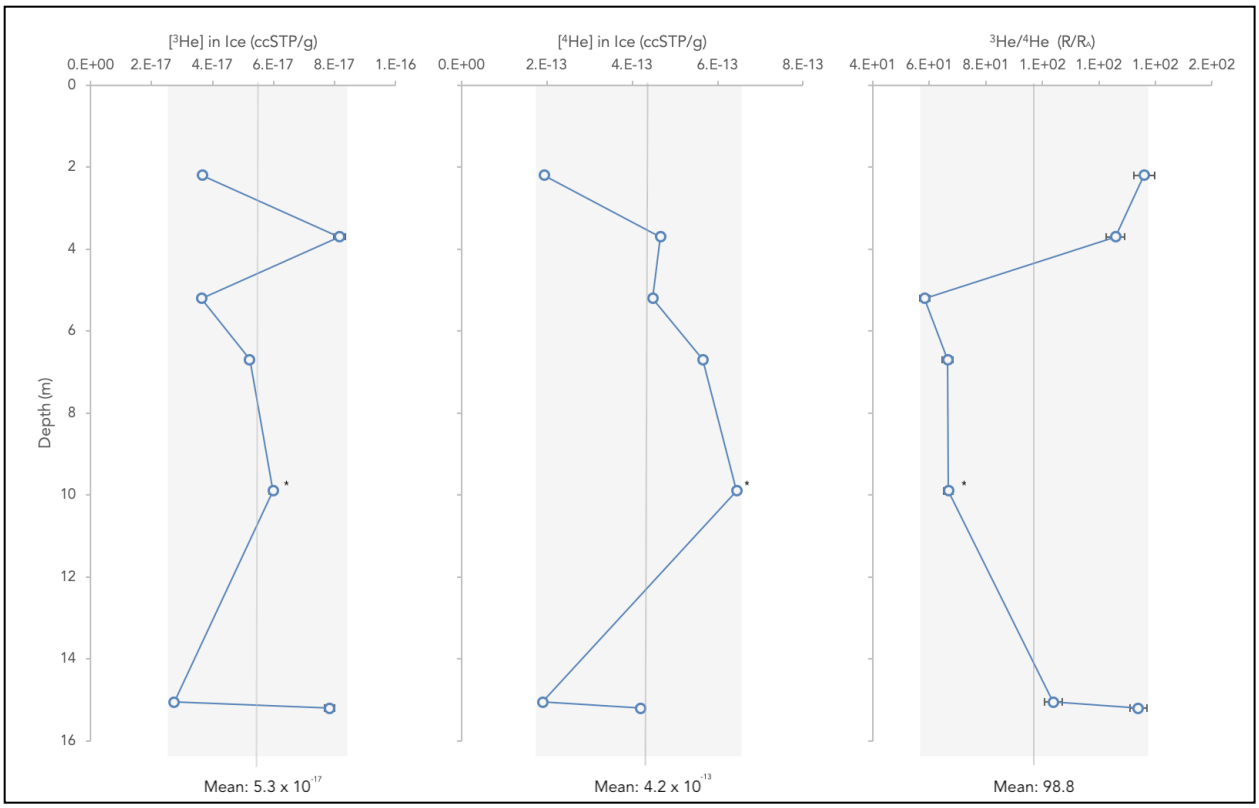

Figure 2.4 : All 7 composite Taylor Glacier samples (excluding high and low accumulation tests) plotted in depth space. Samples span an approximate age range of 53-55 ka. Measured [^{3}He] in ccSTP/g, [^{4}He] in ccSTP/g and ^{3}He/^{4}He in R_A for each sample are presented. Note: the sample at 9.9 m depth was filtered at 5 µm, all other samples were filtered at 0.45 µm. Error bars appear excluded for some depths because they are quite small compared to the sample symbols.

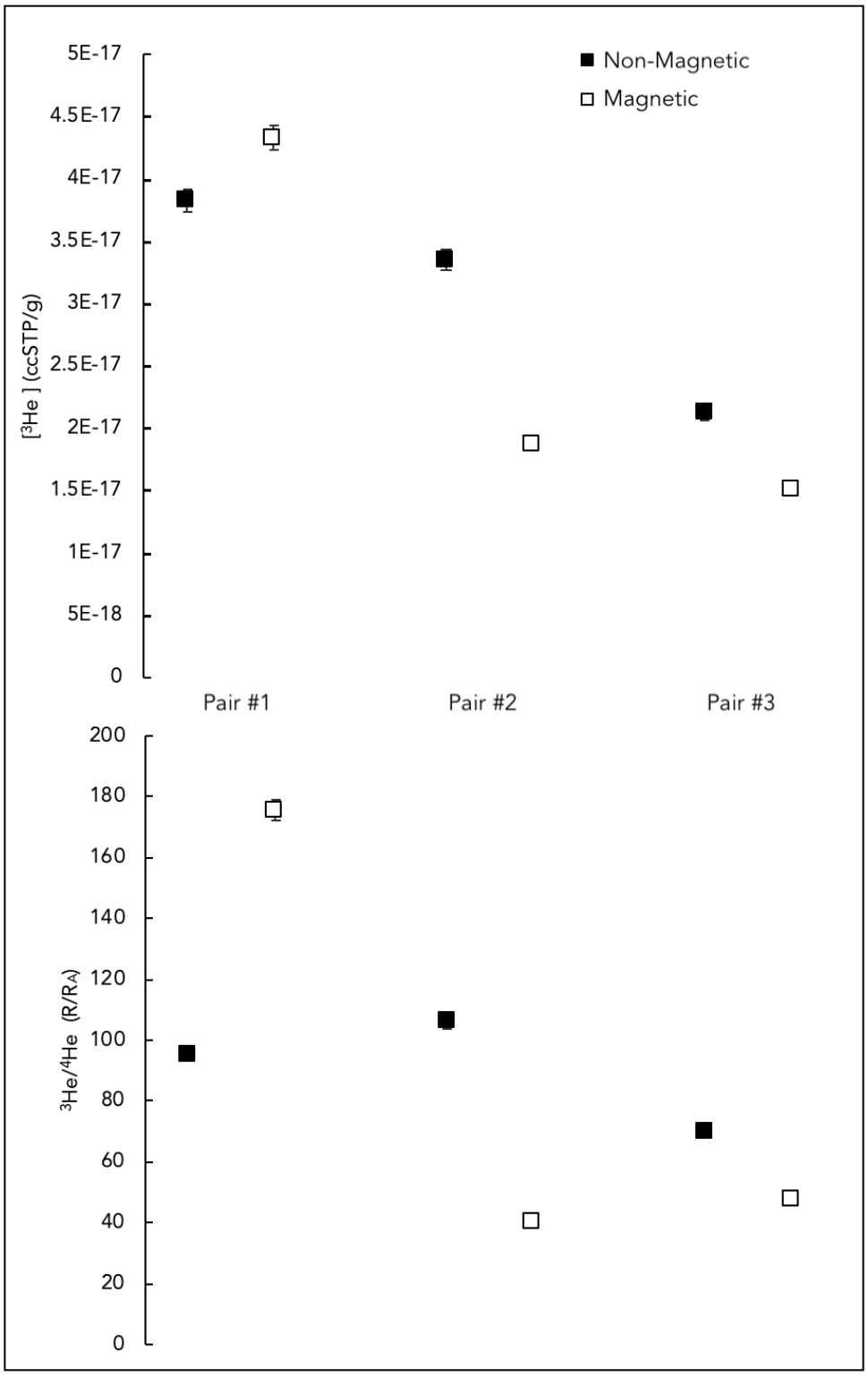

Figure 2.5: 3 magnetic separate pairs from TG sample depths of 3.7m (Pair #1), 6.7m (Pair #2) and 5.2m (Pair #3) respectively, with [^{3}He] in ccSTP/g and ^{3}He/^{4}He in R_A presented for each. Open squares represent magnetic fractions, while closed squares represent non-magnetic fractions. Neither fraction displays a consistently higher [^{3}He] or ^{3}He/^{4}He.

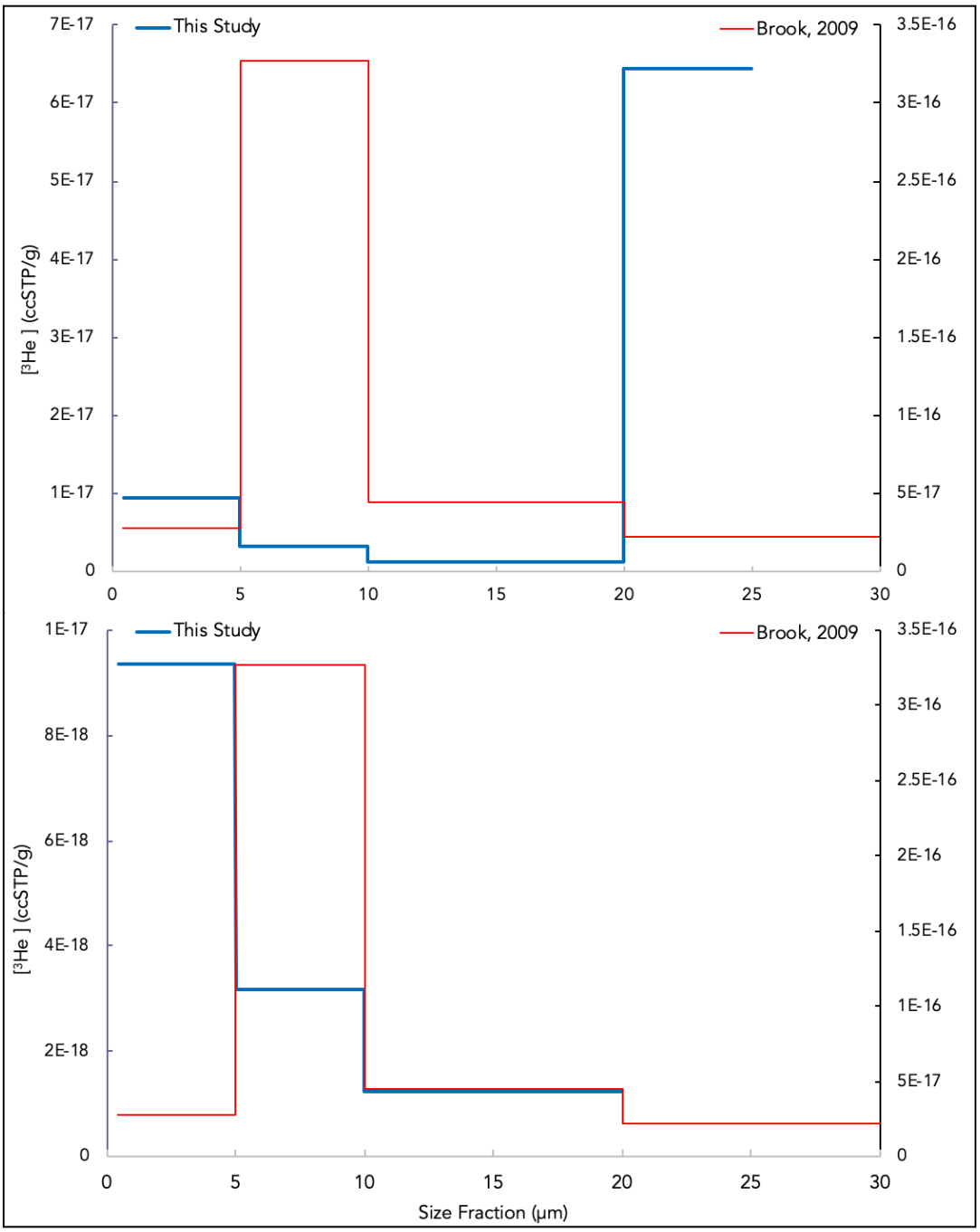

Figure 2.6: Size fraction experiment depicting [^{3}He] among 0.45 – 5 µm , 5 – 10 µm, 10 - 20 µm and 20+ µm diameter particle populations, from TG samples at 15.2m depth (This study, Blue) and from Vostok samples at 112-115m (Brook et al., 2009, Red). Each profile is on a its own relative scale. The upper graph includes the 20+ µm fraction from this study, while the bottom graph excludes it. The unexpectedly high [^{3}He] from the 20+ µm fraction in the upper graph may be due to input from a large, ^{3}He-rich "nugget" particle. If this size fraction is excluded, the profile from this study indicates a maximum input from the 0.45 - 5 µm particle size range.

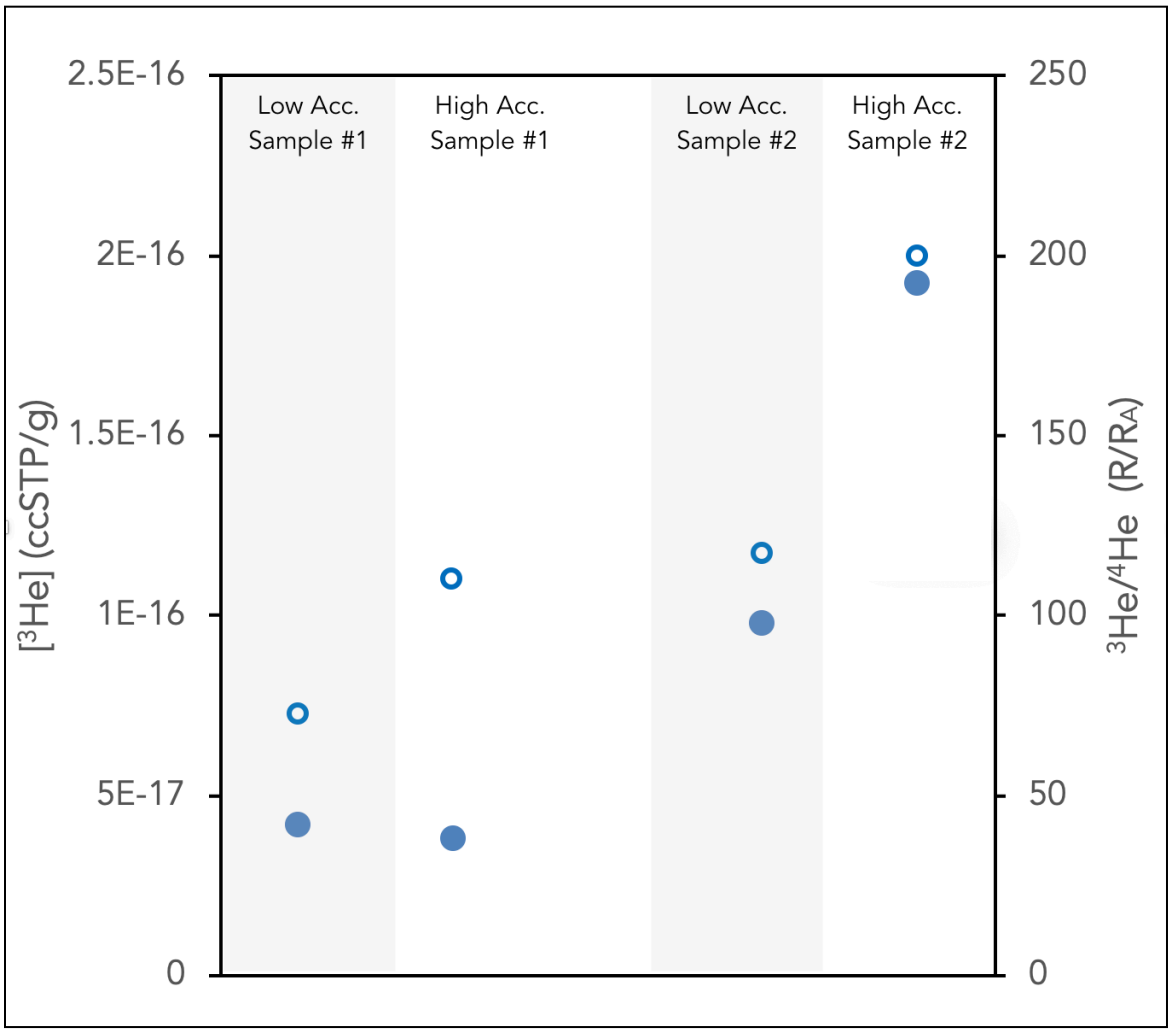

Figure 2.7: Measured [^{3}He] in ccSTP/g (closed circles) and ^{3}He/^{4}He in R_A (open circles) among 2 high accumulation and 2 low accumulation samples from Taylor Glacier- with approximate accumulation rates based on N_2O profiles (~0.15 cm/year for low accumulation, 1.5 cm/year for high accumulation). Low accumulation sample were expected to have higher [^{3}He] and ^{3}He/^{4}He than high accumulation samples. However, it appears on average, the opposite is true. This may indicate that ^{3}He is not an ideal proxy for ice accumulation rates in polar ice cores. Note: Low accumulation samples for this study were very dusty and required multiple filters to complete. During the second measurement of 3 components for low accumulation sample #1, the the furnace failed at 1400°C rather than 1450°C, so these values should be considered a lower estimate.

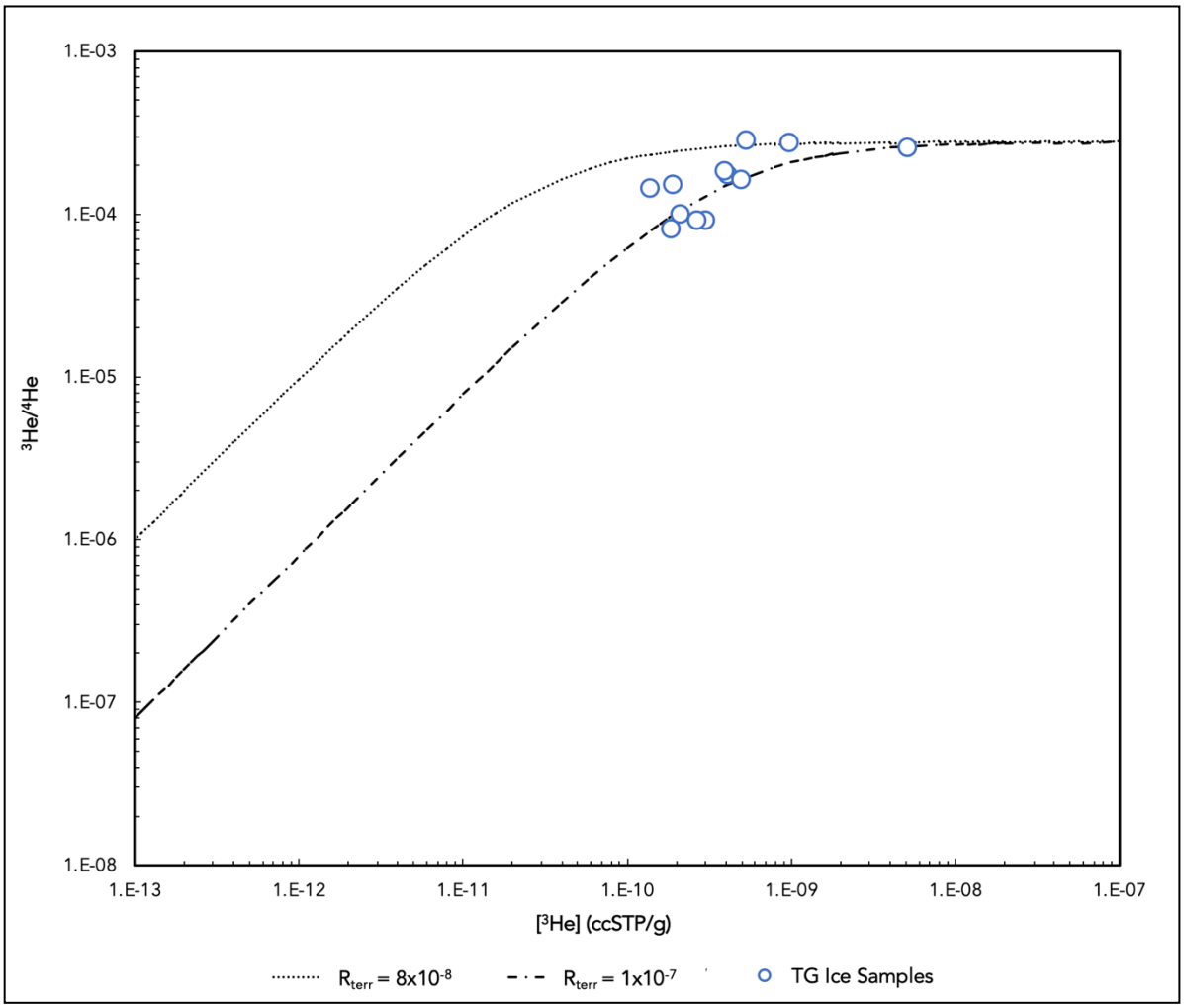

Figure 2.8: 2 Mixing models to determine if samples align with appropriate terrestrial and extraterrestrial end-member values. Upper and lower models were constructed using estimated dust concentrations in ice of 0.4 μg/g based on historic Taylor Glacier insoluble particle counts. Terrestrial ^{3}He/^{4}He ratios of 0.07 R_A (1 x 10^{-7} ^{3}He/^{4}He) and 0.058 R_A (8 x 10^{-8} ^{3}He/^{4}He)in ice were used, while an ET endmember of ~200 R_A (2.8 x 10^{-4} ^{3}He/^{4}He) was used. Measured ice samples agree well with the 2 models, indicating that our results are within the range of expected values.

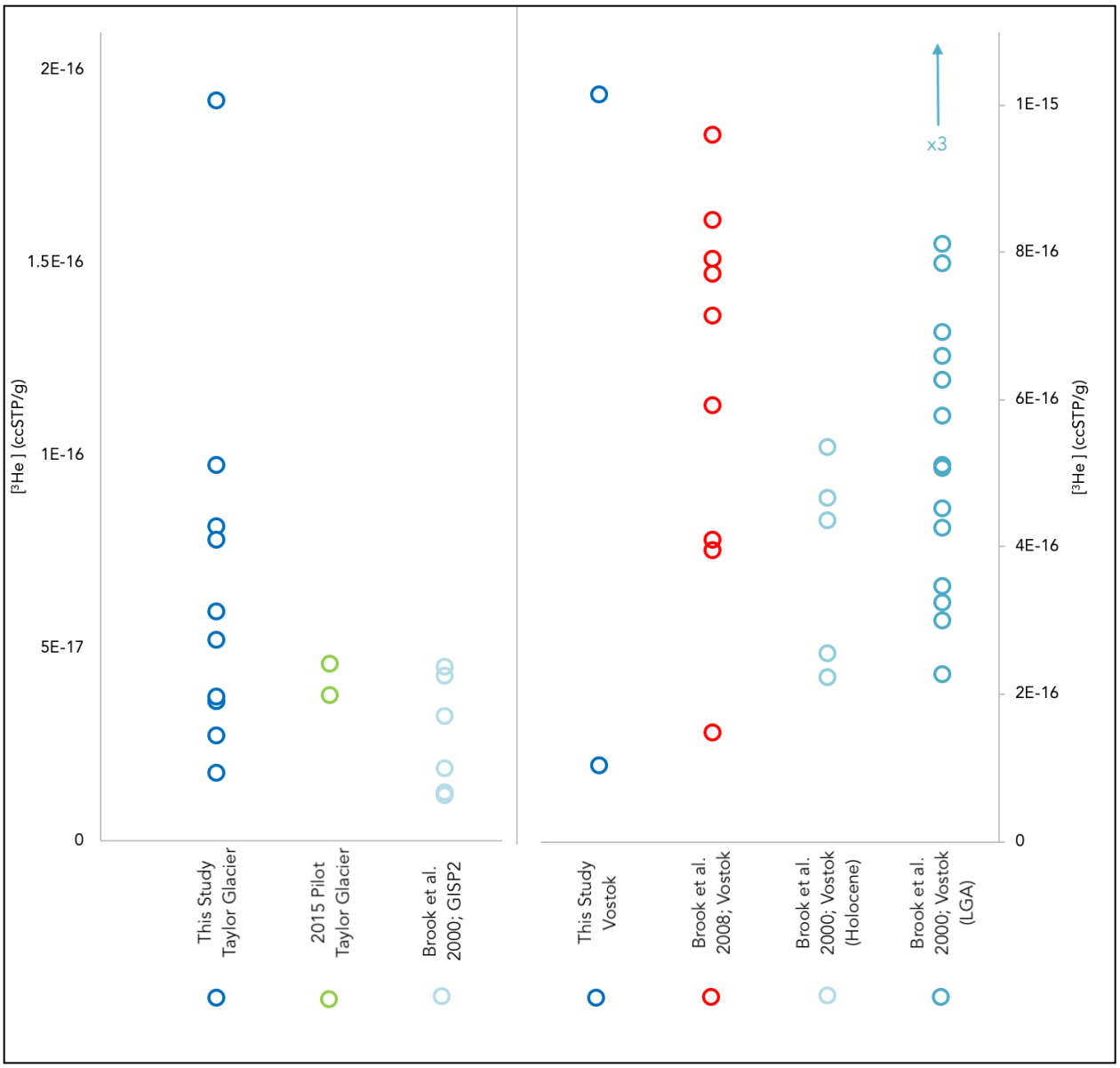

Figure 2.9: Individual sample measurements of [^{3}He] from this study, compared to Brook et al. (2000, 2008). On the left graph, average measurements from Taylor Glacier are higher than those from GISP2, which was expected given their respective accumulation rates. On the right graph, 2 Vostok Holocene estimates from this study compare favorably on average to the Brook et al. (2009) results (they are from very similar depths- see Table 2), which gives us confidence in our extraction procedure. However, the very wide spread in the 2 replicate Vostok samples (as well as the wide spread in most every column), indicate that replicability quite low for ice core samples, likely due to the very small number of IDPs present.

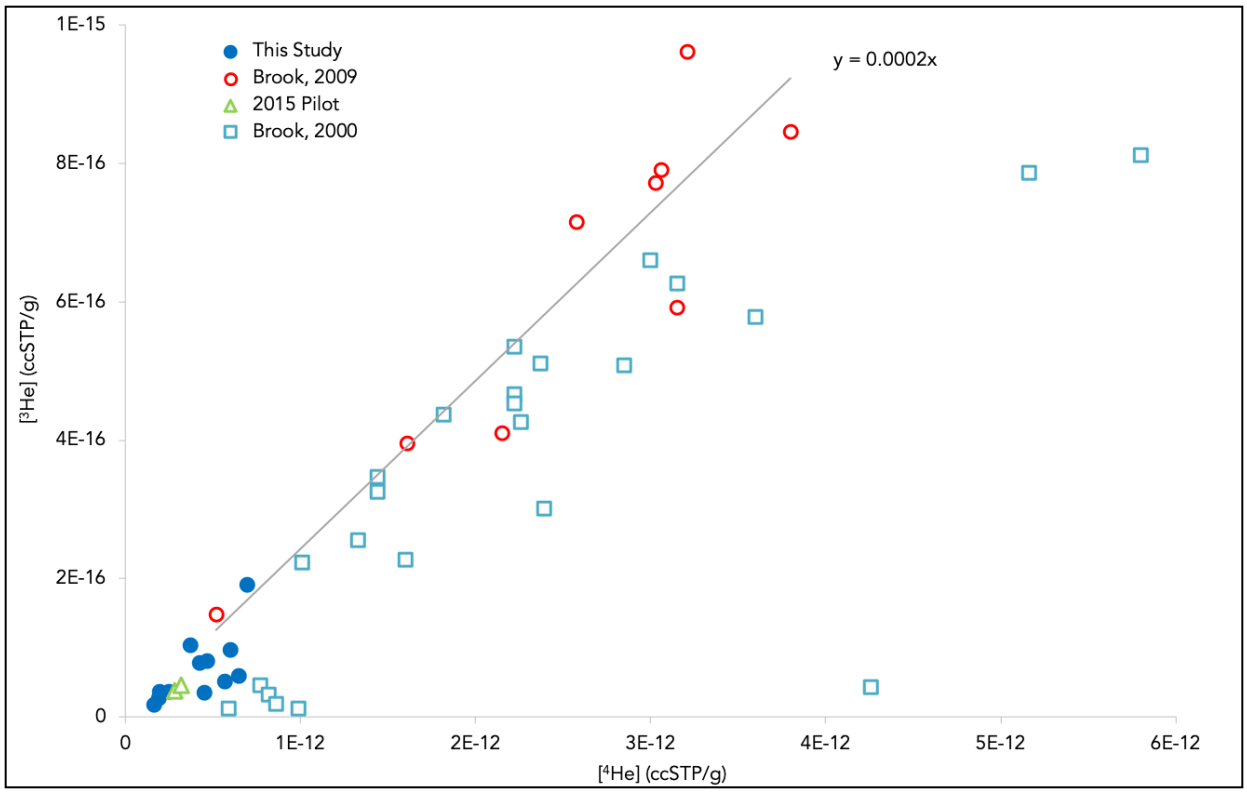

Figure 2.10: Measured [^{3}He] and [^{4}He] for each sample from this study, and from Brook et al. (2000, 2009) lie together along one mixing line which represents an R_A of 143.9. The fact that they lie along the same line suggests that they each contain similar proportions of terrestrial and extraterrestrial dust. 5 samples from GISP2 lie notably to the right of the line, likely because they have a greater proportion of terrestrial dust (and ^{4}He) in them. Samples on the lower left corner of the graph would be expected to have higher accumulation rates than samples in the upper right. Note: 3 outliers from Brook et al. (2000) are omitted, as in Figure 8.

Table 2.1: Summary of all relevant measurements from every blank, trial experiment, magnetic separation, size fraction experiment, accumulation test, and Vostok replicate procedure performed in this study.

Category	Sample	Depth (m)	Mass Ice Filtered (g)	Area Time Product (m^2a)	$^3He/^4He$	±	[^4He] (ccSTP/g)	±	[^3He] (ccSTP/g)	±	Combined [^4He]	±	Combined [^3He]	±	Combined $^3He/^4He$	±
BLANKS	Blank #1		1700				1.13E-14				1.13E-14	NM	NM	NM	NM	NM
	Blank #2		1700		3.51	2.01	1.84E-14		8.99E-20		1.84E-14	NM	8.99E-20	NM	NM	NM
	Blank #3		3000		0.05	1.33	2.09E-14	2.09E-16	1.53E-21	3.87E-20	2.09E-14	2.09E-16	1.53E-21	3.87E-20	NM	NM
TRIALS	TG # 7 0.45um filter	15.05	1700	0.059	103.89	2.82	1.90E-13	1.90E-15	2.74E-17	7.93E-19	1.90E-13	1.90E-15	2.74E-17	7.93E-19	103.89	3.18
	TG #10 0.45 um filter	2.2	3000	0.103	136.06	2.64	1.94E-13	1.94E-15	3.66E-17	7.99E-19	1.94E-13	2.11E-15	3.66E-17	8.75E-19	136.06	3.57
	TG #10 Secondary^		3000	0.103	31.30	3.10	1.75E-14	1.75E-16	7.61E-19	7.57E-20						
	TG # 5 5um filter	9.9	2767	0.095	66.76	1.23	6.45E-13	6.45E-15	5.98E-17	1.25E-18	6.45E-13	6.45E-15	5.98E-17	1.25E-18	66.76	1.55
MAGNETIC SEPARATION	Trial 1 Non-Magnetic		3000	0.103	95.38	2.10	2.89E-13	2.89E-15	3.83E-17	9.24E-19						
	Trial 1 Magnetic	3.7	3000	0.103	175.61	3.65	1.77E-13	1.77E-15	4.33E-17	9.98E-19	4.66E-13	4.66E-15	8.16E-17	1.92E-18	125.91	3.22
	Trial 2 Non-Magnetic		3139	0.108	105.93	2.39	2.27E-13	2.27E-15	3.35E-17	8.27E-19						
	Trial 2 Magnetic	6.7	3139	0.108	39.89	1.10	3.37E-13	3.37E-15	1.87E-17	5.47E-19	5.65E-13	5.65E-15	5.22E-17	1.37E-18	66.47	1.87
	Trial 3 Non-Magnetic		2989	0.103	69.68	1.88	2.20E-13	2.20E-15	2.13E-17	6.13E-19						
	Trial 3 Magnetic	5.2	2989	0.103	47.45	1.39	2.28E-13	2.28E-15	1.50E-17	4.64E-19	4.48E-13	3.63E-17	3.63E-17	1.08E-18	58.37	1.73
SIZE FRACTION	.45um fraction		5650	0.195	106.99	2.89	6.29E-14	6.29E-16	9.35E-18	2.70E-19						
	5um fraction		5650	0.195	92.92	3.36	2.47E-14	2.47E-16	3.19E-18	1.20E-19						
	10um fracton.		5650	0.195	76.15	3.19	1.18E-14	1.18E-16	1.25E-18	5.37E-20						
	20um fraction	15.2	5650	0.195	144.53	2.16	3.21E-13	3.21E-15	6.45E-17	1.16E-18	4.20E-13	4.20E-15	7.83E-17	1.60E-18	133.96	3.05
ACCUMULATION TESTS					86.29	2.53	1.17E-13	1.17E-15	1.40E-17	4.35E-19						
					87.31	3.05	2.53E-14	2.53E-16	3.07E-18	1.12E-19						
					32.41	2.97	1.81E-14	1.81E-16	8.16E-19	7.51E-20						
	TG 5/4-2 Low Acc 1	5.17-5.78	3649	2.433	67.23	1.59	2.58E-13	2.58E-15	2.41E-17	6.19E-19	4.18E-13	4.18E-15	4.20E-17	1.24E-18	72.29	2.29
	TG 5/4-1 High Acc 1	14.1-15.9	3064	0.219	109.88	2.17	2.47E-13	2.47E-15	3.78E-17	8.37E-19	2.47E-13	2.47E-15	3.78E-17	8.37E-19	109.88	2.67
					80.28	2.04	1.70E-13	1.70E-15	1.89E-17	5.18E-19						
					49.28	2.08	8.10E-14	8.10E-16	5.55E-18	2.41E-19						
	TG 5/4-2 Low Acc 2	5.17-5.78	3552	2.368	150.59	2.29	3.49E-13	3.49E-15	7.31E-17	1.33E-18	6.00E-13	6.00E-15	9.76E-17	2.09E-18	117.03	2.77
	TG 5/4-1 High Acc 2	14.1-15.9	3084	0.220	199.70	2.55	6.92E-13	6.92E-15	1.92E-16	3.11E-18	6.92E-13	6.92E-15	1.92E-16	3.11E-18	199.70	3.80
VOSTOK	Vostok Rep 1	122.17-123	2826	0.141	187.82	2.01	3.89E-12	3.89E-14	1.01E-15	1.48E-17	3.89E-12	3.89E-14	1.01E-15	1.48E-17	187.82	3.33
	Vostok Rep 2	122.17-123	3070	0.154	203.23	3.04	3.70E-13	3.70E-15	1.05E-16	1.88E-18	3.70E-13	3.70E-15	1.05E-16	1.88E-18	203.23	4.18

Table 2.2: Summary of Taylor Glacier ice core components used to create the high (~1.5 cm/yr) and low accumulation (~0.15cm/yr) samples for a rudimentary accumulation ice accumulation rate experiment. Samples were left over from the Menking et al. (2019) study.

High Accumulation Replicates
TG 5/4 BID 14-15. 45-60. 14.555 m
TG 5/4 BID 15-16. 30-45. 15.405 m
TG 5/4 BID 14-15. 60-75. 14.705 m
TG 5/4 BID 14-15. 90-97.5. 14.9675 m
TG 5/4 BID 14-15. 75-90. 14.855 m
TG 5/4 BID 15-16. 15-30. 15.255 m
TG 5/4 BID 15-16. 87-98.5. 15.9575 m
TG 5/4 BID 14-15. 0-15. 14.105 m
Low Accumulation Replicates
TG 5/4 BID2 #6. 15-30. 5.175 m
TG 5/4 BID2 #6. 45-60. 5.45 m
TG 5/4 BID2 #6. 75-90. 5.775 m
TG 5/4 BID2 #6. 30-45. 5.325 m

Table 2.3: Vostok 110-123m range sample comparison from this study, and Brook et al. (2000, 2009)

Parameter	**Brook at al. (2000) N = 5**	**Brook et al. (2009) N = 9**	**This Study (2020) N = 2**
Vostok Depths (m)	110.0 - 110.48	112 - 115 (replicate)	122.17 - 123.0 (replicate)
Sample Mass Range (g)	139.5 – 280.35	820.78 – 1200.78	2826 – 3070
Mean [^{3}He] (ccSTP/g ice)	3.83 x 10^{-16}	6.25 x 10^{-16}	5.60 x 10^{-16}
Range [^{3}He] (ccSTP/g ice)	2.23 – 5.35 x 10^{-16}	1.38 – 9.61 x 10^{-16}	1.05 -10.20 x 10^{-16}
Mean ^{3}He/^{4}He R/R_A	159.6	177.9	195.5
Range ^{3}He/^{4}He R/R_A	139.1 – 174.1	136 - 206.1	187.8 – 203.2

Table 2.4: Summary of ^{3}He flux estimates from ice cores. Estimates from this study are unusually low. *Because accumulation rates are poorly constrained in our ice, there is a very wide range of calculated ^{3}He flux. It is possible that accumulation rates are much higher than expected for our samples, and that the flux estimate from our samples should be closer to those from previous studies.

Study	Archive	^{3}He Flux estimate (x 10^{-13} ccSTP cm^{-2} ka^{-1})
Brook et al. (2000)	GISP2, Holocene ice	6.2 ± 2.7
Brook et al. (2000)	Vostok, Holocene ice	7.7 ± 2.5
Winckler & Fischer (2006)	EPICA Dome C Ice, 0-29 ka	7.5 ± 2.9
Brook et al. (2009)	Vostok, Holocene ice	12.5 ± 3.7
This Study	Taylor Glacier, Holocene ice	0.96 ± 0.38 – 1.91 ± 0.76 *

REFERENCES

Alvarez, L. W., Alvarez, W., Asaro, F., & Michel, H. v. (1980). Extraterrestrial cause for the Cretaceous-Tertiary extinction. *Science*, *208*(4448), 1095–1108. http://science.sciencemag.org/content/208/4448/1095.long

Anders, E. (1989). Pre-biotic organic matter from comets and asteroids. *Nature*, *342*(6247), 255–257. https://doi.org/10.1038/342255a0

Anders, E., & Grevesse, N. (1989). Abundances of the elements: Meteoritic and solar. *Geochimica Et Cosmochimica Acta*, *53*(1), 197–214.

Arculus, R. J., & Delano, J. W. (1981). Siderophile element abundances in the upper mantle: evidence for a sulfide signature and equilibrium with the core. *Geochimica et Cosmochimica Acta*, *45*(8), 1331–1343. https://doi.org/https://doi.org/10.1016/0016-7037(81)90226-X

Baales, M., Jöris, O., Street, M., Bittmann, F., Weninger, B., & Wiethold, J. (2002). Impact of the Late Glacial Eruption of the Laacher See Volcano, Central Rhineland, Germany. *Quaternary Research*, *58*(3), 273–288. https://doi.org/DOI: 10.1006/qres.2002.2379

Balcerzak, M. (2009). Methods of Elimination of Hafnium Interference in the Determination of Platinum in Environmental Samples by ICP-MS Technique. *Chemia Analityczna*, *54*, 135–149.

Barbante, C., Boutron, C., Morel, C., Ferrari, C., Jaffrezo, J. L., Cozzi, G., Gaspari, V., & Cescon, P. (2003). Seasonal variations of heavy metals in central Greenland snow deposited from 1991 to 1995. *J. Environ. Monit.*, *5*(2), 328–335. https://doi.org/10.1039/B210460A

Barbante, C., Schwikowski, M., Döring, T., Gäggeler, H. W., Schotterer, U., Tobler, L., van de Velde, K., Ferrari, C., Cozzi, G., & Turetta, A. (2004). Historical record of European emissions of heavy metals to the atmosphere since the 1650s from Alpine snow/ice cores drilled near Monte Rosa. *Environmental Science & Technology*, *38*(15), 4085–4090.

Barbante, C., Veysseyre, A., Ferrari, C., van de Velde, K., Morel, C., Capodaglio, G., Cescon, P., Scarponi, G., & Boutron, C. (2001). Greenland Snow Evidence of Large Scale Atmospheric Contamination for Platinum, Palladium, and Rhodium. *Environmental Science & Technology*, *35*(5), 835–839. https://doi.org/10.1021/es000146y

Borovička, J., Spurný, P., Brown, P., Wiegert, P., Kalenda, P., Clark, D., & Shrbený, L. (2013). The trajectory, structure and origin of the Chelyabinsk asteroidal impactor. *Nature*, *503*(7475), 235–237. https://doi.org/10.1038/nature12671

Briffa, K. R., Jones, P. D., Schweingruber, F. H., & Osborn, T. J. (1998). Influence of volcanic eruptions on Northern Hemisphere summer temperature over the past 600 years. *Nature*, *393*(6684), 450–455. https://doi.org/10.1038/30943

Broecker, W. S. (2006). Was the Younger Dryas Triggered by a Flood? *Science*, *312*(5777), 1146 LP – 1148. https://doi.org/10.1126/science.1123253

Broecker, W. S., Denton, G. H., Edwards, R. L., Cheng, H., Alley, R. B., & Putnam, A. E. (2010). Putting the Younger Dryas cold event into context. *Quaternary Science Reviews*, *29*(9), 1078–1081. https://doi.org/https://doi.org/10.1016/j.quascirev.2010.02.019

Brownlee, D. E. (1985). Cosmic Dust - Collection and Research. *Annual Review of Earth and Planetary Sciences*, *13*, 147–173. https://doi.org/DOI 10.1146/annurev.ea.13.050185.001051

Brownlee, D. E. (2016). Cosmic Dust: Building Blocks of Planets Falling from the sky. *Elements*, *12*(3), 165–170. https://doi.org/10.2113/gselements.12.3.165

Buizert, C., Gkinis, V., Severinghaus, J. P., He, F., Lecavalier, B. S., Kindler, P., Leuenberger, M., Carlson, A. E., Vinther, B., Masson-Delmotte, V., White, J. W. C., Liu, Z., Otto-Bliesner, B., & Brook, E. J. (2014). Greenland temperature response to climate forcing during the last deglaciation. *Science*, *345*(6201), 1177 LP – 1180. https://doi.org/10.1126/science.1254961

Bunch, T. E., Hermes, R. E., Moore, A. M. T., Kennett, D. J., Weaver, J. C., Wittke, J. H., DeCarli, P. S., Bischoff, J. L., Hillman, G. C., Howard, G. A., Kimbel, D. R., Kletetschka, G., Lipo, C. P., Sakai, S., Revay, Z., West, A., Firestone, R. B., & Kennett, J. P. (2012). Very high-temperature impact melt products as evidence for cosmic airbursts and impacts 12,900 years ago. *Proceedings of the National Academy of Sciences*, *109*(28), E1903 LP-E1912. https://doi.org/10.1073/pnas.1204453109

Chyba, C. F., Thomas, P. J., & Zahnle, K. J. (1993). The 1908 Tunguska explosion: atmospheric disruption of a stony asteroid. *Nature*, *361*(6407), 40–44. https://doi.org/10.1038/361040a0

Cole-Dai, J., Mosley-Thompson, E., & Thompson, L. G. (1997). Annually resolved southern hemisphere volcanic history from two Antarctic ice cores. *Journal of Geophysical Research: Atmospheres*, *102*(D14), 16761–16771. https://doi.org/10.1029/97JD01394

Curtius, J., Weigel, R., Vössing, H.-J., Wernli, H., Werner, A., Volk, C.-M., Konopka, P., Krebsbach, M., Schiller, C., Roiger, A., Schlager, H., Dreiling, V., & Borrmann, S. (2005). Observations of meteoric material and implications for aerosol nucleation in the winter Arctic lower stratosphere derived from in situ particle measurements. *Atmos. Chem. Phys.*, *5*(11), 3053–3069. https://doi.org/10.5194/acp-5-3053-2005

Dai, J., Mosley-Thompson, E., & Thompson, L. G. (1991). Ice core evidence for an explosive tropical volcanic eruption 6 years preceding Tambora. *Journal of Geophysical Research: Atmospheres*, *96*(D9), 17361–17366. https://doi.org/10.1029/91JD01634

Fan, Z. Y., Plane, J. M. C., Gumbel, J., Stegman, J., & Llewellyn, E. J. (2007). Satellite measurements of the global mesospheric sodium layer. *Atmospheric Chemistry and Physics*, *7*(15), 4107–4115. https://doi.org/10.5194/acp-7-4107-2007

Felitsyn, S. B., & Vaganov, P. A. (1988). IRIDIUM IN THE ASH OF KAMCHATKAN VOLCANOES. *International Geology Review*, *30*(12), 1288–1291. https://doi.org/10.1080/00206818809466110

Firestone, R. B., West, A., Kennett, J. P., Becker, L., Bunch, T. E., Revay, Z. S., Schultz, P. H., Belgya, T., Kennett, D. J., & Erlandson, J. M. (2007). Evidence for an extraterrestrial impact 12,900 years ago that contributed to the megafaunal extinctions and the Younger Dryas cooling. *Proceedings of the National Academy of Sciences*, *104*(41), 16016–16021.

Gabrielli, P, Barbante, C., Plane, J. M. C., Boutron, C. F., Jaffrezo, J. L., Mather, T. A., Stenni, B., Gaspari, V., Cozzi, G., Ferrari, C., & Cescon, P. (2008). Siderophile metal fallout to Greenland from the 1991 winter eruption of Hekla (Iceland) and during the global atmospheric perturbation of Pinatubo. *Chemical Geology*, *255*(1–2), 78–86. https://doi.org/10.1016/j.chemgeo.2008.06.012

Gabrielli, P, Plane, J. M. C., Boutron, C. F., Hong, S. M., Cozzi, G., Cescon, P., Ferrari, C., Crutzen, P. J., Petit, J. R., Lipenkov, V. Y., & Barbante, C. (2006). A climatic control on the accretion

of meteoric and super-chondritic iridium-platinum to the Antarctic ice cap. *Earth and Planetary Science Letters*, *250*(3–4), 459–469. https://doi.org/10.1016/j.epsl.2006.08.015

Gabrielli, Paolo, Barbante, C., Plane, J. M. C., Varga, A., Hong, S., Cozzi, G., Gaspari, V., Planchon, F. A. M., Cairns, W., & Ferrari, C. (2004). Meteoric smoke fallout over the Holocene epoch revealed by iridium and platinum in Greenland ice. *Nature*, *432*(7020), 1011.

Gabrielli, Paolo, Varga, A., Barbante, C., Boutron, C., Cozzi, G., Gaspari, V., Planchon, F., Cairns, W., Hong, S., & Ferrari, C. (2004). Determination of Ir and Pt down to the sub-femtogram per gram level in polar ice by ICP-SFMS using preconcentration and a desolvation system. *Journal of Analytical Atomic Spectrometry*, *19*(7), 831–837.

Gardner, C. S., Chu, X., Espy, P. J., Plane, J. M. C., Marsh, D. R., & Janches, D. (2011). Seasonal variations of the mesospheric Fe layer at Rothera, Antarctica (67.5°S, 68.0°W). *Journal of Geophysical Research: Atmospheres*, *116*(D2). https://doi.org/10.1029/2010JD014655

Gupta, S., Zhao, D., & Rai, S. S. (2009). Seismic imaging of the upper mantle under the Erebus hotspot in Antarctica. *Gondwana Research*, *16*(1), 109–118. https://doi.org/https://doi.org/10.1016/j.gr.2009.01.004

Hammer, C. U. (1977). Past volcanism revealed by Greenland Ice Sheet impurities. *Nature*, *270*(5637), 482–486. https://doi.org/10.1038/270482a0

Hans Wedepohl, K. (1995). The composition of the continental crust. *Geochimica et Cosmochimica Acta*, *59*(7), 1217–1232. https://doi.org/https://doi.org/10.1016/0016-7037(95)00038-2

Haynes, W. M., Lide, D. R., & Bruno, T. J. (2016). *CRC handbook of chemistry and physics : a ready-reference book of chemical and physical data.*

Hou, Q. L., Ma, P. X., & Kolesnikov, E. M. (1998). Discovery of iridium and other element anomalies near the 1908 Tunguska explosion site. *Planetary and Space Science*, *46*(2), 179–188. https://doi.org/https://doi.org/10.1016/S0032-0633(97)00174-8

Hsu, J., Prather, M. J., & Wild, O. (2005). Diagnosing the stratosphere-to-troposphere flux of ozone in a chemistry transport model. *Journal of Geophysical Research: Atmospheres*, *110*(D19). https://doi.org/10.1029/2005JD006045

Janches, D., Heinselman, C. J., Chau, J. L., Chandran, A., & Woodman, R. (2006). Modeling the global micrometeor input function in the upper atmosphere observed by high power and large aperture radars. *Journal of Geophysical Research: Space Physics*, *111*(A7). https://doi.org/10.1029/2006JA011628

Jarvis, I., Totland, M. M., & Jarvis, K. E. (1997). Determination of the platinum-group elements in geological materials by ICP-MS using microwave digestion, alkali fusion and cation-exchange chromatography. *Chemical Geology*, *143*(1), 27–42. https://doi.org/https://doi.org/10.1016/S0009-2541(97)00098-3

Kahl, J. D. W., Martinez, D. A., Kuhns, H., Davidson, C. I., Jaffrezo, J.-L., & Harris, J. M. (1997). Air mass trajectories to Summit, Greenland: A 44-year climatology and some episodic events. *Journal of Geophysical Research: Oceans*, *102*(C12), 26861–26875. https://doi.org/10.1029/97JC00296

Karner, D. B., Levine, J., Muller, R. A., Asaro, F., Ram, M., & Stolz, M. R. (2003). Extraterrestrial accretion from the GISP2 ice core. *Geochimica Et Cosmochimica Acta*, *67*(4), 751–763.

Kelley, M. C., Seyler, C. E., & Larsen, M. F. (2009). Two-dimensional turbulence, space shuttle plume transport in the thermosphere, and a possible relation to the Great Siberian Impact Event. *Geophysical Research Letters*, *36*(14). https://doi.org/10.1029/2009GL038362

Kennett, D. J., Kennett, J. P., West, A., Mercer, C., Hee, S. S. Q., Bement, L., Bunch, T. E., Sellers, M., & Wolbach, W. S. (2009). Nanodiamonds in the Younger Dryas boundary sediment layer. *Science*, *323*(5910), 94.

Kennett, D. J., Kennett, J. P., West, A., West, G. J., Bunch, T. E., Culleton, B. J., Erlandson, J. M., Hee, S. S. Q., Johnson, J. R., & Mercer, C. (2009). Shock-synthesized hexagonal diamonds in Younger Dryas boundary sediments. *Proceedings of the National Academy of Sciences*, *106*(31), 12623–12628.

Kjær, K. H., Larsen, N. K., Binder, T., Bjørk, A. A., Eisen, O., Fahnestock, M. A., Funder, S., Garde, A. A., Haack, H., Helm, V., Houmark-Nielsen, M., Kjeldsen, K. K., Khan, S. A., Machguth, H., McDonald, I., Morlighem, M., Mouginot, J., Paden, J. D., Waight, T. E., … MacGregor, J. A. (2018). A large impact crater beneath Hiawatha Glacier in northwest Greenland. *Science Advances*, *4*(11), eaar8173. https://doi.org/10.1126/sciadv.aar8173

Koeberl, C. (1989). Iridium enrichment in volcanic dust from blue ice fields, Antarctica, and possible relevance to the K/T boundary event. *Earth and Planetary Science Letters*, *92*(3), 317–322. https://doi.org/https://doi.org/10.1016/0012-821X(89)90056-3

Kvasnytsya, V., Wirth, R., Dobrzhinetskaya, L., Matzel, J., Jacobsen, B., Hutcheon, I., Tappero, R., & Kovalyukh, M. (2013). New evidence of meteoritic origin of the Tunguska cosmic body. *Planetary and Space Science*, *84*, 131–140. https://doi.org/https://doi.org/10.1016/j.pss.2013.05.003

Lanci, L, Delmonte, B., Kent, D. v, Maggi, V., Biscaye, P. E., & Petit, J.-R. (2012). Magnetization of polar ice: a measurement of terrestrial dust and extraterrestrial fallout. *Quaternary Science Reviews*, *33*, 20–31. https://doi.org/https://doi.org/10.1016/j.quascirev.2011.11.023

Lanci, L, & Kent, D. v. (2006). Meteoric smoke fallout revealed by superparamagnetism in Greenland ice. *Geophysical Research Letters*, *33*(13). https://doi.org/10.1029/2006GL026480

Lanci, Luca, Kent, D. v, & Biscaye, P. E. (2007). Meteoric smoke concentration in the Vostok ice core estimated from superparamagnetic relaxation and some consequences for estimates of Earth accretion rate. *Geophysical Research Letters*, *34*(10).

Larsen, E., Fernelius, W. C., & Quill, L. (1943). Concentration of Hafnium. Preparation of Hafnium-Free Zirconia. *Industrial & Engineering Chemistry Analytical Edition*, *15*(8), 512–515. https://doi.org/10.1021/i560120a015

Legrand, M., & Mayewski, P. (1997). Glaciochemistry of polar ice cores: A review. *Reviews of Geophysics*, *35*(3), 219–243. https://doi.org/10.1029/96RG03527

Love, S. G., & Brownlee, D. E. (1993). A direct measurement of the terrestrial mass accretion rate of cosmic dust. *Science*, *262*(5133), 550–553.

Lyne, J. E., & Tauber, M. (1995). Origin of the Tunguska event. *Nature*, *375*(6533), 638–639. https://doi.org/10.1038/375638a0

Mathews, J. D., Janches, D., Meisel, D. D., & Zhou, Q.-H. (2001). The micrometeoroid mass flux into the upper atmosphere: Arecibo results and a comparison with prior estimates. *Geophysical Research Letters*, *28*(10), 1929–1932. https://doi.org/10.1029/2000GL012621

Matsumoto, A., & Hinkley, T. K. (2001). Trace metal suites in Antarctic pre-industrial ice are consistent with emissions from quiescent degassing of volcanoes worldwide. *Earth and Planetary Science Letters*, *186*(1), 33–43. https://doi.org/https://doi.org/10.1016/S0012-821X(01)00228-X

Mayewski, P A, Meeker, L. D., Whitlow, S., Twickler, M. S., Morrison, M. C., Bloomfield, P., Bond, G. C., Alley, R. B., Gow, A. J., Meese, D. A., Grootes, P. M., Ram, M., Taylor, K. C., & Wumkes, W. (1994). Changes in Atmospheric Circulation and Ocean Ice Cover over the North Atlantic During the Last 41,000 Years. *Science*, *263*(5154), 1747–1751. https://doi.org/10.1126/science.263.5154.1747

Mayewski, Paul Andrew. (1999). *GISP2 Ions: Deep (D) Core (Detailed)*. PANGAEA. https://doi.org/10.1594/PANGAEA.55533

McConnell, J. R., Edwards, R., & Banta, R. (2005). A novel method for high-resolution, broad spectrum ice core analyses using ICP-OES and dual HR-ICP-MS. *Geophys. Res. Abstr*, *7*(10,713).

McCormick, M. P., Thomason, L. W., & Trepte, C. R. (1995). Atmospheric effects of the Mt Pinatubo eruption. *Nature*, *373*(6513), 399–404. https://doi.org/10.1038/373399a0

McDonough, W. F., & Sun, S.-S. (1995). The composition of the Earth. *Chemical Geology*, *120*(3–4), 223–253.

Meija, J., Coplen, T. B., Berglund, M., Brand, W. A., Bièvre, P. de, Gröning, M., Holden, N. E., Irrgeher, J., Loss, R. D., Walczyk, T., & Prohaska, T. (2016). Isotopic compositions of the elements 2013 (IUPAC Technical Report). *Pure and Applied Chemistry*, *88*(3), 293–306. https://doi.org/https://doi.org/10.1515/pac-2015-0503

Melott, A. L., Thomas, B. C., Dreschhoff, G., & Johnson, C. K. (2010). Cometary airbursts and atmospheric chemistry: Tunguska and a candidate Younger Dryas event. *Geology*, *38*(4), 355–358. https://doi.org/10.1130/G30508.1

Murrell, M. T., Davis, P. A., Nishiizumi, K., & Millard, H. T. (1980). Deep-sea spherules from Pacific clay: mass distribution and influx rate. *Geochimica et Cosmochimica Acta*, *44*(12), 2067–2074. https://doi.org/https://doi.org/10.1016/0016-7037(80)90204-5

Oppenheimer, C. (2003). Climatic, environmental and human consequences of the largest known historic eruption: Tambora volcano (Indonesia) 1815. *Progress in Physical Geography: Earth and Environment*, *27*(2), 230–259. https://doi.org/10.1191/0309133303pp379ra

Pearson, D. G., & Woodland, S. J. (2000). Solvent extraction/anion exchange separation and determination of PGEs (Os, Ir, Pt, Pd, Ru) and Re–Os isotopes in geological samples by isotope dilution ICP-MS. *Chemical Geology*, *165*(1–2), 87–107.

Petaev, M. I., Huang, S., Jacobsen, S. B., & Zindler, A. (2013). Large Pt anomaly in the Greenland ice core points to a cataclysm at the onset of Younger Dryas. *Proceedings of the National Academy of Sciences*, *110*(32), 12917–12920.

Pino, M., Abarzúa, A. M., Astorga, G., Martel-Cea, A., Cossio-Montecinos, N., Navarro, R. X., Lira, M. P., Labarca, R., LeCompte, M. A., Adedeji, V., Moore, C. R., Bunch, T. E., Mooney, C., Wolbach, W. S., West, A., & Kennett, J. P. (2019). Sedimentary record from Patagonia, southern Chile supports cosmic-impact triggering of biomass burning, climate change, and megafaunal extinctions at 12.8 ka. *Scientific Reports*, *9*(1), 4413. https://doi.org/10.1038/s41598-018-38089-y

Pinter, N., Scott, A. C., Daulton, T. L., Podoll, A., Koeberl, C., Anderson, R. S., & Ishman, S. E. (2011). The Younger Dryas impact hypothesis: A requiem. *Earth-Science Reviews*, *106*(3), 247–264.

Plane, J. M. C. (2003). Atmospheric chemistry of meteoric metals. *Chemical Reviews*, *103*(12), 4963–4984.

Plane, J. M. C. (2012). Cosmic dust in the Earth's atmosphere. *Chemical Society Reviews*, *41*(19), 6507–6518.

Ram, M., & Koenig, G. (1997). Continuous dust concentration profile of pre-Holocene ice from the Greenland Ice Sheet Project 2 ice core: Dust stadials, interstadials, and the Eemian. *Journal of Geophysical Research: Oceans*, *102*(C12), 26641–26648. https://doi.org/10.1029/96JC03548

Rasmussen, K. L., Clausen, H. B., & Kallemeyn, G. W. (1995). No iridium anomaly after the 1908 Tunguska impact: Evidence from a Greenland ice core. *Meteoritics*, *30*(6), 634–638.

Rasmussen, K. L., Olsen, H. J. F., Gwozdz, R., & Kolesnikov, E. M. (1999). Evidence for a very high carbon/iridium ratio in the Tunguska impactor. *Meteoritics & Planetary Science*, *34*(6), 891–895.

Rasmussen, S. O., Andersen, K. K., Svensson, A. M., Steffensen, J. P., Vinther, B. M., Clausen, H. B., Siggaard-Andersen, M.-L., Johnsen, S. J., Larsen, L. B., Dahl-Jensen, D., Bigler, M., RöThlisberger, R., Fischer, H., Goto-Azuma, K., Hansson, M. E., & Ruth, U. (2006). A new Greenland ice core chronology for the last glacial termination. *Journal of Geophysical Research (Atmospheres)*, *111*, D06102. https://doi.org/10.1029/2005JD006079

Saunders, R W, Dhomse, S., Tian, W. S., Chipperfield, M. P., & Plane, J. M. C. (2012). Interactions of meteoric smoke particles with sulphuric acid in the Earth's stratosphere. *Atmos. Chem. Phys.*, *12*(10), 4387–4398. https://doi.org/10.5194/acp-12-4387-2012

Saunders, Russell W, & Plane, J. M. C. (2011). A photo-chemical method for the production of olivine nanoparticles as cosmic dust analogues. *Icarus*, *212*(1), 373–382. https://doi.org/https://doi.org/10.1016/j.icarus.2010.12.019

Sengupta, A., Airan, Y., Thulasidas, S. K., & Natarajan, V. (2015). Evaluation of Spectral Interference of Lutetium on Analytes Including Specified Rare Earth Elements Using a CCD Detector-based ICP-AES. *Atomic Spectroscopy*, *36*, 82–95.

Soyol-Erdene, T.-O., Huh, Y., Hong, S., & Hur, S. do. (2011). A 50-year record of platinum, iridium, and rhodium in Antarctic snow: volcanic and anthropogenic sources. *Environmental Science & Technology*, *45*(14), 5929–5935.

Stothers, R. B. (1984). The Great Tambora Eruption in 1815 and Its Aftermath. *Science*, *224*(4654), 1191 LP – 1198. https://doi.org/10.1126/science.224.4654.1191

Suavet, C., Rochette, P., Gattacceca, J., & Folco, L. (2008). Micrometeorites: A possible bias on the sedimentary magnetic record. *Geochemistry, Geophysics, Geosystems*, *9*(11). https://doi.org/10.1029/2008GC002160

Sun, N., Brandon, A. D., Forman, S. L., Waters, M. R., & Befus, K. S. (2020). Volcanic origin for Younger Dryas geochemical anomalies ca. 12,900 cal B.P. *Science Advances*, *6*(31), eaax8587. https://doi.org/10.1126/sciadv.aax8587

Tankersley, K. B., Dunning, N. P., Owen, L. A., Huff, W. D., Park, J. H., Kim, C., Lentz, D. L., & Sparks-Stokes, D. (2018). Positive Platinum anomalies at three late Holocene high

magnitude volcanic events in Western Hemisphere sediments. *Scientific Reports*, *8*(1), 11298. https://doi.org/10.1038/s41598-018-29741-8

Taylor, S., Lever, J. H., & Harvey, R. P. (1998). Accretion rate of cosmic spherules measured at the South Pole. *Nature*, *392*(6679), 899–903. https://doi.org/10.1038/31894

Toutain, J.-P., & Meyer, G. (1989). Iridium-bearing sublimates at a hot-spot volcano (Piton De La Fournaise, Indian Ocean). *Geophysical Research Letters*, *16*(12), 1391–1394. https://doi.org/10.1029/GL016i012p01391

Tseren-Ochir, S.-E., Huh, Y., Hong, S.-M., Hwang, H., & Hur, S. do. (2011). Quantification of Ultra-Trace Levels of Pt, Ir and Rh in Polar Snow and Ice Using ICP-SFMS Coupled with a Pre-Concentration and Desolvation Nebulization System. *Bulletin of the Korean Chemical Society*, *32*, 2105–2108. https://doi.org/10.5012/bkcs.2011.32.6.2105

US Ice Drilling Program. (2019). *Blue Ice Drill Operations and Maintenance Manual*.

Vondrak, T., Plane, J. M. C., Broadley, S., & Janches, D. (2008). A chemical model of meteoric ablation. *Atmos. Chem. Phys.*, *8*(23), 7015–7031. https://doi.org/10.5194/acp-8-7015-2008

Wasson, J. T. (1999). Trapped melt in IIIAB irons; solid/liquid elemental partitioning during the fractionation of the IIIAB magma. *Geochimica et Cosmochimica Acta*, *63*, 2875–2889. https://doi.org/10.1016/S0016-7037(99)00283-5

Wasson, J. T., & Choe, W.-H. (2009). The IIG iron meteorites: Probable formation in the IIAB core. *Geochimica et Cosmochimica Acta*, *73*(16), 4879–4890. https://doi.org/https://doi.org/10.1016/j.gca.2009.05.062

Watson, A. J., Bakker, D. C. E., Ridgwell, A. J., Boyd, P. W., & Law, C. S. (2000). Effect of iron supply on Southern Ocean CO2 uptake and implications for glacial atmospheric CO2. *Nature*, *407*(6805), 730–733. https://doi.org/10.1038/35037561

WDOWIAK, T. J., ARMENDAREZ, L. P., AGRESTI, D. G., WADE, M. L., WDOWIAK, S. Y., CLAEYS, P., & IZETT, G. (2001). Presence of an iron-rich nanophase material in the upper layer of the Cretaceous-Tertiary boundary clay. *Meteoritics & Planetary Science*, *36*(1), 123–133. https://doi.org/10.1111/j.1945-5100.2001.tb01814.x

ZOLLER, W. H., PARRINGTON, J. R., & KOTRA, J. M. P. (1983). Iridium Enrichment in Airborne Particles from Kilauea Volcano: January 1983. *Science*, *222*(4628), 1118 LP – 1121. https://doi.org/10.1126/science.222.4628.1118

Zreda-Gostynska, G., Kyle, P. R., Finnegan, D., & Prestbo, K. M. (1997). Volcanic gas emissions from Mount Erebus and their impact on the Antarctic environment. *Journal of Geophysical Research: Solid Earth*, *102*(B7), 15039–15055. https://doi.org/10.1029/97JB00155